Refinement of plume models in
the infrared spectral region

By

Kenneth E. Harwell

University of Tennessee Space Institute
30 June 1978

20. ABSTRACT (Continue on reverse side if necessary and identify by block number)

The MIRADCOM Radiation Model was improved and used successfully to predict CO_2 and H_2O radiation emitted from a turbojet exhaust plume and a rocket exhaust plume. The model was validated using experimental data. Two existing gas dynamics models (LAPP and REP3) were employed to calculate the flow field properties required as input to the radiation computer codes. A new finite difference code was developed, but was only partially successfully in predicting imbedded shock waves.

DISPOSITION INSTRUCTIONS

DISCLAIMER

TRADE NAMES

Final Report for
Contract DAAK40-77-C-0032

REFINEMENT OF PLUME MODELING IN
THE INFRARED SPECTRAL REGION

Kenneth E. Harwell
The University of Tennessee Space Institute
Tullahoma, Tennessee 37388

30 June 1978

Approved for public release; distribution unlimited

Prepared for
Advanced Sensors Directorate
U.S. Army Missile Research and Development Command
Redstone Arsenal, Alabama 35809

TABLE OF CONTENTS

ACKNOWLEDGEMENTS

ABSTRACT

A research program was conducted to develop a validated numerical model for the prediction of radiation emitted in the infrared wavelength spectral band from turbojet and rocket exhaust plumes. Two existing gas dynamics models (LAPP and REP3) were employed to calculate the flow field properties (temperature and species concentrations) required as input for the radiation computer codes. A new finite difference computer code, which was developed as part of this project, and includes the calculation of imbedded shock waves in the exhaust plume along with finite-rate chemistry and turbulent mixing, was only partially successful. A refined version of the MIRADCOM Radiation Model was developed and was used successfully to predict CO_2 and H_2O radiation emitted from several cases for which experimental data were available.

1. INTRODUCTION

During the past few years, considerable effort has been expended to design infrared seeker systems for ground-to-air and air-to-air missile guidance systems. Since the next generation of seeker systems must possess head-on capability, infrared radiation from the missile exhaust plume is an important component of the overall infrared signature of a missile system. In order to characterize completely the missile seeker-target interaction, it is necessary to develop infrared radiation predictive models which have the capability of predicting all the pertinent physical phenomena associated with the plume infrared signature.

Infrared radiation emitted from the hot gases in an exhaust plume is characterized by the types of radiating species and their number densities and the environmental conditions (temperature and pressure). All radiative predictive models require a knowledge of these parameters, so that the first step in developing a model is to develop or to obtain a gas dynamics model which yields the spatial distribution of radiating specie concentrations, temperature, and pressure.

Unfortunately, the exhaust plumes of turbojet aircraft and rockets are characterized by the existence of a complex shock wave structure and the presence of a turbulent viscous mixing layer between the inner hot jet flow and the external freestream flow. The inner flow usually consists of a high-temperature, high-velocity, chemically-reacting gas produced by the combustion of a hydrocarbon fuel while the external flow usually is low-temperature, low-velocity air that flows around the exterior of the aircraft or missile body.

Even though considerable progress had been made in developing workable gas dynamics computational models,[1-17] at the time this project was initiated, there was no available model which adequately predicted the mixed supersonic and subsonic flow regions present in the central core of the exhaust plumes. This report describes the results of a research program which was initiated to develop a finite difference computer code which would include the calculation of imbedded shock waves and Mach discs along with finite-rate chemistry and turbulent mixing phenomena.

During the course of this project, a gas dynamics computer code developed by Dr. Brian Spalding for the Rocket Propulsion Establishment in the United Kingdom was made available to the U.S. Army MIRADCOM as part of the TTCP program with Great Britain. This program was modified by the Principal Investigator to operate on the MIRADCOM computer. The results of a few limited calculations are described in this report.

The MIRADCOM Radiation Model (developed by H. Tracy Jackson, Jr. and extended by K. E. Harwell) was refined as part of the research effort described in this report. Results obtained using this model will be described and a comparison made between the theoretical predictions and experimental data.

2. THEORETICAL FOUNDATIONS

2.1 Gas Dynamics Theoretical Models

A complete review of the theory for turbulent exhaust plumes is beyond the scope of this report. A description of the flow theories is given by Jackson, Poslajko, and Harwell in Ref. 18.

The appropriate equations of motion for the gas are the conservation equations:

Conservation of Mass: $\quad \frac{\partial \rho}{\partial t} + \nabla \cdot \rho \vec{V} = 0$

Conservation of Momentum:

$$\rho \left[\frac{\partial \vec{V}}{\partial t} + (\vec{V} \cdot \nabla) \vec{V} \right] = - \nabla p + \nabla \cdot \underline{\underline{\tau}}$$

Conservation of Energy:

$$\rho \frac{DE}{Dt} = \rho \frac{D \left[e + \frac{\vec{V} \cdot \vec{V}}{2} \right]}{Dt} = - \nabla \cdot (p\vec{V}) + \nabla \cdot \underline{\underline{\tau}} \cdot \vec{V} - \nabla \cdot \vec{q}$$

After supplementing these conservation equations with an Equation of State

$$e = e\ (T,p)$$

and constitutive relations relations relating the shearing stress τ to strain of the fluid element and ultimately to the velocity gradients in the flow, a complete system of flow equations is obtained. For example, the laminar shear stress can be expressed as

$$\tau_{ij} = \lambda \nabla \cdot \vec{V} \delta_{ij} + 2\mu \left(\frac{\partial V_j}{\partial X_i} + \frac{\partial V_i}{\partial X_j} \right)$$

The theoretical approach to the development of the turbulent shear stress model is not described here, but the model employed was the eddy diffusivity model proposed by Donaldson and Gray [19] for the compressible free mixing of a primary jet with quiescent air:

$$\tau_t = -\bar{\rho}\ \overline{u'v'} = K\ \bar{\rho}\ LU_s\ \frac{\partial \bar{u}}{\partial r}$$

where K is the mixing rate factor, L is a typical local scale length, ρ is the local density, and U_s is a typical velocity difference. These parameters are defined in Refs. [12 and 19].

It had been intended to incorporate the Turbulent Kinetic Energy (TKE) turbulence model approach into the computer model. However, due to problems with the basic computer code, this was not accomplished. In this model [see Ref. 11], an additional conservation equation for the turbulent kinetic energy is added to the previous set of conservation equations. This equation for an axisymmetric flow becomes

$$\rho \bar{u}\ \frac{\partial \bar{k}}{\partial X} + \rho \bar{v}\ \frac{\partial \bar{k}}{\partial r} = \left[\frac{\rho}{P_{r_k}}\ \varepsilon_t\ \frac{\partial \bar{k}}{\partial r} \right] + \rho\varepsilon_t \left(\frac{\partial \bar{u}}{\partial r} \right)^2 - a_2\ \frac{\bar{k}^{3/2}}{\ell_k}$$

where

$$\bar{k} = \frac{1}{2}\left[\overline{(u')^2} + \overline{(v')^2} \right]$$

$$\varepsilon_t = \tau_t / \rho\ \frac{\partial \bar{u}}{\partial r}$$

$$\tau_t = a_1\ \bar{\rho}\ \bar{k}$$

and

$$P_{r_k} = \bar{\rho}\ C_p\ \frac{\varepsilon t}{\bar{k}}\ .$$

-4-

a_1 and a_2 are Universal empirical relationships and ℓ_k is a length scale for the TKE. The reader is referred to Harsha [20] for a detailed formulation of this model. Suffice it to state that the addition of the TKE equation in the matrix formulation of the computer model is straightforward and can be accomplished without major difficulty.

The chemical reaction relations employed in the gas dynamics model was identical to those employed in the Low Altitude Plume Program (LAPP) developed for the U.S. Air Force Rocket Propulsion Laboratory [5]. The reader is referred to the LAPP report [5] for a detailed description of the formalism.

2.1.1 Gas Dynamics Finite Difference Computer Model

A finite difference numerical scheme was used to approximate the gas dynamics conservation equations described in the previous section.

A method developed by Daniel Matuska of the USAF Weapons Laboratory for computing hydrodynamic properties of fluids was modified to include the viscous stress tensor.

The finite differencing technique used was the standard one in which the derivative of the function F is defined as $[F(X + H) - F(X)]/H$ where H is finite.

The degree of success in using the finite difference technique to solve the differential equations depends on the "stability," "convergence" and "compatibility" of the method. The method is stable if any bounded starting procedure yields a uniformly bounded solution of the difference equation as H goes to zero. A method is convergent if the values of $Y(N)$, the solution of the finite difference expression approximating the difference equation, tend to the values of $Y(T)$ of the exact solution. The method is compatible

if the truncation error goes to zero as H goes to zero. The difference between the true solution of the differential equation and the finite difference equation method is influenced by the step size H and may require very small values of H to be stable and convergent.

One of the major advantages of the finite difference approach is that the problem is reduced to an initial value problem with well defined boundary conditions which results in a unique time-dependent solution. The major advantage in terms of the present problem of interest, is that the mixed subsonic/transonic/supersonic flow problem can be solved without using a patching solution.

The main disadvantages of the approach are that the complete boundary must be defined as a function of time, that small steps may be required which results in a fine computational mesh which in turn requires a large computer memory if realistic resolution is desired, and that computational times may become prohibitive.

The calculation procedure used in the present program is to treat the problem in two phases. In the first phase, the "Lagrangian terms" (coordinate system fixed to the fluid element) are integrated. In the second phase, the convective terms are integrated (mass momentum and energy is transported across boundaries). The details of the calculation procedure are described in Ref. [21].

2.2 Infrared Radiation Theoretical Model

A numerical infrared radiation band model was developed to predict the infrared spectral and spatial radiation intensity distributions in exhaust plumes. The model essentially extends the models of Jackson [22,23], which were developed for CO_2 radiation from aircraft plumes, to include water vapor radiation and to include the capability of treating higher temperatures than the Jackson code.

The statistical band model and spectral parameters used in the code were developed for application to rocket plume studies [24]. The transmissivity τ_R, in the model becomes

$$\tau_R = \exp\left[-P/(1 + P^2/4Q)^{\frac{1}{2}}\right]$$

where $P = \int k\,du$

$$Q = \int \frac{k\gamma}{d}\,du$$

$k(\omega,T)$ = absorption coefficient

u = optical depth

γ = average line width, and

$d(\omega,T)$ = average line spacing

The absorption coefficients k and reciprocal line spacings, $1/d$, are tabulated as a function of frequency, ω and temperature, T in Ref. [24].

The average line width was computed using the relation

$$\gamma = [120.1\ P_{H_2O}/T] + [.09(P_{H_2O} + P_{N_2}) + .04\ P_{O_2} + .12\ P_{CO_2}]\ [273/T]^{\frac{1}{2}}$$

2.2.1 Infrared Radiation Computer Model

The infrared radiation computational model combined a water vapor emissivity formalism developed by Reardon [25] with the plume integration

scheme developed by Jackson [23] for carbon dioxide emission from aircraft plumes.

The computation of radiance from a jet exhaust plume was accomplished by dividing the plume into sufficiently small incremental blocks so that average conditions could be assigned and the blocks treated as homogeneous. The approach used in the geometric division of the plume is described in detail by Jackson [23]. The plume is subdivided into slabs parallel to the line of sight. Each slab is then cut into horizontal strips which lie along the line-of-sight vector.

The radiation from each of these strips is computed by integration using the modified Curtis-Godson approximation [24].

Integration is accomplished over the length of the strip to obtain the parameters P and Q as shown earlier,

$$P = \int k\,du$$

$$Q = \int \frac{kY}{d}\,du$$

The transmittance $\tau_R = \exp\left[-P/(1 + P^2/4Q)^{\frac{1}{2}}\right]$ is then computed.

Radiance is then calculated by integrating over the strip emissivity. For a homogeneous block, Radiance = (Blackbody) (emissivity) so that the inhomogeneous strip radiance is

$$\text{STRIP RADIANCE} = \int (\text{Blackbody})\,d\varepsilon$$

Since $d\varepsilon = -\,d\tau_R$ the computational algorithm

$$\text{STRIP RADIANCE} = -\sum_i (\text{Blackbody})_i \Delta\tau_{R_i}.$$

The algorithms used for calculating the radiation from inhomogeneous strips were tested by applying them to homogeneous strips and comparing with direct radiation calculations. The differences in calculated values were less than

one percent.

A listing of the infrared computer program is given in Appendix I.
A list of the input requirements is given in Appendix II. Appendix III includes
a listing of a sample case with output.

3. DISCUSSION OF RESULTS

This section contains a discussion of the results obtained as part of the contract effort. The procedure used to validate the infrared radiation computer code is described in Section 3.1. Section 3.2 presents the results of the infrared radiation code predictions for a turbojet flight test for which there are experimental data. The prediction of the infrared radiation emitted from a small kerosene/gaseous oxygen rocket engine exhaust plume is presented in Section 3.3. A discussion of the progress in developing the Gas Dynamics Finite Difference Computer Model is described in Section 3.4. Some preliminary results obtained using the REP3 Computer Code are described in Section 3.5.

3.1 Validation of the UTSI Infrared Radiation Code

In order to validate the Infrared Radiation Code, the spectral radiance of water vapor and carbon dioxide mixtures experimental data are available [Refs. 24, 27-29]. Sukanek and Davis [26] performed a similar assessment of the NASA band model formulation developed by Reardon [25]. It was decided that several selected cases used by Sukanek and Davis would be used for the evaluation since this would provide a comparison of the present model calculations with the experimental data and with the predictions of the NASA/Reardon Radiation Code. The cases selected for the comparison are given in Table 3.1.

The spectral radiance of 60-cm thick slabs of hot H_2O vapor and CO_2 were computed for the 2.7-μ and 4.3-μ wavelength bands. Figures 3.1-3.8 present the results of the computations.

The comparison between the measured and predicted values of the spectral radiance in the 2.7-μ band for an isothermal slab of water vapor is presented

TABLE 3.1 CASES CONSIDERED FOR COMPARISON

Subject	Fig. No.	Particle Pressure (mmHg)					Temperature Profile	Length (m)
		H_2O	CO_2	N_2	CO	H_2		
Isothermal Hot H_2O	1	38.0		38.7			1215	0.6
Isothermal Hot CO_2	2		38.0	38.0			1202	0.6
Isothermal Hot CO_2	3		7.58	68.43			1200	0.6
Isothermal Mixture	4	35.26	7.58	27.09	1.44	4.64	1200	0.6
Isothermal Mixture	5	35.26	7.58	27.06	1.47	4.62	1200	0.6
Nonisothermal H_2O	6	670					382/537/723/953/1128/1160/990/751/558/389	0.6
Nonisothermal CO_2	7		760				386/528/719/953/1130/1160/975/737/541/387	0.6
Nonisothermal Mixture	8	57	28	675			378/537/723/958/1127/1158/990/752/555/383	0.6

NOTE: The temperature of the gas was either homogenous, in which case one temperature is reported, or was inhomogeneous, in which case the temperatures are given at the center of each 6 cm wide cell.

in Fig. 3.1. At the center of the spectral band the computed values are slightly lower than the measured ones. The NASA code predicts slightly higher values than the UTSI code, but in general the agreement is fairly good between the calculated and measured values. The calculated values are within 20% of the measured ones.

The measured and predicted values of spectral radiance in the 2.7-μ and 4.3-μ wavelength bands for an isothermal slab of CO_2 are presented in Figs. 3.2 and 3.3. In contract to the H_2O predictions, the predictions of the spectral randiance for CO_2 do not agree very well with the measurements. Errors of 30 to 50 percent are observed. Similar disagreement was found by Lindquist and others [27-29] who attributed to the probable cause of the disagreement to the lack of knowledge of the CO_2 broadening parameters at low pressures. Ludwig and others [24] show better agreement between the predictions and measurements at higher pressures (P_{CO_2} = 1-2 atmospheres).

Figures 3.4 and 3.5 present the results for the spectral radiance of an isothermal mixture of CO_2 and H_2O in the 4.3 and 2.7-μ bands, respectively. The calculated values are higher than the measurements in the center of the spectral bands. Both codes yield results which are in fair agreement with the measured values.

Figure 3.6 presents the results for a nonisothermal slab of water vapor. There is fairly good agreement between the predicted and measured values, but the present code appears to predict values which are below the measured and calculated values using the NASA code.

Figure 3.7 presents the comparison between the predicted and measured values of spectral radiance in the 2.7-μ spectral band of a nonisothermal slab of CO_2. The agreement between the predicted and measured values is quite good.
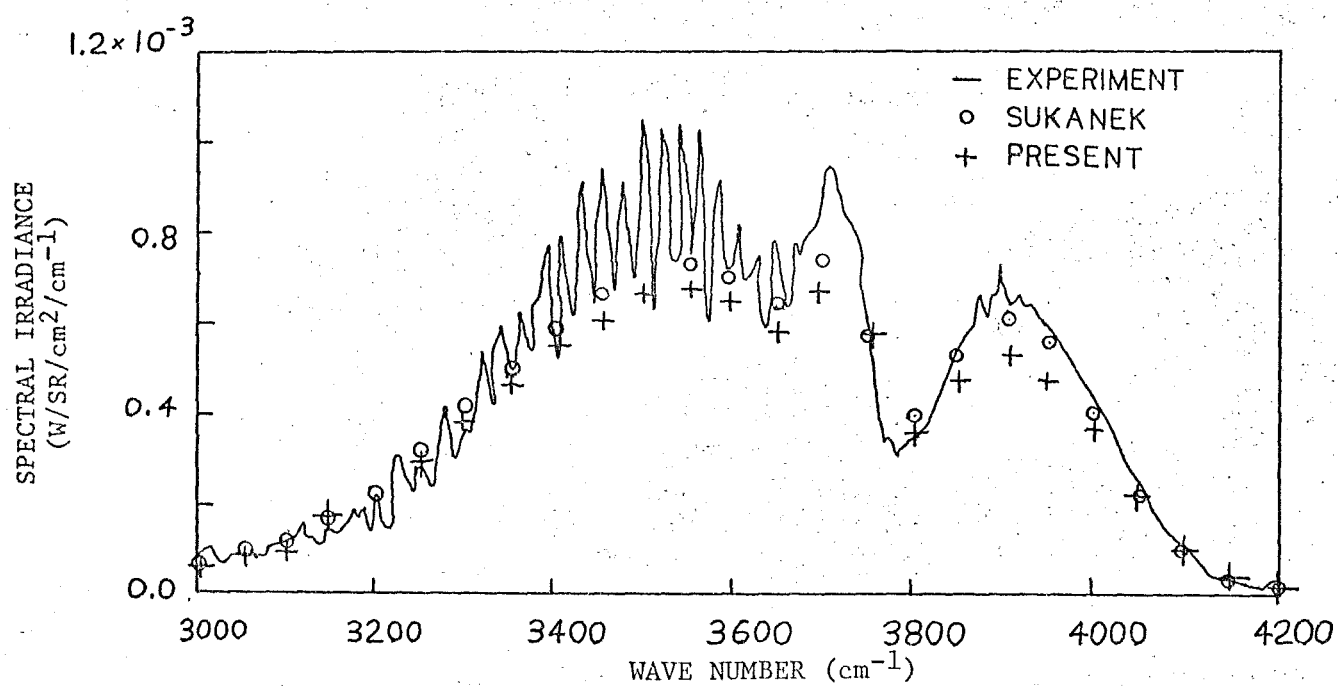
Fig. 3.1   SPECTRAL RADIANCE IN THE 2.7-μm BAND FOR AN ISOTHERMAL
SLAB OF H_2O VAPOR.
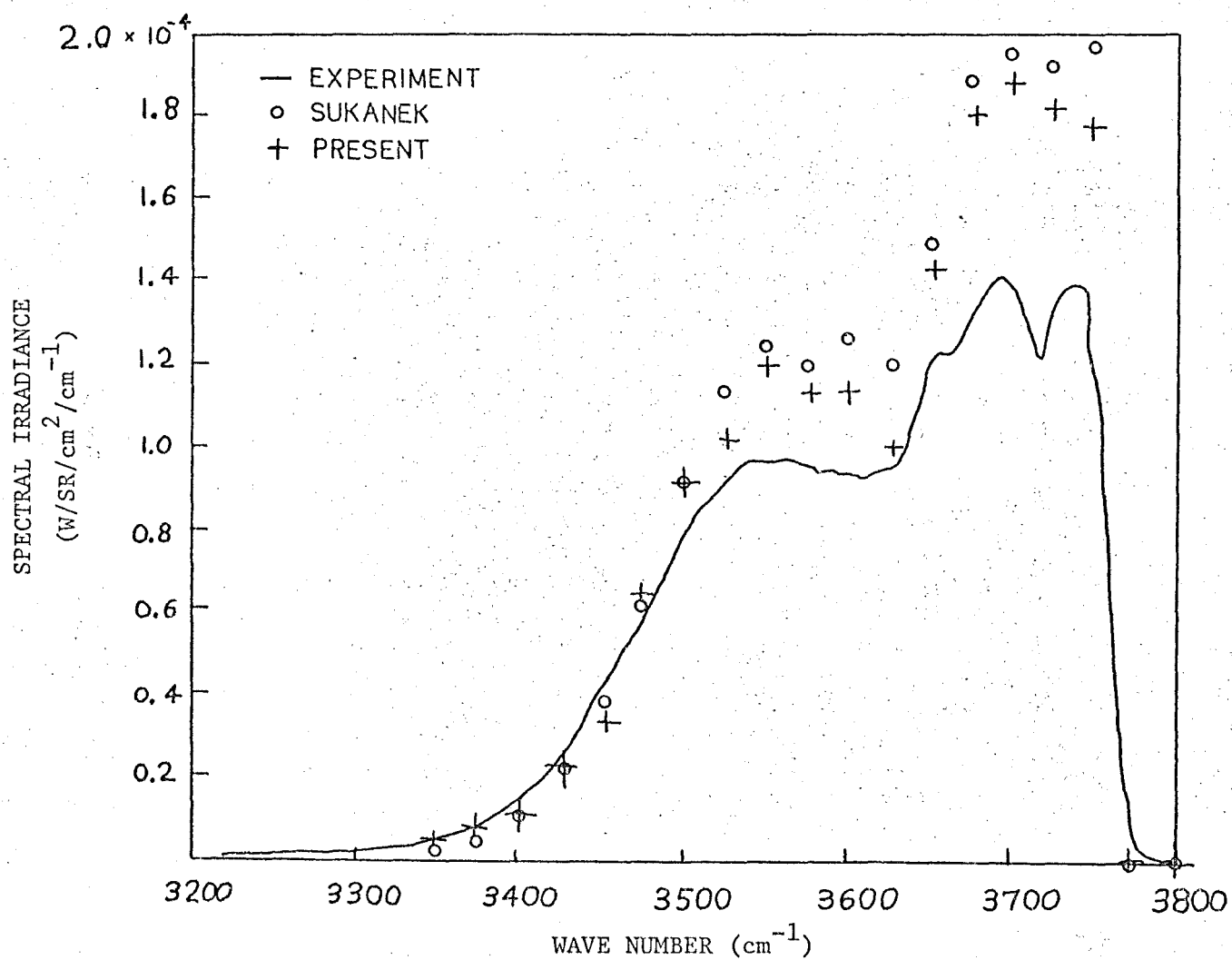
Fig. 3.2 SPECTRAL RADIANCE IN THE 2.7-μm BAND FOR AN ISOTHERMAL SLAB OF CO_2.
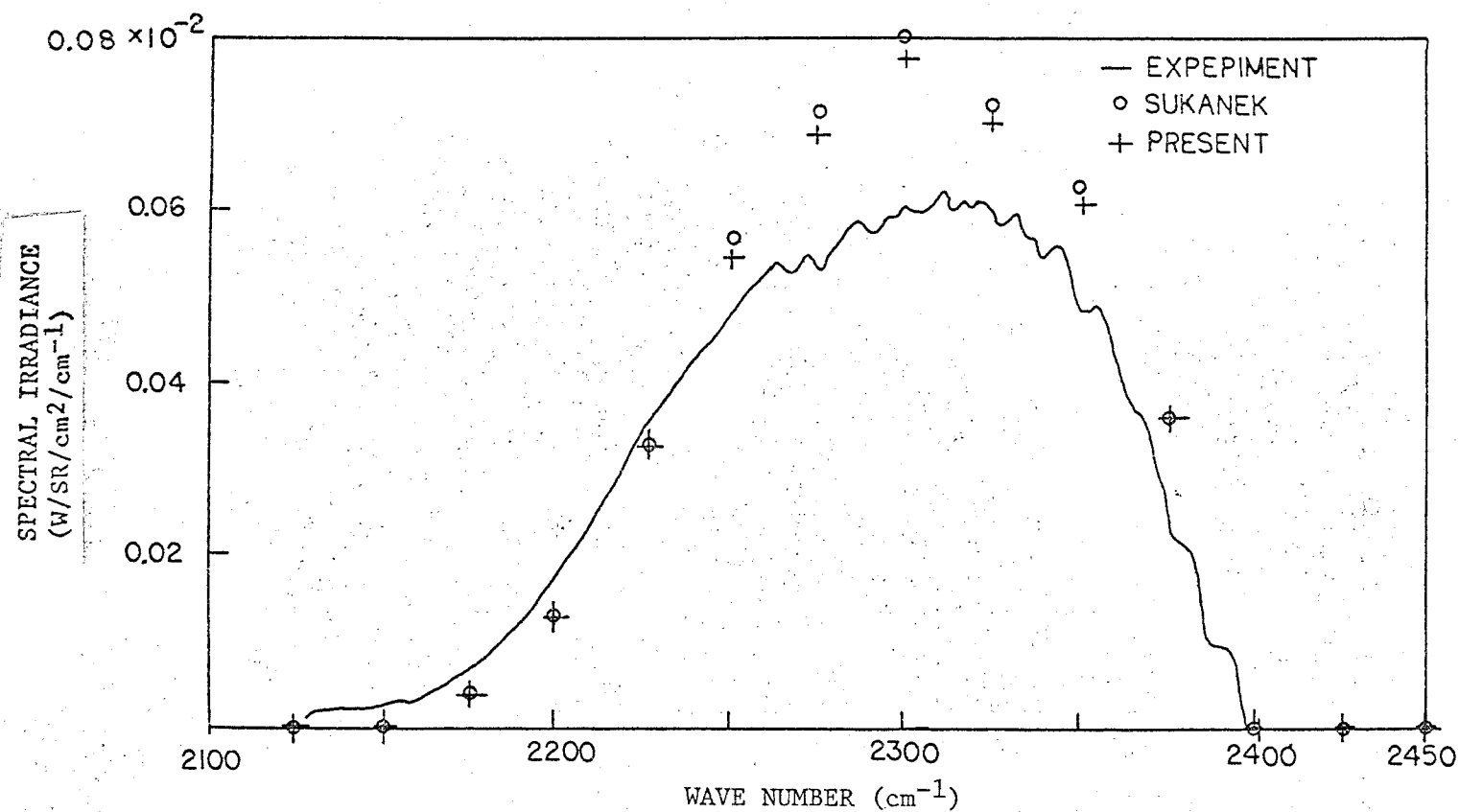
Fig. 3.3 SPECTRAL RADIANCE IN THE 4.3-μm BAND FOR AN ISOTHERMAL SLAB OF CO_2.
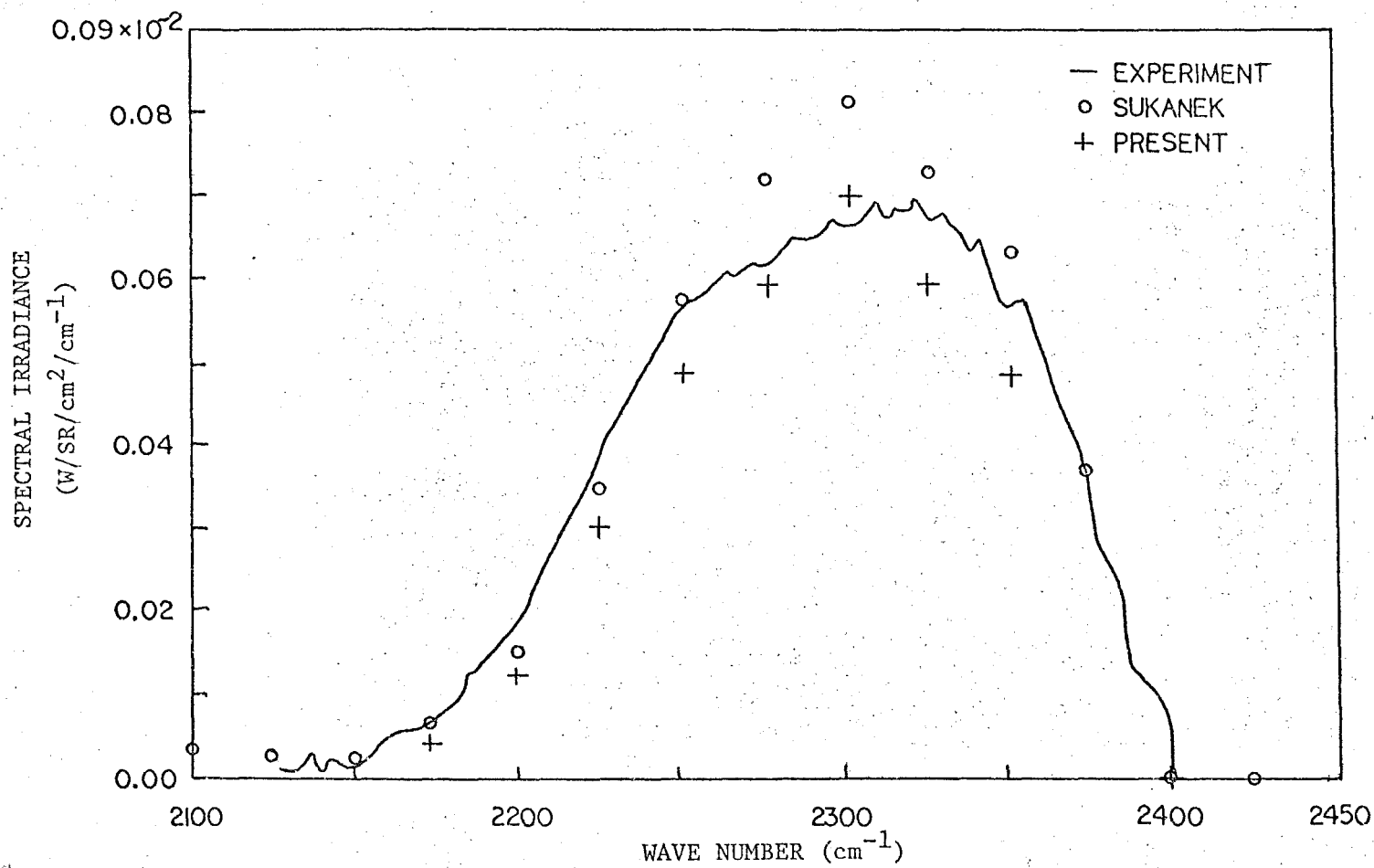
Fig. 3.4 SPECTRAL RADIANCE IN THE 4.3-μm BAND FOR AN ISOTHERMAL MIXTURE OF CO_2 and H_2O.
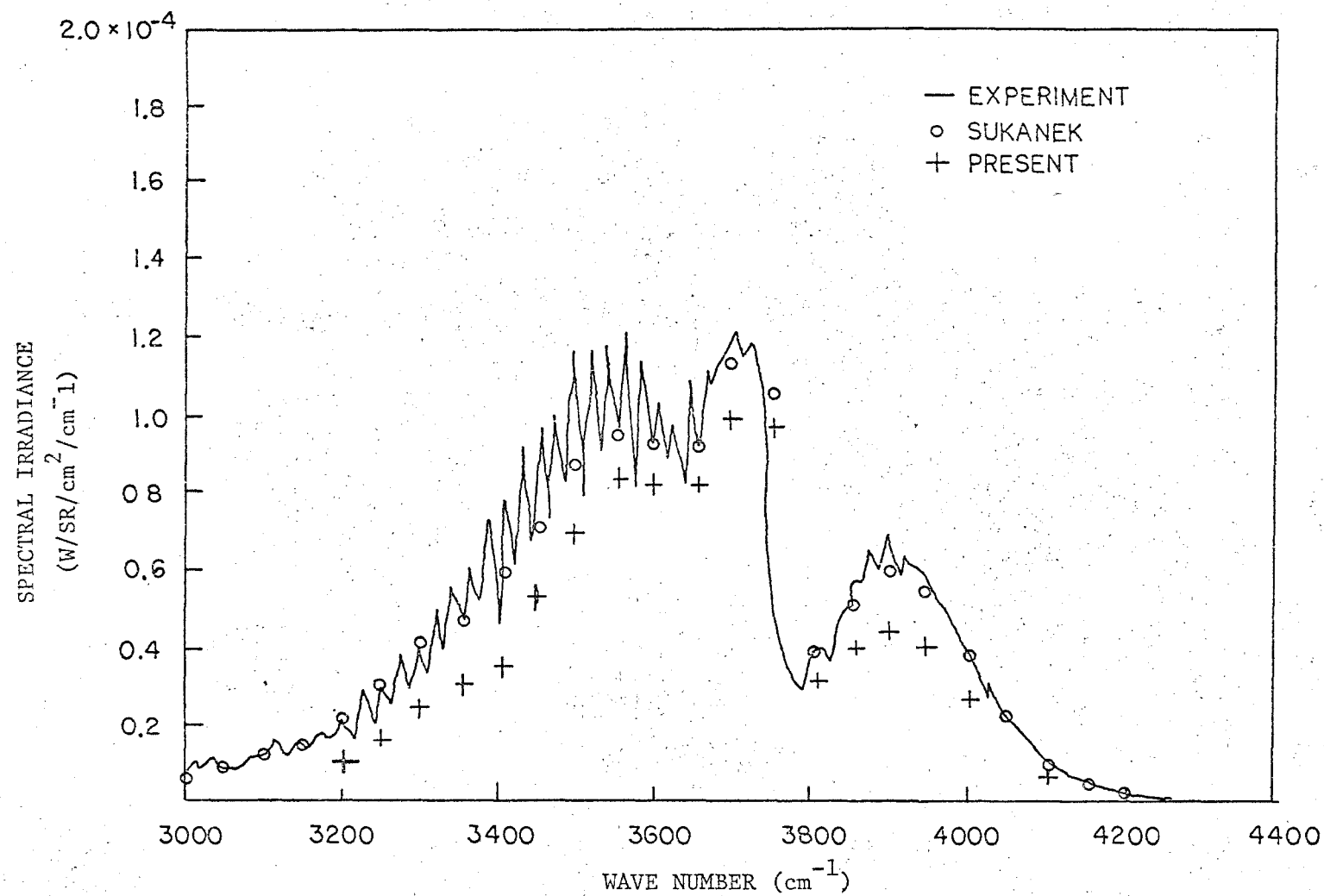
Fig. 3.5 SPECTRAL RADIANCE IN THE 2.7-µm BAND FOR AN ISOTHERMAL MIXTURE OF CO_2 and H_2O.
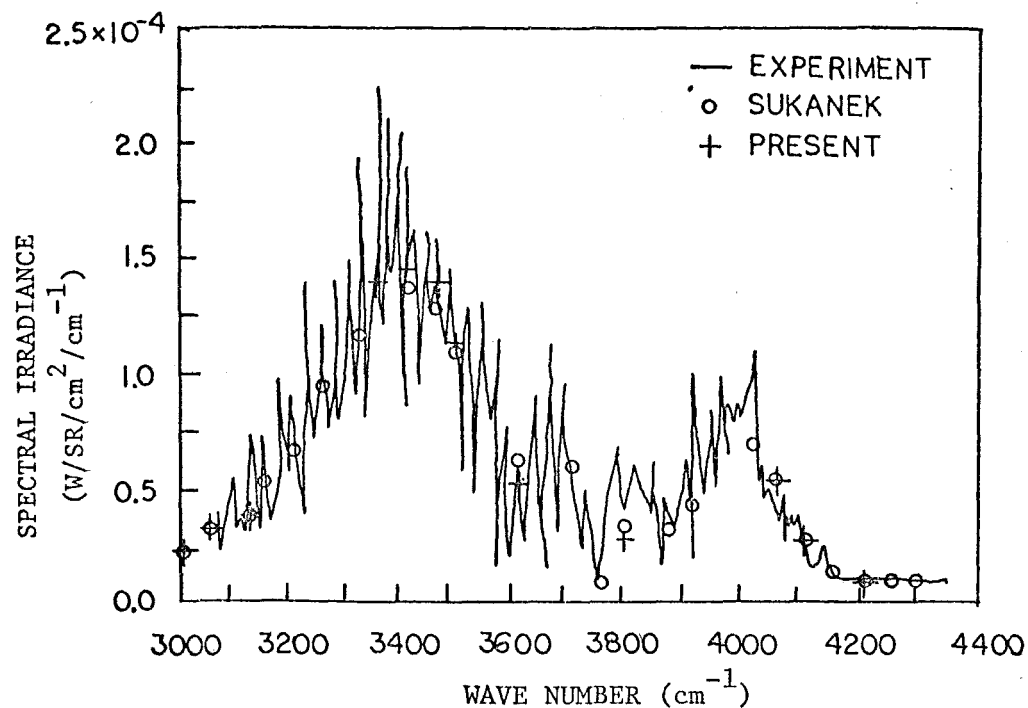
Fig. 3.6 SPECTRAL RADIANCE IN THE 2.7-μm BAND FOR A NONISOTHERMAL SLAB OF H_2O VAPOR.
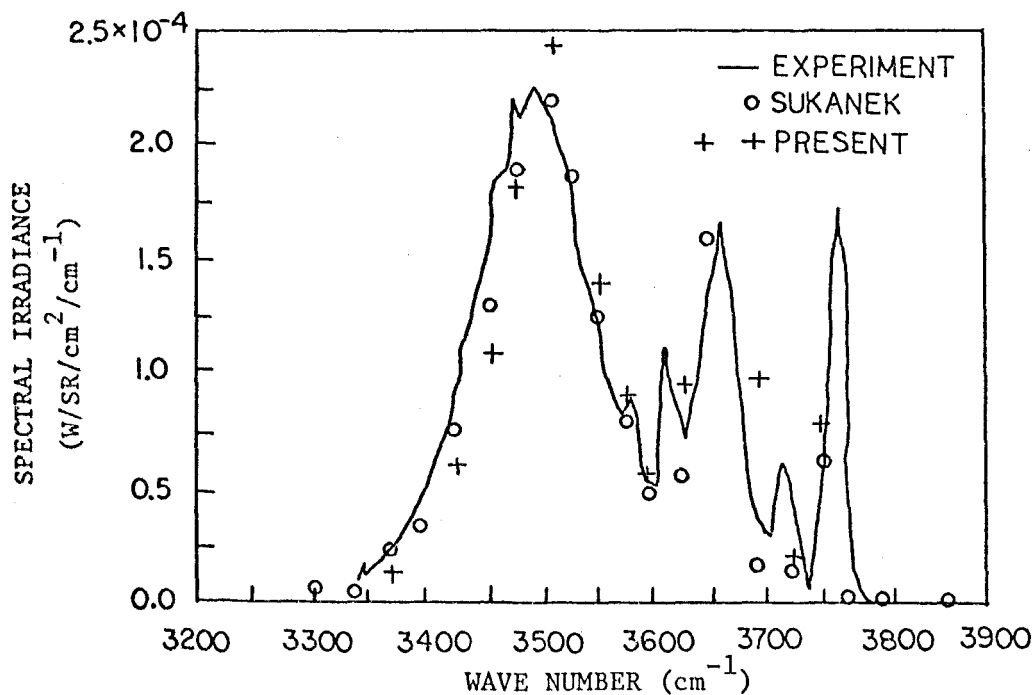
Fig. 3.7 SPECTRAL RADIANCE IN THE 2.7-μm BAND FOR A NONISOTHERMAL SLAB OF CO_2.

Figure 3.8 presents the results for a nonisothermal mixture of CO_2 and H_2O. There is fairly good agreement over the entire 2.7-μ wavelength band.

In summary, the UTSI radiation code appears to yield results which agree fairly well with the NASA code even though there are some differences. With the exception of the low pressure CO_2 cases, the predicted values are within $\pm$ 20% of the measured values.
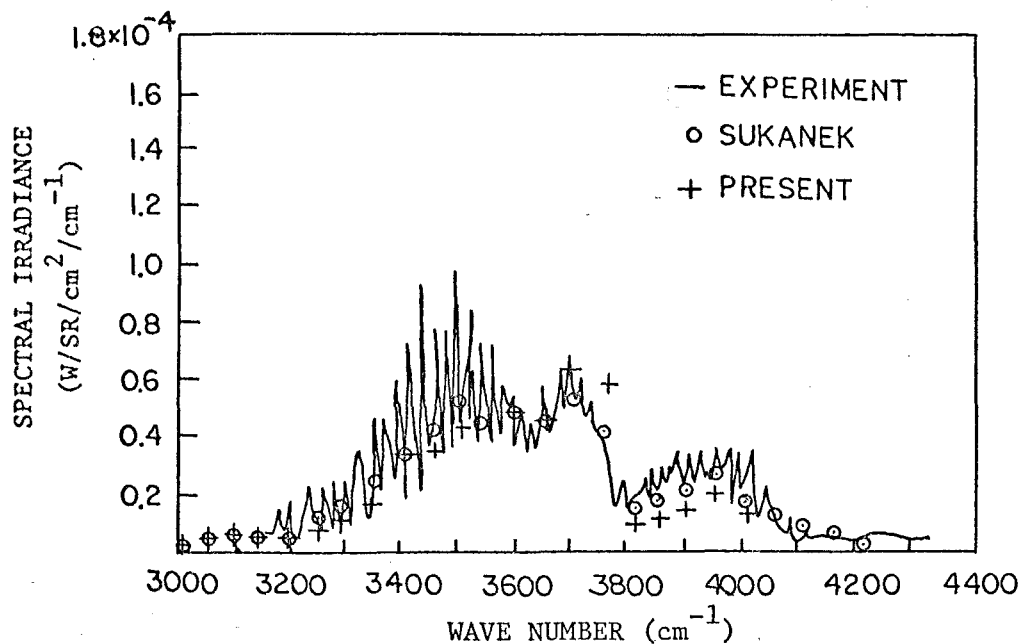
Fig. 3.8 SPECTRAL RADIANCE IN THE 2.7-μm BAND FOR A NONISOTHERMAL MIXTURE OF CO_2 AND H_2O.

3.2 Infrared Radiation Predictions for Turbojet Flight Test

The UTSI Infrared Radiation Code was utilized to calculate the infrared radiation emitted in the wavelength interval from 4 to 5 microns from a turbojet aircraft exhaust for which experimental data are available. H. Tracy Jackson, Jr. at MIRADCOM provided the data given in Table 3.2.

The Low Altitude Plume Program (LAPP) was exercised for the input data given in Table 3.2. The first portion of the LAPP code output for this case, labeled "FLT1-PASS 7," is included as Figs. 3.9-3.11. The output data from the LAPP code was then used as input data for the Infrared Radiation Code. Refer to Fig. 3.12 for a typical set of input data.

The results of the computations are presented in Figs. 3.13-3.15. The CO_2 contribution to the radiation per length of plume (Watts/SR/cm) is given in Fig. 3.13 while the H_2O contribution is given in Fig. 3.14. The H_2O radiation is very small compared to the CO_2 radiation.

The spatial distribution of the radiation is given in Fig. 3.15. Also, shown on the figure is the centerline temperature distribution. The total radiation emitted from the plume in the 4.0 to 5.0 micron wavelength interval was 165.7 Watts/SR. This radiation is at the plume and is uncorrected for detector response characteristics or for atmospheric attenuation between the plume and the detector.

It had been anticipated that the Jackson MIRADCOM Radiation Code would be used to calculate the radiation for the same test flight so that a comparison could be made between the two codes. Unfortunately, the results from the MIRADCOM Code did not become available prior to the completion of the project.

-20-

TABLE 3.2

TURBOJET FLIGHT TEST DATA

Flight 10, Pass 7

TPT = 790° K

Vel = 512 Kts. = 263 m/sec.

Asp. α = 19°

O/F = 62

Range - 2212 meters

$T\infty$ = 526°R

$p\infty$ = 1955 lb/ft^2

C^* = 1124 ft/sec.

Air Flow 182 lb/sec., 99% RPM

V jet = 1801.6 ft/sec.

F UT1- PASS 7

PRESSURE(CONSTANT) = 1.0000000E 00 ATMOSPHERES

NOZZLE RADIUS= 8.9999998E-01 FEET

LEWIS NUMBER(CONSTANT)= 1.0000000E 00   PRANDTL NUMBER(CONSTANT)= 6.9999999E-01

X INITIAL(FEET)= 0.0   X FINAL(FEET)= 3.0000000E 01

PRINT INCREMENT= 1.0000000E 00   MINIMUM STEP SIZE= 9.9999994E-11

DONALDSON/GRAY VISCOSITY MODEL

		JET	EDGE
TEMPERATURE(DEG. KELVIN)		7.9000000E 02	2.9200000E 02
VELOCITY (FEET/SECOND)		1.8000000E 03	1.0000000E 02
MOLE FRACTION	H	2.8829817E-07	2.8849433E-07
MOLE FRACTION	H2	2.8829817E-07	2.8849433E-07
MOLE FRACTION	H2O	3.3150621E-02	2.8849433E-07
MOLE FRACTION	CO	2.8829817E-07	2.8849433E-07
MOLE FRACTION	CO2	3.2630604E-02	3.2879249E-04
MOLE FRACTION	O	2.8829817E-07	2.8649433E-07
MOLE FRACTION	OH	2.8829817E-07	2.8849433E-07
MOLE FRACTION	O2	1.5670282E-01	2.0846844E-01
MOLE FRACTION	N2	7.7751452E-01	7.9120100E-01

	REACTIONS BEING CONSIDERED				KK=A*EXP(B/RT)/T**N	A	N	B	(MOLECULE-ML-SEC UN
1	O	+	O	+ M	=	O2	+ M		1.000E-29	1.0	0.0
2	H	+	H	+ M	=	H2	+ M		1.000E-29	1.0	0.0
3	O	+	H	+ M	=	OH	+ M		1.000E-29	1.0	0.0
4	H	+	OH	+ M	=	H2O	+ M		1.000E-28	1.0	0.0
5	CO	+	O	+ M	=	CO2	+ M		5.000E-29	1.0	-4000.0
6	OH	+	OH		=	H2O	+ O		1.000E-11	0.0	-1000.0
7	OH	+	H2		=	H2O	+ H		4.000E-11	0.0	-5500.0
8	O	+	H2		=	OH	+ H		3.000E-11	0.0	-8200.0
9	H	+	O2		=	OH	+ O		3.000E-10	0.0	-16500.0
10	CO	+	OH		=	CO2	+ H		5.000E-13	0.0	-600.0

Fig. 3.9   Initial Conditions for LAPP Computer Program

X/R	DELTA X FEET	PRESS(ATM)
0.0	8.999991E-02	1.000000E 00

HALF RADIUS/R	INNER MIXING ZONE RADIUS/R	MACH NUMBER AT HALF RADIUS	MIXING RATE COEFFICIENT
1.137226E 00	1.013722E 00	6.269119E-01	4.209092E-02

Y/R	VELOCITY FEET/SEC	TEMPERATURE K	DENSITY GM/CC	MACH NO.	ENTHALPY CAL/GM	VISCOSITY LB/FT/SEC	ELECTRON DENSITY(1/ML)	PSI
0.0	1.800000E 03	7.900000E 02	4.448628E-04	9.920356E-01	-4.688548E 01	1.104238E-01	0.0	
0.1000	1.800000E 03	7.900000E 02	4.448628E-04	9.920356E-01	-4.688548E 01	1.104238E-01	1.121742E-01	
0.2000	1.800000E 03	7.900000E 02	4.448628E-04	9.920356E-01	-4.688548E 01	1.104238E-01	2.243484E-01	
0.3000	1.800000E 03	7.900000E 02	4.448628E-04	9.920356E-01	-4.688548E 01	1.104238E-01	3.365226E-01	
0.4000	1.800000E 03	7.900000E 02	4.448628E-04	9.920356E-01	-4.688548E 01	1.104238E-01	4.486969E-01	
0.5000	1.800000E 03	7.900000E 02	4.448628E-04	9.920356E-01	-4.688548E 01	1.104238E-01	5.608711E-01	
0.6000	1.800000E 03	7.900000E 02	4.448628E-04	9.920356E-01	-4.688548E 01	1.104238E-01	6.730453E-01	
0.7000	1.800000E 03	7.900000E 02	4.448628E-04	9.920356E-01	-4.688548E 01	1.104238E-01	7.852195E-01	
0.8000	1.800000E 03	7.900000E 02	4.448628E-04	9.920356E-01	-4.688548E 01	1.104238E-01	8.973937E-01	
0.9000	1.800000E 03	7.900000E 02	4.448628E-04	9.920356E-01	-4.688548E 01	1.104238E-01	1.009567E 00	
1.0000	1.800000E 03	7.900000E 02	4.448628E-04	9.920356E-01	-4.688548E 01	1.104238E-01	1.121741E 00	
1.2745	1.000000E 02	2.920000E 02	1.204386E-03	8.888811E-02	-2.495791E 00	2.989527E-01	1.233916E 00	
1.6838	1.000000E 02	2.920000E 02	1.204386E-03	8.888811E-02	-2.495791E 00	2.989527E-01	1.345090E 00	

Fig. 3.10 Sample Output of LAPP Computer Program

PSET   FLTI-PASS I   PAGE 1

MODE FRACTIONS

	H_2	H_2O	CO	CO2	O	OH	PT
2.xx298E-07	2.8829xE-07	3.31506E-02	2.88298E-07	3.26306E-02	2.88298E-07	2.88298E-07	1
2.xx298E-07	2.8829xE-07	3.31506E-02	2.88298E-07	3.26306E-02	2.88298E-07	2.88298E-07	2
2.xx298E-07	2.8829xE-07	3.31506E-02	2.88298E-07	3.26306E-02	2.88298E-07	2.88298E-07	3
2.xx298E-07	2.8829xE-07	3.31506E-02	2.88298E-07	3.26306E-02	2.88298E-07	2.88298E-07	4
2.xx298E-07	2.8829xE-07	3.31506E-02	2.88298E-07	3.26306E-02	2.88298E-07	2.88298E-07	5
2.xx298E-07	2.8829xE-07	3.31506E-02	2.88298E-07	3.26306E-02	2.88298E-07	2.88298E-07	6
2.xx298E-07	2.8829xE-07	3.31506E-02	2.88298E-07	3.26306E-02	2.88298E-07	2.88298E-07	7
2.xx298E-07	2.8829xE-07	3.31506E-02	2.88298E-07	3.26306E-02	2.88298E-07	2.88298E-07	8
2.xx298E-07	2.8829xE-07	3.31506E-02	2.88298E-07	3.26306E-02	2.88298E-07	2.88298E-07	9
2.xx298E-07	2.8829xE-07	3.31506E-02	2.88298E-07	3.26306E-02	2.88298E-07	2.88298E-07	10
2.xx298E-07	2.8829xE-07	3.31506E-02	2.88298E-07	3.26306E-02	2.88298E-07	2.88298E-07	11
2.xx494E-07	2.88494E-07	2.88494E-07	2.88494E-07	3.28792E-04	2.88494E-07	2.88494E-07	12
2.xx494E-07	2.88494E-07	2.88494E-07	2.88494E-07	3.28792E-04	2.88494E-07	2.88494E-07	13

NET RATE OF PRODUCTION (W=DOT/RHO*U)

A	H_2	H_2O	CO	CO2	O	OH	PT
-6.xx31xE-08	5.31415E-10	-1.89146E-09	2.77323E-11	-2.77323E-11	6.40717E-08	6.87579E-08	1
-6.xx37xE-08	5.31415E-10	-1.89145E-09	2.77323E-11	-2.77323E-11	6.40717E-08	6.87579E-08	2
-6.xx37xE-08	5.31415E-10	-1.89145E-09	2.77323E-11	-2.77323E-11	6.40717E-08	6.87579E-08	3
-6.xx316E-08	5.31415E-10	-1.89146E-09	2.77323E-11	-2.77323E-11	6.40717E-08	6.87579E-08	4
-6.xx37xE-08	5.31415E-10	-1.89146E-09	2.77323E-11	-2.77323E-11	6.40717E-08	6.87579E-08	5
-6.xx37xE-08	5.31415E-10	-1.89146E-09	2.77323E-11	-2.77323E-11	6.40717E-08	6.87579E-08	6
-6.xx315E-08	5.31415E-10	-1.89146E-09	2.77323E-11	-2.77323E-11	6.40717E-08	6.87579E-08	7
-6.xx316E-08	5.31415E-10	-1.89146E-09	2.77323E-11	-2.77323E-11	6.40717E-08	6.87579E-08	8
-6.xx316E-08	5.31415E-10	-1.89146E-09	2.77323E-11	-2.77323E-11	6.40717E-08	6.87579E-08	9
-6.xx37xE-08	5.31415E-10	-1.89145E-09	2.77323E-11	-2.77323E-11	6.40717E-08	6.87579E-08	10
-6.xx316E-08	5.31415E-10	-1.89146E-09	2.77323E-11	-2.77323E-11	6.40717E-08	5.87579E-08	11

Fig. 3.11   Sample Output of LAPP Computer Program

-24-

MOLE FRACTIONS

F/R	O2	N2	B	SRMO	MED	2	PI
0.0	1.5670E-01	7.7751E-01	0.0	0.0	0.0	0.0	1
0.10000	1.5670E-01	7.7751E-01	0.0	0.0	0.0	0.0	2
0.20000	1.5670E-01	7.7751E-01	0.0	0.0	0.0	0.0	3
0.30000	1.5670E-01	7.7751E-01	0.0	0.0	0.0	0.0	4
0.40000	1.5670E-01	7.7761E-01	0.0	0.0	0.0	0.0	5
0.50000	1.5670E-01	7.7751E-01	0.0	0.0	0.0	0.0	6
0.60000	1.5670E-01	7.7751E-01	0.0	0.0	0.0	0.0	7
0.70000	1.5670E-01	7.7751E-01	0.0	0.0	0.0	0.0	8
0.80000	1.5670E-01	7.7751E-01	0.0	0.0	0.0	0.0	9
0.90000	1.5670E-01	7.7751E-01	0.0	0.0	0.0	0.0	10
1.00000	1.5670E-01	7.7751E-01	0.0	0.0	0.0	0.0	11
1.27445	2.0429E-01	7.9120E-01	0.0	0.0	0.0	0.0	12
1.6?3	2.0429E-01	7.9120E-01	0.0	0.0	0.0	0.0	13

NET RATE OF PRODUCTION (W-DOT/RHO*U)

	O2	N2	B	SRMO	MED	2	PI
	-6.5150E-08	0.0	0.0	0.0	0.0	0.0	1
	-6.5145E-08	0.0	0.0	0.0	0.0	0.0	2
	-6.5153E-08	0.0	0.0	0.0	0.0	0.0	3
	-6.5455E-08	0.0	0.0	0.0	0.0	0.0	4
	-6.5455E-08	0.0	0.0	0.0	0.0	0.0	5
	-6.5455E-08	0.0	0.0	0.0	0.0	0.0	6
	-6.5453E-08	0.0	0.0	0.0	0.0	0.0	7
	-6.5455E-08	0.0	0.0	0.0	0.0	0.0	8
	-6.5453E-08	0.0	0.0	0.0	0.0	0.0	9
	-6.5451E-08	0.0	0.0	0.0	0.0	0.0	10
	-6.5451E-08	0.0	0.0	0.0	0.0	0.0	11

LESS THAN INLET

Fig. 3.11 (cont.)

.1000E 01 0.2720E 02 120

0.0 = X POSITION (cm)

R(cm)	T(°K)	PN2	PCO	PCO2	PH2O	PO2
0.0	0.7900E 03	0.1000E-19	0.1000E-19	0.3263E-01	0.3315E-01	0.1000E-19
0.2720E 01	0.7900E 03	0.1000E-19	0.1000E-19	0.3263E-01	0.3315E-01	0.1000E-19
0.5440E 01	0.7900E 03	0.1000E-19	0.1000E-19	0.3263E-01	0.3315E-01	0.1000E-19
0.8160E 01	0.7900E 03	0.1000E-19	0.1000E-19	0.3263E-01	0.3315E-01	0.1000E-19
0.1088E 02	0.7900E 03	0.1000E-19	0.1000E-19	0.3263E-01	0.3315E-01	0.1000E-19
0.1360E 02	0.7900E 03	0.1000E-19	0.1000E-19	0.3263E-01	0.3315E-01	0.1000E-19
0.1632E 02	0.7900E 03	0.1000E-19	0.1000E-19	0.3263E-01	0.3315E-01	0.1000E-19
0.1904E 02	0.7900E 03	0.1000E-19	0.1000E-19	0.3263E-01	0.3315E-01	0.1000E-19
0.2176E 02	0.7900E 03	0.1000E-19	0.1000E-19	0.3263E-01	0.3315E-01	0.1000E-19
0.2448E 02	0.7900E 03	0.1000E-19	0.1000E-19	0.3263E-01	0.3315E-01	0.1000E-19
0.2720E 02	0.7900E 03	0.1000E-19	0.1000E-19	0.3263E-01	0.3315E-01	0.1000E-19
0.3400E 02	0.2920E 03	0.1000E-19	0.1000E-19	0.3288E-03	0.2885E-06	0.1000E-19

0.3820E 02 = X (cm)

	T(°K)	PN2	PCO	PCO2	PH2O	PO2
0.0	0.7900E 03	0.1000E-19	0.1000E-19	0.3263E-01	0.3315E-01	0.1000E-19
0.2720E 01	0.7900E 03	0.1000E-19	0.1000E-19	0.3263E-01	0.3315E-01	0.1000E-19
0.5440E 01	0.7900E 03	0.1000E-19	0.1000E-19	0.3263E-01	0.3315E-01	0.1000E-19
0.8160E 01	0.7900E 03	0.1000E-19	0.1000E-19	0.3263E-01	0.3315E-01	0.1000E-19
0.1088E 02	0.7900E 03	0.1000E-19	0.1000E-19	0.3263E-01	0.3315E-01	0.1000E-19
0.1360E 02	0.7900E 03	0.1000E-19	0.1000E-19	0.3263E-01	0.3315E-01	0.1000E-19
0.1632E 02	0.7900E 03	0.1000E-19	0.1000E-19	0.3263E-01	0.3315E-01	0.1000E-19
0.1904E 02	0.7899E 03	0.1000E-19	0.1000E-19	0.3263E-01	0.3315E-01	0.1000E-19
0.2176E 02	0.7876E 03	0.1000E-19	0.1000E-19	0.3245E-01	0.3296E-01	0.1000E-19
0.2448E 02	0.7640E 03	0.1000E-19	0.1000E-19	0.3061E-01	0.3108E-01	0.1000E-19
0.2728E 02	0.6561E 03	0.1000E-19	0.1000E-19	0.2319E-01	0.2346E-01	0.1000E-19
0.3123E 02	0.4492E 03	0.1000E-19	0.1000E-19	0.9216E-02	0.9121E-02	0.1000E-19
0.3968E 02	0.3143E 03	0.1000E-19	0.1000E-19	0.1604E-02	0.1309E-02	0.1000E-19
0.5252E 02	0.2935E 03	0.1000E-19	0.1000E-19	0.4128E-03	0.6655E-04	0.1000E-19
0.6351E 02	0.2920E 03	0.1000E-19	0.1000E-19	0.3288E-03	0.2885E-06	0.1000E-19

0.720E 02

	T(°K)	PN2	PCO	PCO2	PH2O	PO2
0.0	0.7900E 03	0.1000E-19	0.1000E-19	0.3263E-01	0.3315E-01	0.1000E-19
0.2720E 01	0.7900E 03	0.1000E-19	0.1000E-19	0.3263E-01	0.3315E-01	0.1000E-19
0.5440E 01	0.7900E 03	0.1000E-19	0.1000E-19	0.3263E-01	0.3315E-01	0.1000E-19
0.8160E 01	0.7900E 03	0.1000E-19	0.1000E-19	0.3263E-01	0.3315E-01	0.1000E-19
0.1088E 02	0.7900E 03	0.1000E-19	0.1000E-19	0.3263E-01	0.3315E-01	0.1000E-19
0.1360E 02	0.7899E 03	0.1000E-19	0.1000E-19	0.3263E-01	0.3314E-01	0.1000E-19
0.1632E 02	0.7892E 03	0.1000E-19	0.1000E-19	0.3257E-01	0.3309E-01	0.1000E-19
0.1903E 02	0.7848E 03	0.1000E-19	0.1000E-19	0.3222E-01	0.3273E-01	0.1000E-19
0.2175E 02	0.7607E 03	0.1000E-19	0.1000E-19	0.3078E-01	0.3125E-01	0.1000E-19
0.2449E 02	0.7178E 03	0.1000E-19	0.1000E-19	0.2694E-01	0.2731E-01	0.1000E-19
0.2744E 02	0.6269E 03	0.1000E-19	0.1000E-19	0.2022E-01	0.2041E-01	0.1000E-19

Fig. 3.12 Typical Set of Input Data for Radiation Code

X(cm)	W/SR/CM	STATION RADIATION (W/SR)
0.0	0.8030024E 00	0.1062637E 01
38.19	0.6650596E 00	0.2803171E 02
71.97	0.5855711E 00	0.2112463E 02
102.27	0.5204300E 00	0.1675532E 02
135.10	0.4548181E 00	0.1600888E 02
165.70	0.3968118E 00	0.1302993E 02
195.02	0.3400359E 00	0.1190510E 02
228.89	0.2897733E 00	0.9721726E 01
259.24	0.2418252E 00	0.8068358E 01
298.38	0.1936032E 00	0.8521406E 01
329.39	0.1511664E 00	0.5345317E 01
359.86	0.1196913E 00	0.4125719E 01
395.49	0.9243929E-01	0.3779300E 01
429.76	0.7282054E-01	0.2831890E 01
462.94	0.5788064E-01	0.2166581E 01
494.77	0.4560884E-01	0.1562521E 01
525.78	0.3838268E-01	0.1317710E 01
560.59	0.3459402E-01	0.1270374E 01
594.32	0.2598157E-01	0.1021555E 01
626.96	0.2198615E-01	0.7828305E 00
658.51	0.1888854E-01	0.6446391E 00
689.25	0.1645325E-01	0.5431341E 00
723.25	0.1424051E-01	0.5217939E 00
755.43	0.1251272E-01	0.4438905E 00
785.80	0.1109931E-01	0.3821360E 00
820.08	0.9954126E-02	0.3292734E 00
850.82	0.1471464E-01	0.3791106E 00
884.27	0.8120896E-02	0.3819935E 00
909.64	0.0	0.1036170E 00

* RADIATION VALUE WAS CALCULATED BASED ON THE SLOPE BETWEEN THE PREVIOUS TWO POINTS

TOTAL RADIATION EMITTED=0.1612E 03 WATTS/STER

CENTROID= 0.1921E 03CM

Fig. 3.13 CO_2 Contribution to Infrared Radiation per Length of Plume

FL1.PASS7

		STATION RADIATION (W/SR)
0.0	0.2072786E-01	0.1062637E 01
38.19	0.1714092E-01	0.7230808E 00
71.97	0.1537959E-01	0.5493103E 00
102.27	0.1386401E-01	0.4430514E 00
135.10	0.1225346E-01	0.4287230E 00
165.70	0.1080529E-01	0.3527966E 00
198.02	0.9366962E-02	0.3259194E 00
228.89	0.8083675E-02	0.2693681E 00
259.24	0.6870915E-02	0.2269739E 00
298.38	0.5615367E-02	0.2443608E 00
329.39	0.4495639E-02	0.1567802E 00
359.86	0.3643198E-02	0.1240656E 00
395.49	0.2894438E-02	0.1165030E 00
429.76	0.2336578E-02	0.8953859E-01
462.94	0.1902269E-02	0.7033050E-01
494.77	0.1566058E-02	0.5518754E-01
525.78	0.1313538E-02	0.4464533E-01
560.59	0.1114177E-02	0.4226155E-01
594.32	0.9213609E-03	0.3432756E-01
625.96	0.7910719E-03	0.2794681E-01
658.51	0.6881284E-03	0.2333586E-01
689.25	0.6061282E-03	0.1989019E-01
723.25	0.5306695E-03	0.1932555E-01
756.43	0.4710052E-03	0.1651962E-01
788.60	0.4216461E-03	0.1444663E-01
820.03	0.3811687E-03	0.1255593E-01
850.82	0.3897771E-03	0.1184792E-01
884.27	0.3154260E-03	0.1179666E-01
909.84	0.0	0.4032392E-02

* RADIATION VALUE WAS CALCULATED BASED ON THE SLOPE BETWEEN THE PREVIOUS TWO POINTS

TOTAL RADIATION EMITTED=0.4459E 01 WATTS/STER

CENTROID= 0.2050E 03CM

Fig. 3.14 H_2O Contribution to Infrared Radiation per Length of Plume
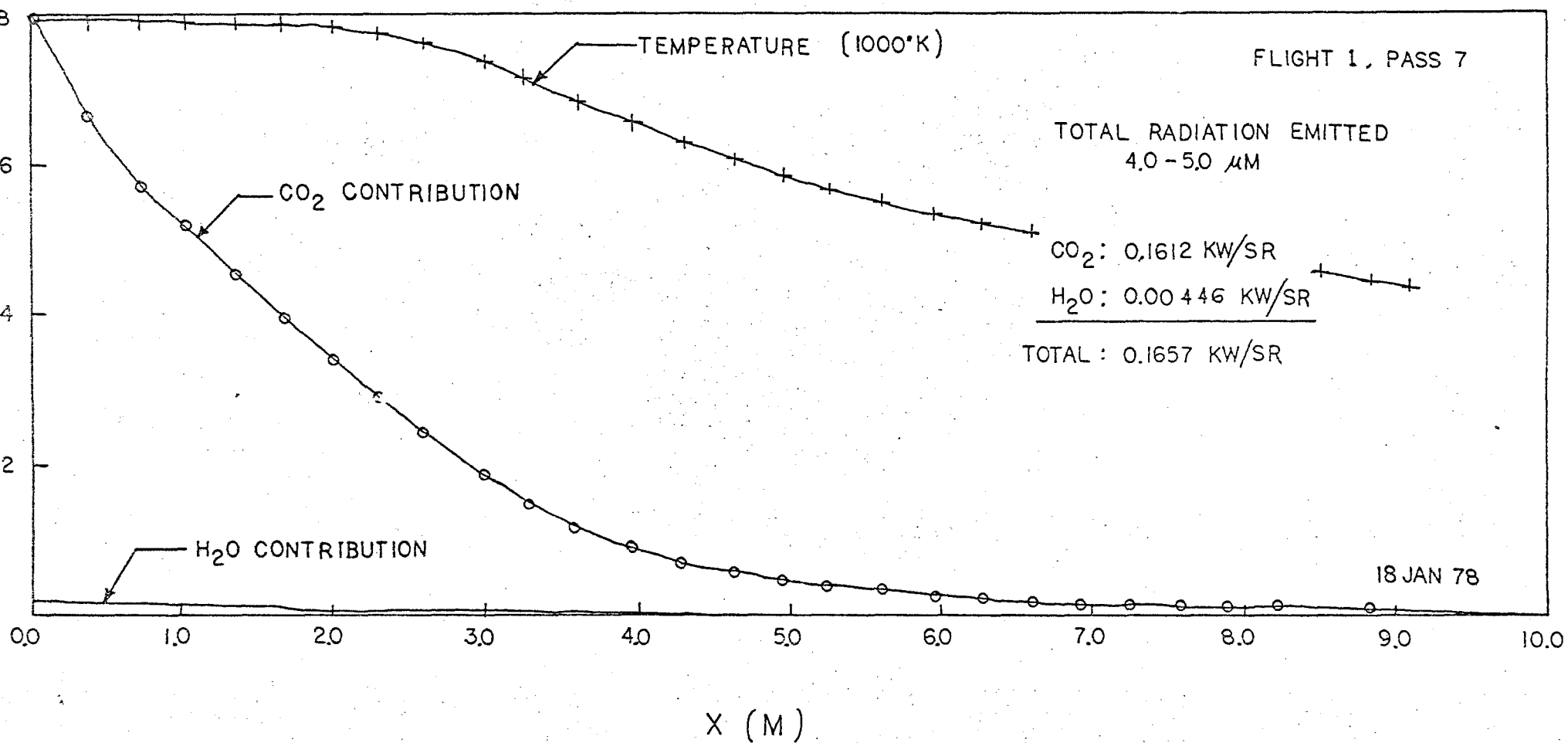
Fig. 3.15 SPATIAL DISTRIBUTION OF TEMPERATURE AND RADIATION IN THE TURBOJET EXHAUST.

3.3 Infrared Radiation Predictions for a Small Kerosene/Gaseous Oxygen Rocket Engine

Two gas dynamics and the UTSI infrared radiation computational models were used to predict the physical properties in hot rocket exhaust plumes. Experimental data were obtained in the exhaust plume of a small kerosene/gaseous oxygen rocket engine using a three-dimensional laser Doppler velocimeter system to measure the velocity distribution. The spatial distribution of radiated energy in the 4-5 μ wavelength band was measured using an infrared radiometer. Detailed comparisons between the computational and experimental results are described in this section.

3.3.1 Description of Experimental Equipment

Small Laboratory Rocket Engine: The exhaust plumes studied in these measurements were produced by a small kerosene/gaseous oxygen rocket engine [30] operating in the NASA Laser Doppler Velocimeter Facility [31]. Engine design and performance parameters are listed in Table 3.3. Data were taken at a variety of oxidizer/fuel (O/F) ratios and at two chamber pressures. The experimental data used to compare with the theoretical calculations were obtained at a chamber pressure of 11.1 atm. and an O/F ratio of 2.25.

NASA Laser Doppler Velocimeter Facility: The NASA Marshall three-dimensional laser Doppler velocimeter [31] was used to measure the velocity distribution in the exhaust plume and mixing layer produced by the inner hot rocket exhaust jet mixing with an outer subsonic airflow. A schematic diagram of the LDV experimental arrangement showing the installation of the small rocket engine is shown in Fig. 3.16. As described in Ref. [18] the simultaneous measurement of the three Doppler velocity components yielded the three velocity components u,v, and w.

TABLE 3.3

ENGINE DESIGN AND PERFORMANCE PARAMETERS

Fuel	Kerosene
Oxidizer	Gaseous oxygen
Purge	Nitrogen 100 psig
Coolant	Water at 3 gal/min
Chamber pressure	50 and 148 psig
Fuel flow rate	
50 psig	1.38 g/sec
148 psig	3.80 g/sec
Oxygen flow rate	
50 psig	3.05 g/sec
148 psig	8.70 g/sec
Throat diameter	0.200 in.
Exit diameter	0.310 in.
Throat area	0.0314 in.^{2}
Exit area	0.0755 in.^{2}
Area ratio (A_E/A_t)	2.40
O/F ratio	2.25
Chamber diameter	0.780 in.
Chamber length	1.620 in.
L^*	25.20 in.
C^* at 148 psig	6045 fps

AEROSOL
GENERATOR

LASER
POWER
SUPPLY

LASER CAVITY

O_2 AND N_2 CYLINDERS

HOT JET
CONTROL
PANEL

EXHAUST
DUCT

EXHAUST
JET

LDV INSTRUMENT

AIR
HEATERS

AIR REGULATION
PANEL

ELECTRONICS

WIND TUNNEL
AIR SUPPLY
(DRY AIR)

TAPE
RECORDER
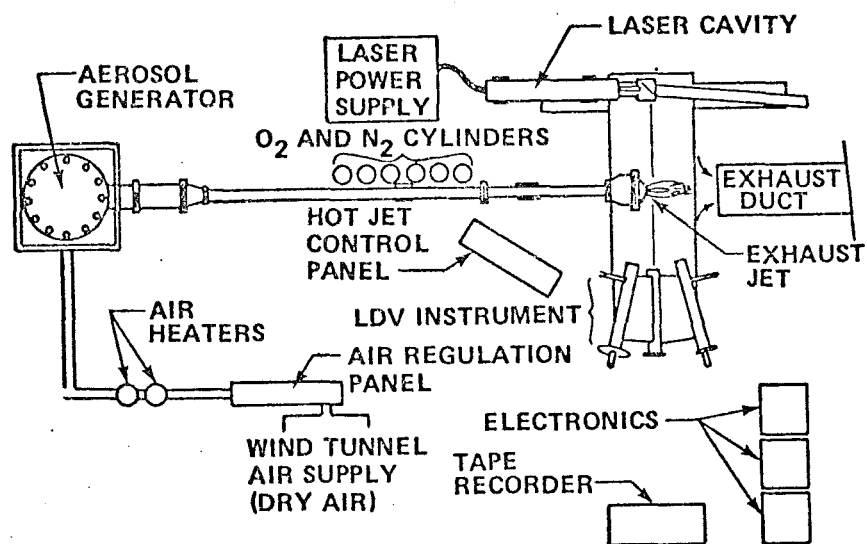
3.16 SCHEMATIC DIAGRAM OF LASER VELOCIMETER ARRANGEMENT

In order to simulate external airflow around the small rocket entine,
an outer flow nozzle was used to produce an external flow velocity of 61 m/sec.
A schematic diagram of the rocket engine and outer flow nozzle is presented
in Fig. 3.17.

Infrared Radiation Diagnostic Equipment: The primary instrument used to
obtain the radiation intensity data was an Electro-Optical Industries Model 470
Radiometer. The data were obtained using a fixed filter, which transmitted
radiation in the 4-5 μ band.

A large metal shield with a 1-mm aperture was moved in the axial direction
to obtain the variation of radiant intensity along the exhaust plume centerline.
A second set of measurements was made using a 1-mm vertical slot in the large
metal shield. The slot length was greater than the diameter of the exhaust
plume. The experimental setup is shown in Fig. 3.18.

3.3.2 Typical Experimental Results

Velocity Distribution Data: Experimental data for mean flow velocities
$(\bar{u},\bar{v},\bar{w})$, turbulent intensities [$\overline{(u')^2}$, $\overline{(v')^2}$, $\overline{(w')^2}$], and turbulent velocity
correlations were obtained in the radial direction at various axial locations
downstream from the nozzle exit plane. Data were obtained at X/D locations
of 2.4, 4.8, 8.4, 11.3, and 14.2, where X is the distance measured from the
nozzle exit plane and D is the diameter of the exit nozzle. Typical data
obtained at X/D = 11.3 for the mean axial flow velocity are presented in
Fig. 3.19. Other data are described in Ref. [18].

Infrared Radiation Data: The infrared radiation data have been described
previously [30]. Typical data obtained at an O/F ratio of 2.25 and an ex-
ternal flow velocity of 210 fps are presented in Figs. 3.20 and 3.21 for the
1-mm aperture and slot, respectively. The centerline radiation intensity
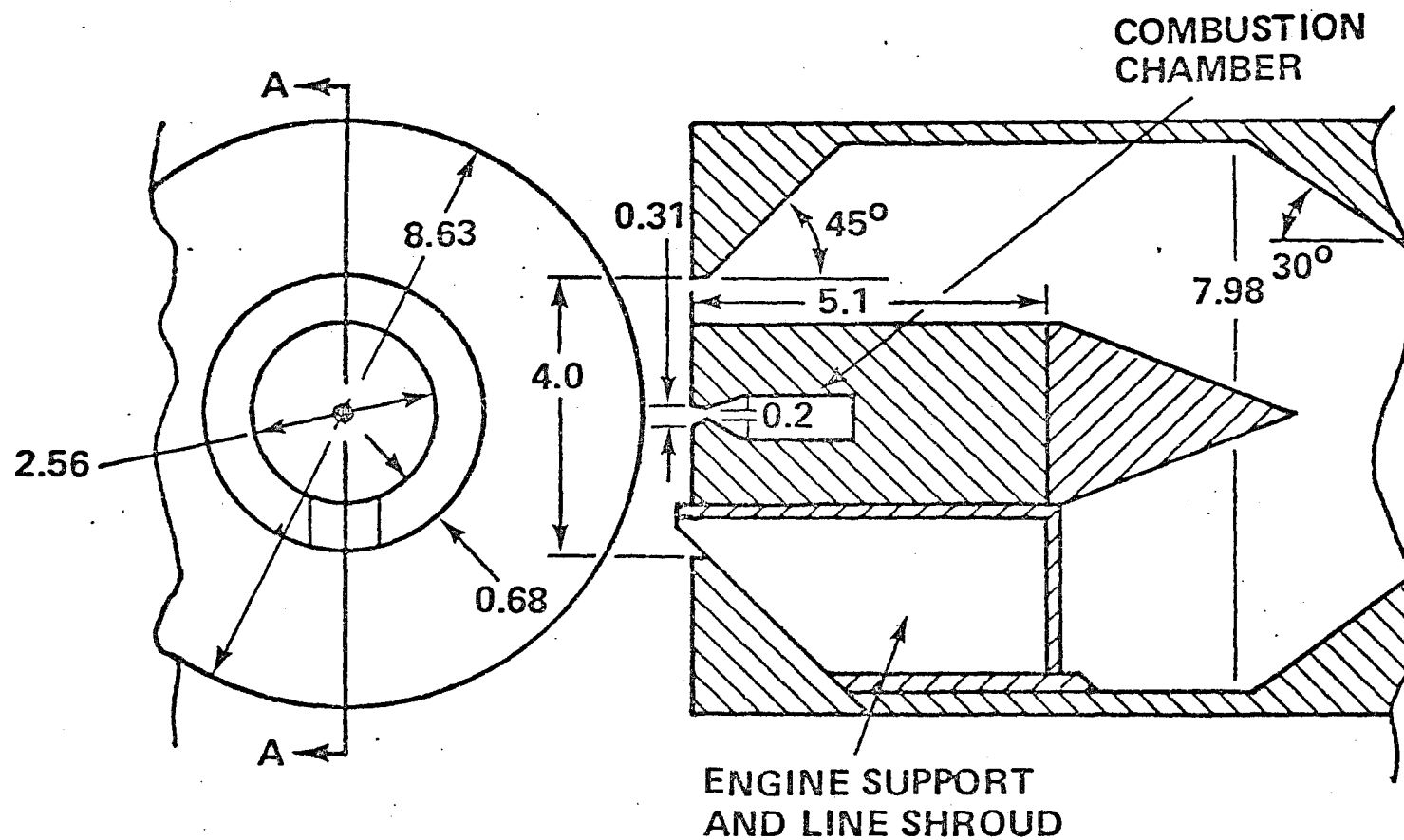
Fig. 3.17 Schematic of the exhaust plume and external flow aparatus.
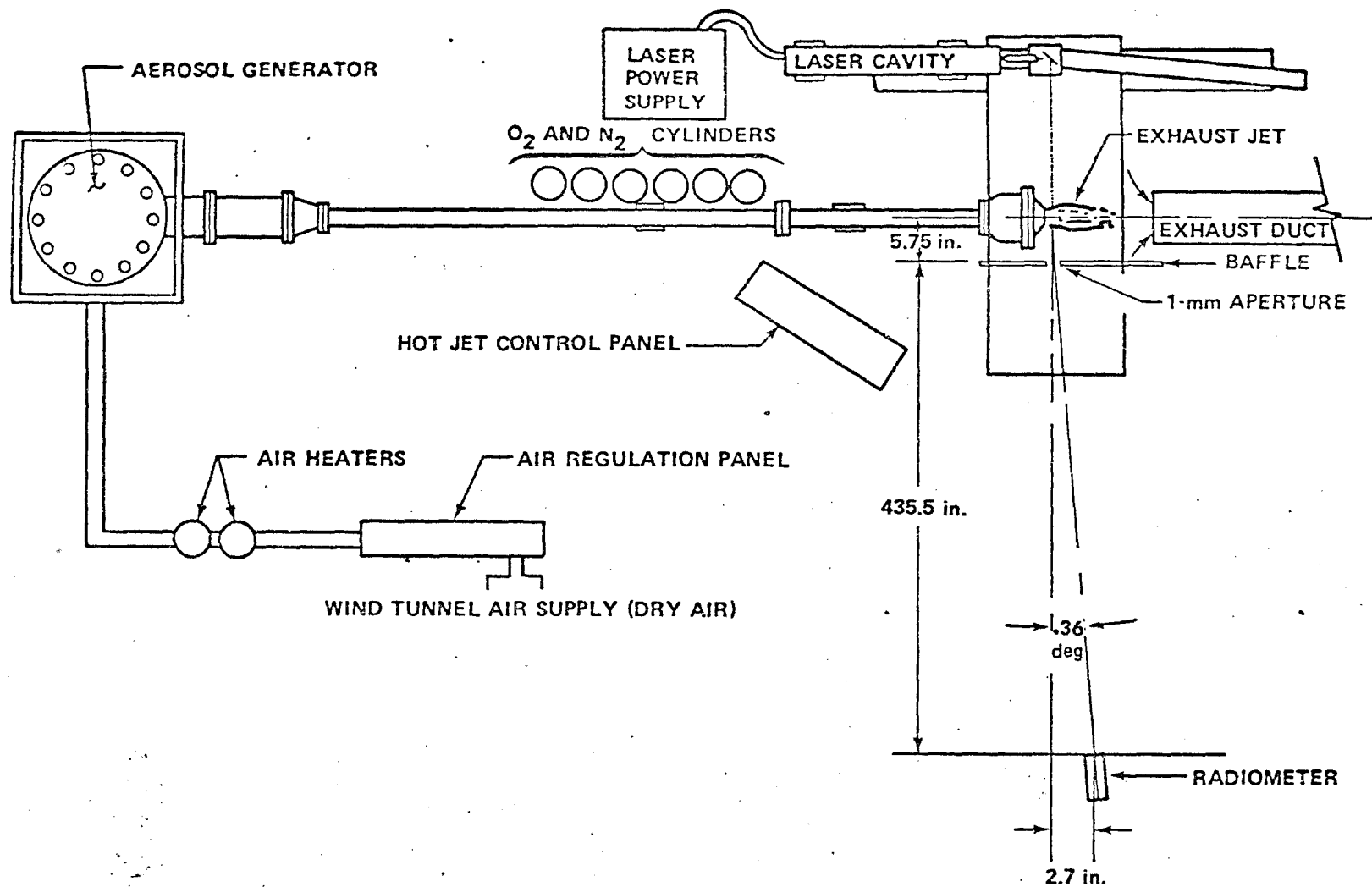
Fig. 3.18 Exhaust plume test arrangement in NASA LDV facility.
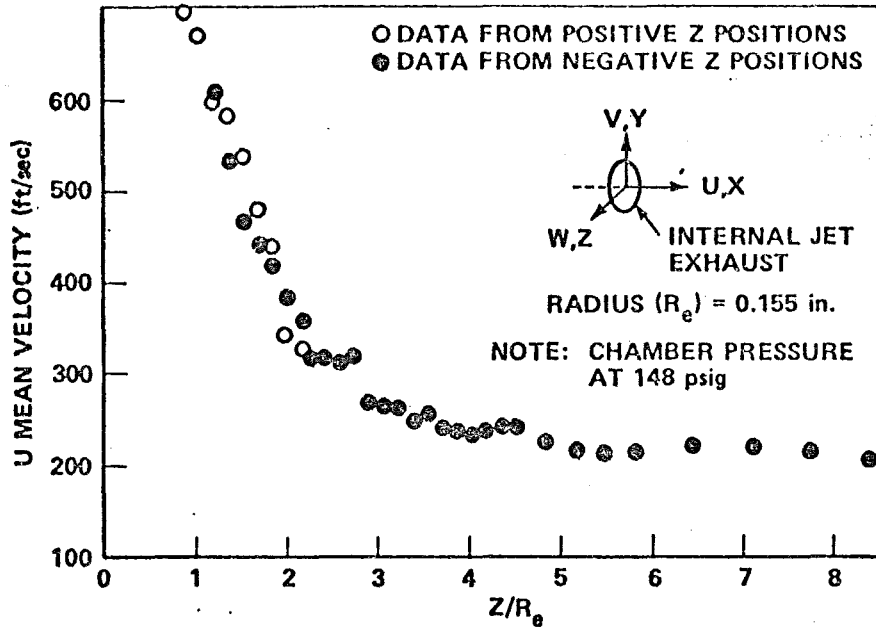
Fig. 3.19. Profile of u mean velocity component
at X/D = 11.3
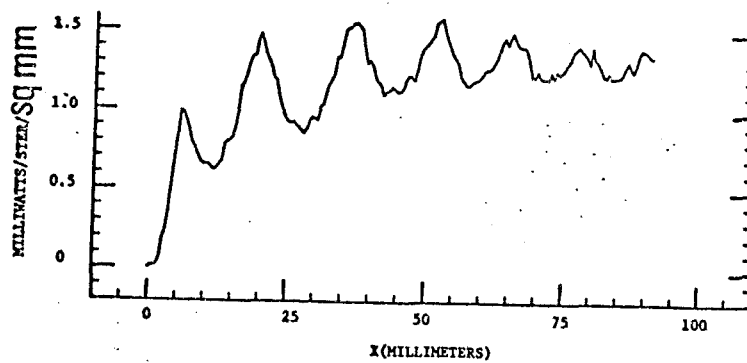
Fig. 3.20 Spatial distribution of radiation along
axis of plume for aperture diameter = 1-mm;
O/F = 2.25, velocity = 150 fps.
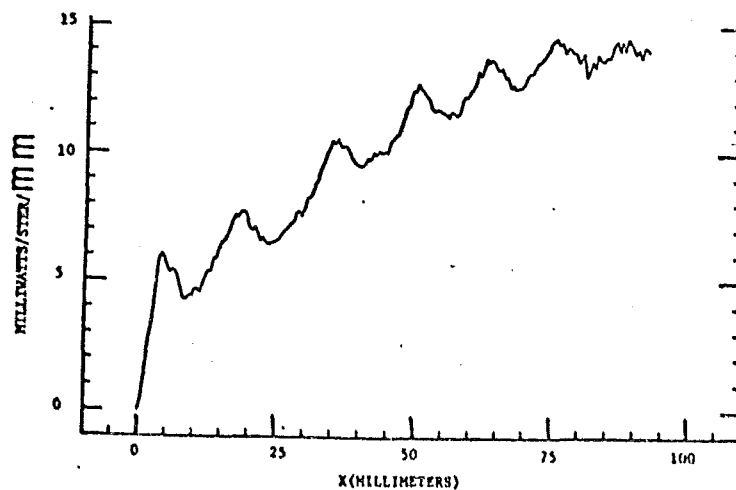
Fig. 3.21 Spatial distribution of radiation along
axis of plume for 1-mm slot width; O/F = 2.25,
velocity = 210 fps.

distribution in Fig. 3.20 clearly shows the presence and influence of shocks and/or Mach disks in the exhaust plume. The effect of afterburning in the mixing layers on the infrared signature is shown clearly in Fig. 3.21 where the shock-induced radiation peaks are superimposed on an axially increasing radiation intensity. The data presented in Figs. 3.20 and 3.21 were obtained in the near field of the exhaust plume (X/D less than 12) and indicate that the peak radiation intensity has not been reached. Typically, the axial distribution of radiation is similar to that shown in Fig. 3.22. Even though the data presented in Fig. 3.22 are for a lower mass flow and chamber pressure, the axial variation is similar to that obtained for the high-chamber-pressure cases. The data presented here are only samples selected to indicate the measured trends in preparation for a discussion of the comparison between theory and experiment.

3.3.3 Comparison of Calculated and Measured Results

The LAPP and TKE computer codes were exercised for the rocket performance parameters listed in Table 3.3. The NASA Lewis Chemical Equilibrium Computer Program was used to calculate the exit plane gas properties. Because of the short expansion nozzle length, the chemical species were assumed to be frozen at the throat values. These exit plane conditions then were used as initial conditions for the LAPP and TKE computer codes.

The results predicted by the LAPP and TKE computer codes are presented in Figs. 3.23-3.28. The variation of the centerline velocity with distance from the nozzle exit plane is presented in Fig. 3.23. The LAPP code predicts a constant-velocity core having a length approximately equal to X/D = 5, which is followed by an exponential velocity decay due to turbulent mixing predicted by the Donaldson-Gray viscosity model. The TKE (REP3) code predicts a sharp decrease in velocity at approximately an S/D value of one. There are also
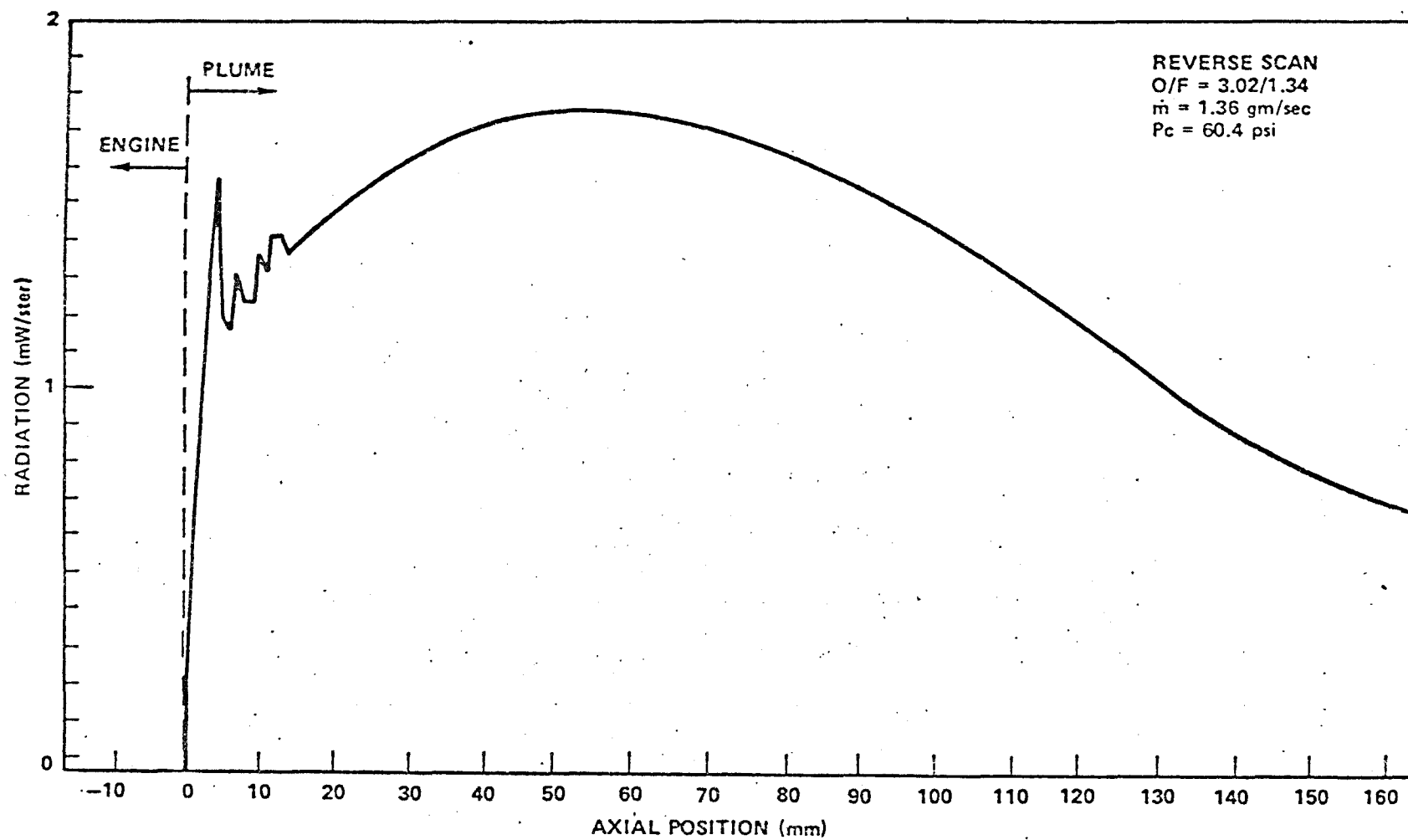
Fig. 3.22 Axial variation of radiation at O/F ratio of 2.27.

-38-
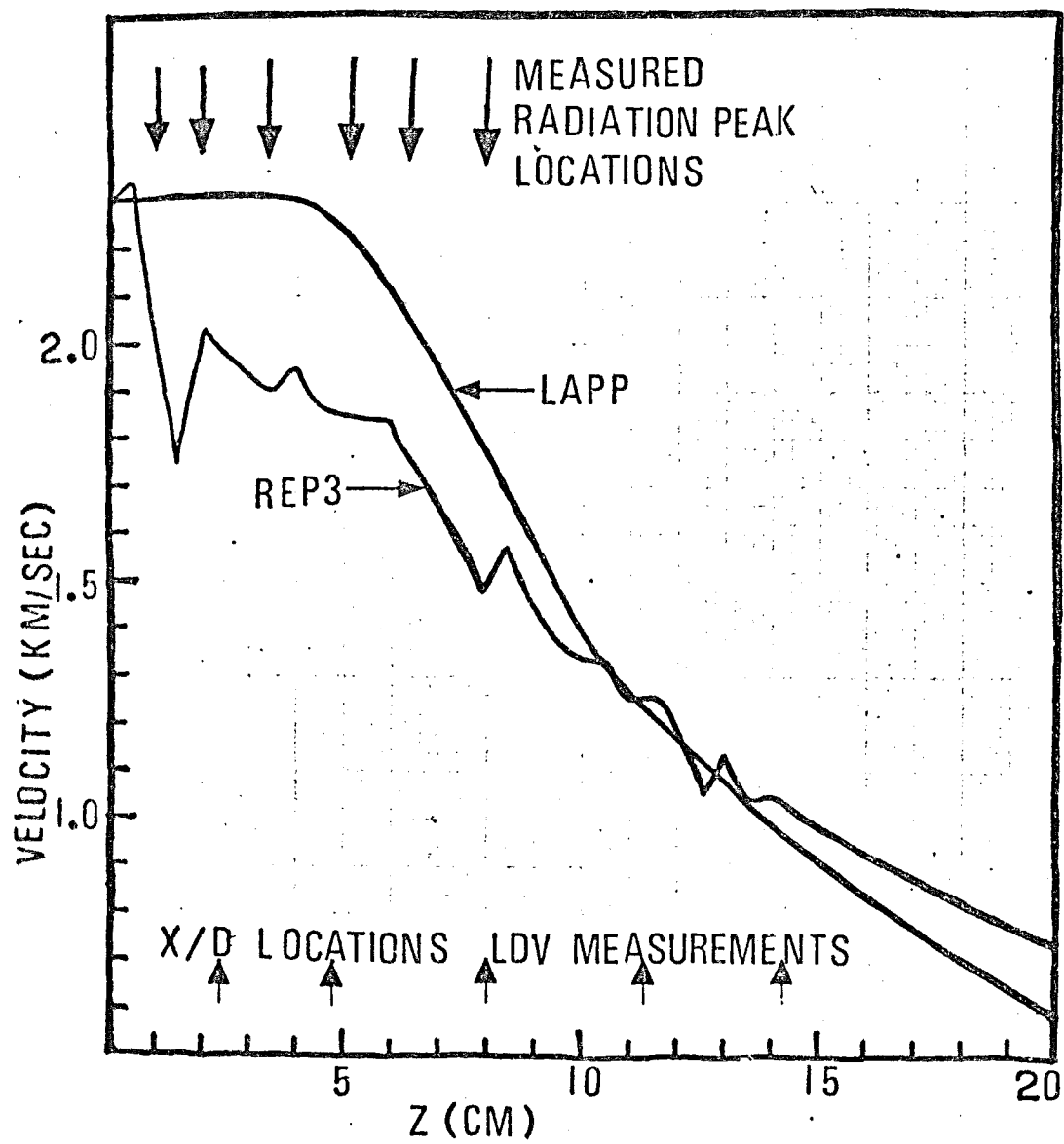
Fig. 3.23 Calculated axial velocity distribution.

several other oscillations in velocity, as shown by the jagged nature of the curve. A particularly large decrease in velocity occurs near an X/D value of 8. Also noted in Fig. 3.23 are the locations of the measured radiation peaks shown previously in Fig. 3.20. The X/D locations for the LDV measurements also are indicated on Fig. 3.23.

The predicted variations of temperature at the jet centerline with axial distance are given in Fig. 3.24. The LAPP code predicts a small temperature rise due to afterburning in the exhaust plume. The TKE code predicts a sharp rise in temperature at an X/D value of one, which then is followed by a series of oscillations in temperature. The predicted oscillations do not agree with the measured locations of radiation peaks (denoted by arrows on the Figs.). It is quite obvious that neither of the computer codes does an adequate job of predicting the spatial variation of velocity and temperature produced by shock waves and Mach disks in the near field of the exhaust plume. This is not surprising since LAPP has no provision for treating shocks.

Figures 3.25-3.38 present the variation of the axial component of the velocity with radial distance from the jet centerline. As shown in Fig. 3.25 for an X/D value of 2.4, the predicted results (curves) do not agree with the experimental measurements (symbols). Because of the limited number of particles in the hot core of the jet, the NASA LDV system was not able to make measurements closer to the jet centerline than about one exit nozzle radius. The variation of the radial velocity component also is shown. The TKE code predicts an increasing value of v with radius, whereas the measured value decreases with radial distance. The external flow is an axial flow at 61 m/sec.

The lack of agreement between theory and experiment also is indicated in Fig. 3.26 for the velocity profile at an X/D value of 8.0. The LAPP and TKE
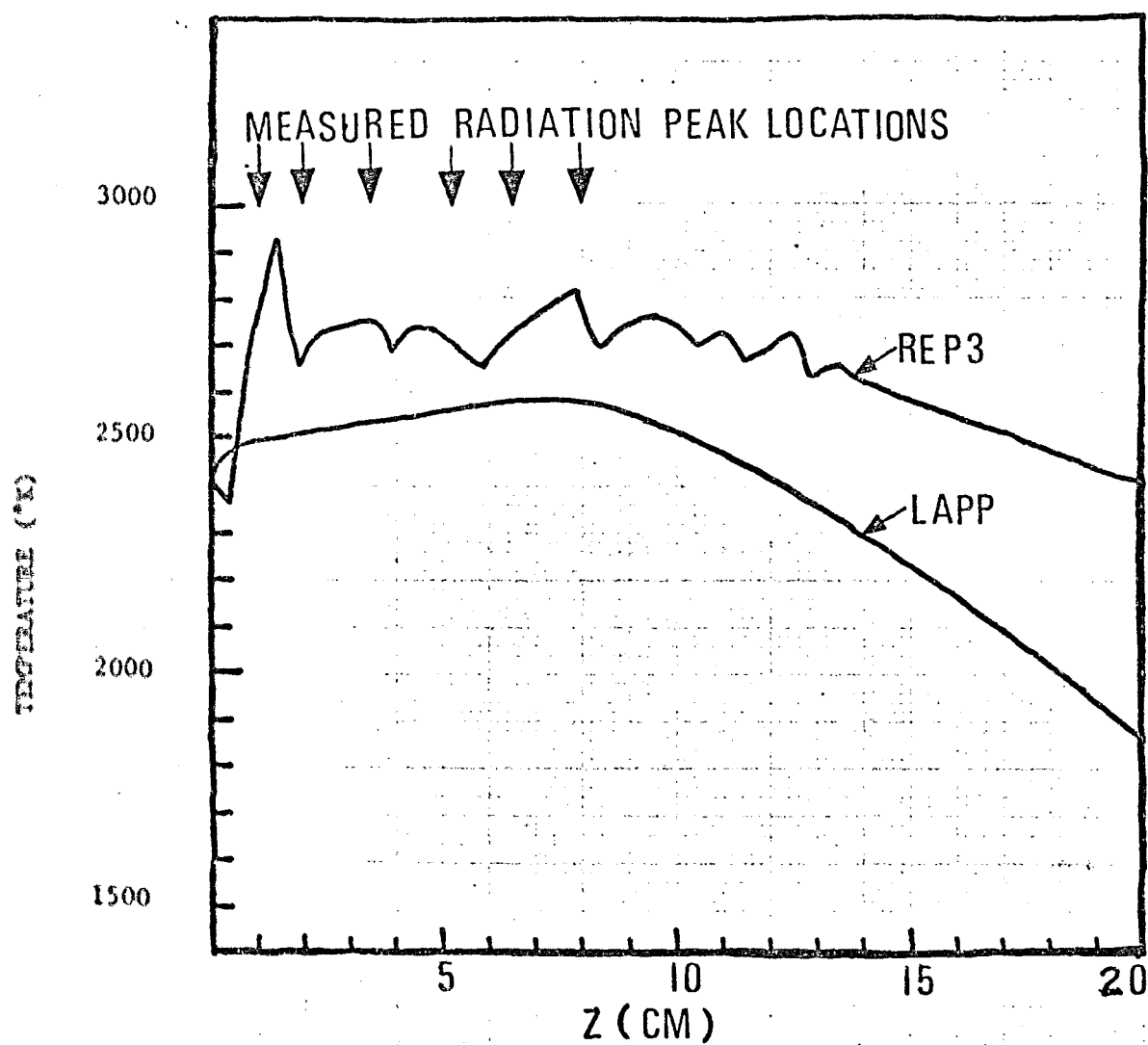
Fig. 3.24 Calculated temperature distribution.
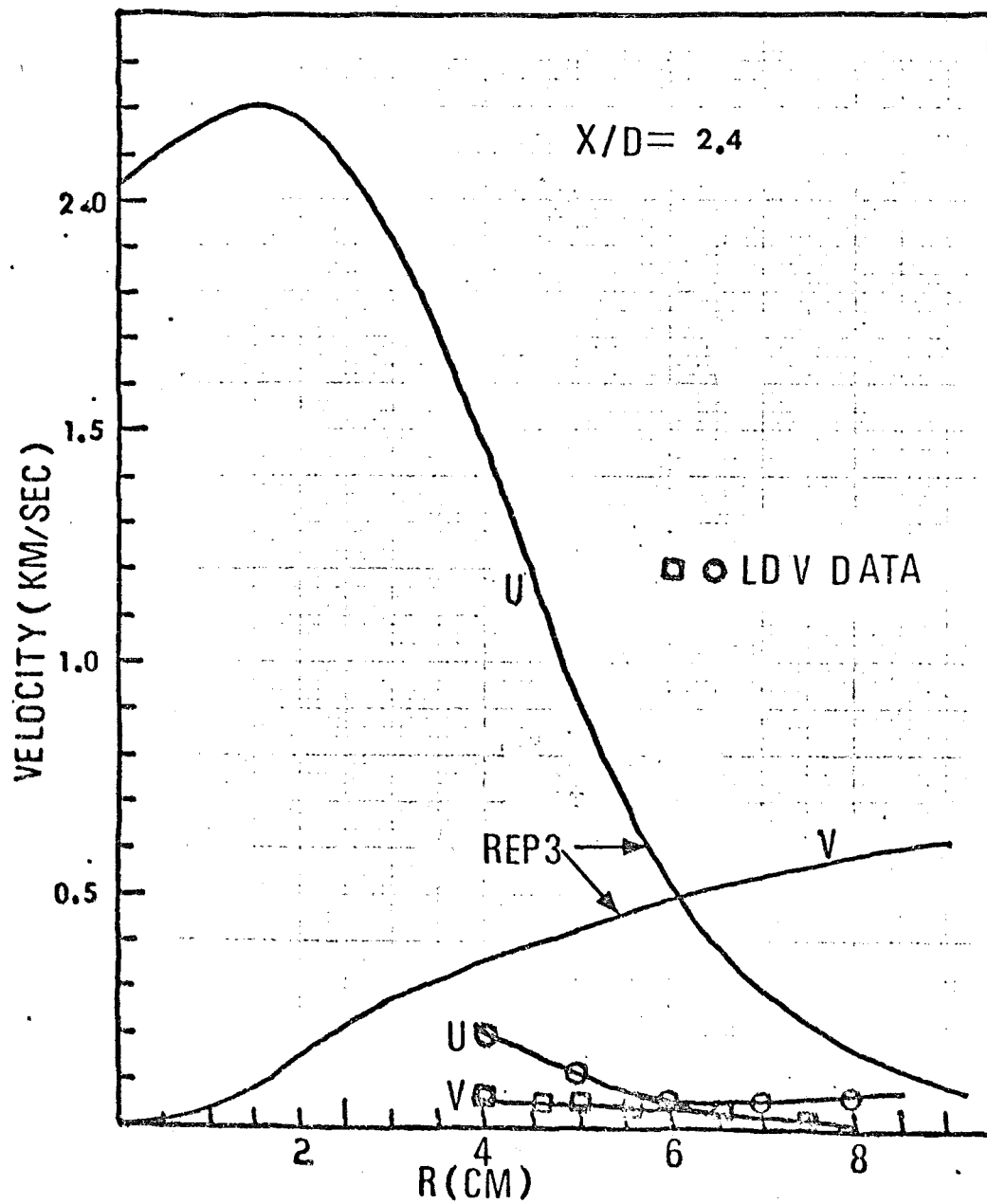
Fig. 3.25 Velocity profiles at X/D = 2.4
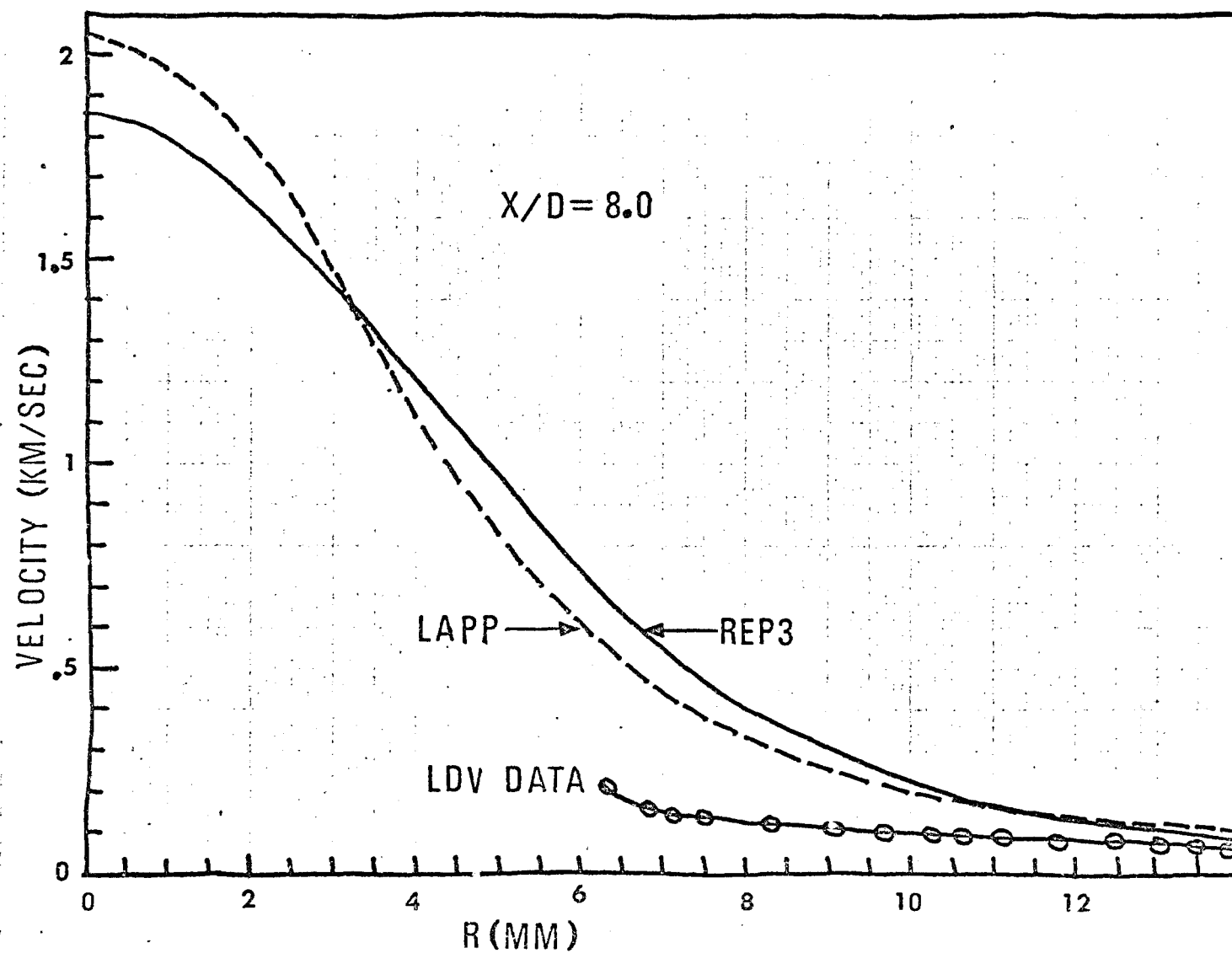
Fig. 3.26 Velocity profiles at X/D = 8.0

calculated results are similar but are in excess of the experimental values. Similar results are presented in Figs. 3.27 and 3.28 for X/D values of 11.3 and 14.2.

The LDV data indicate that the exhaust plume is much narrower than predicted by the LAPP and TKE gas dynamics models. Since both the LAPP and TKE models assumed that turbulent mixing began at the nozzle exit plane and ignored the large recirculation (base flow) region, it is expected that turbulent mixing occurs too fast compared to the physical situation where turbulent mixing begins at the end of the recirculation zone, which is several nozzle diameters downstream from the exit. It is known that the base flow region can have a pronounced effect on exhaust plume spread and initial turbulent mixing layer growth. Because of time and budget constraints, we were unable to use a base flow model to assess its effect on the calculated temperature and velocity profiles.

The infrared radiation band model program was used to calculate the variation of infrared radiation along the exhaust plume for the temperature and species concentration profiles predicted by the LAPP and TKE gas dynamics computer codes. The computed results are shown in Fig. 3.29. The lack of agreement between theory and experiments was not unexpected, since the calculated temperature distributions did not yield the spatial structure due to shock waves that are evident in the measured infrared data and are visible in photographs of the exhaust plume.

It is not clear what causes the difference between the REP3 and LAPP calculations. The LAPP code plus the radiation code yield results that are within a factor of 1.5 of the measured results while the factor is approximately 2.5 for the REP3 plus radiation code results.
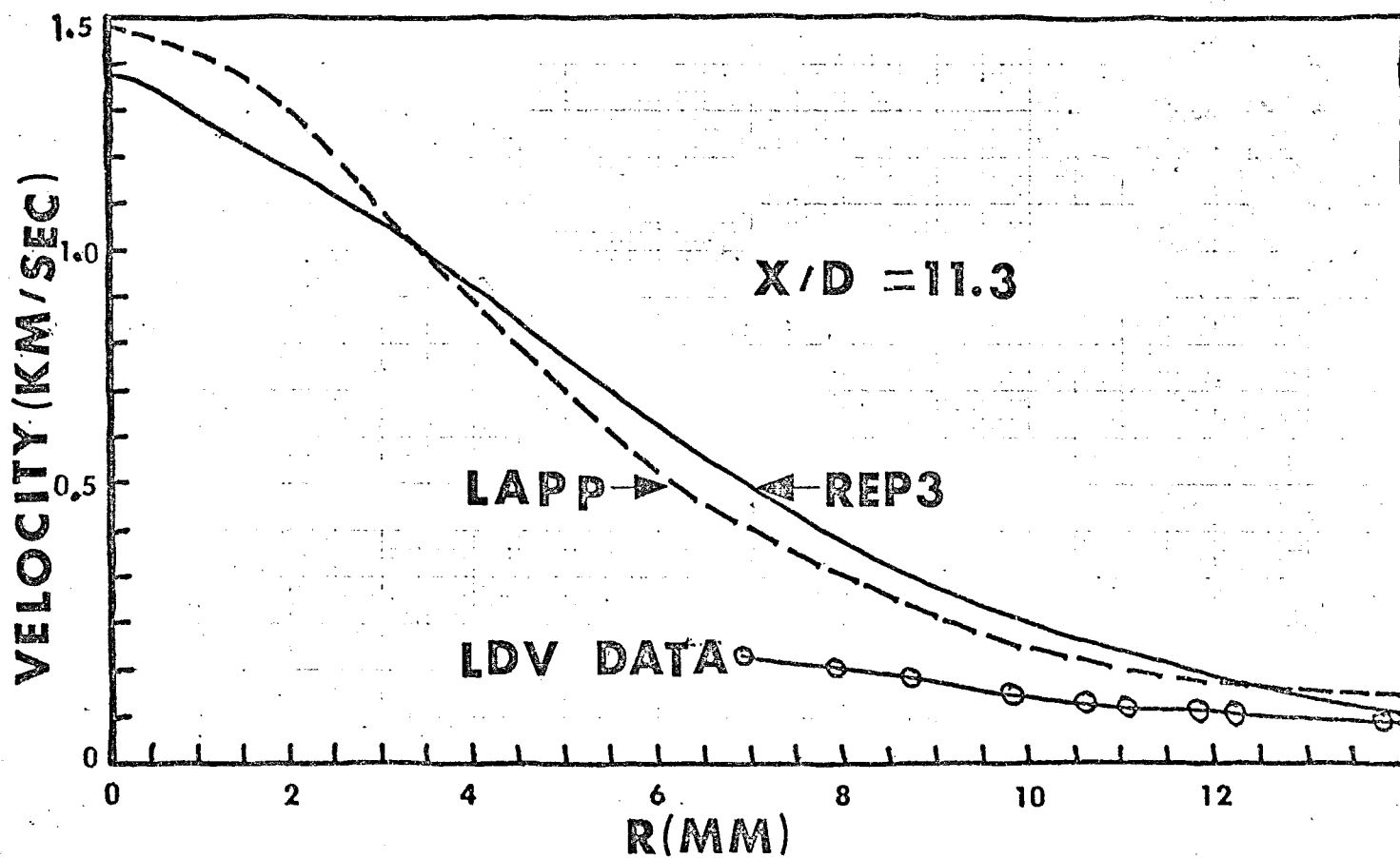
Fig. 3.27   Velocity profiles at X/D = 11.3
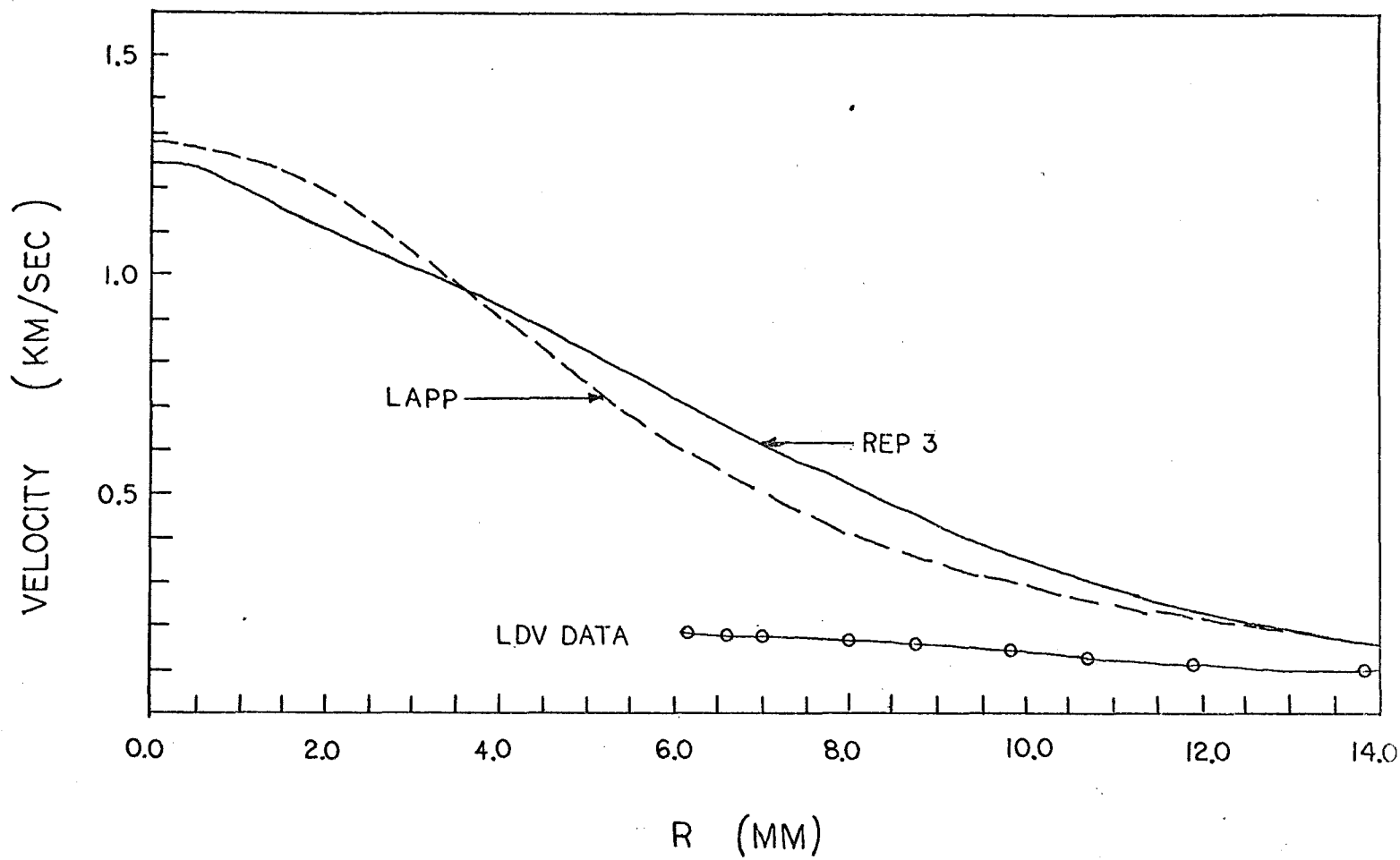
Fig. 3.28   VELOCITY PROFILES AT X/D = 14.2
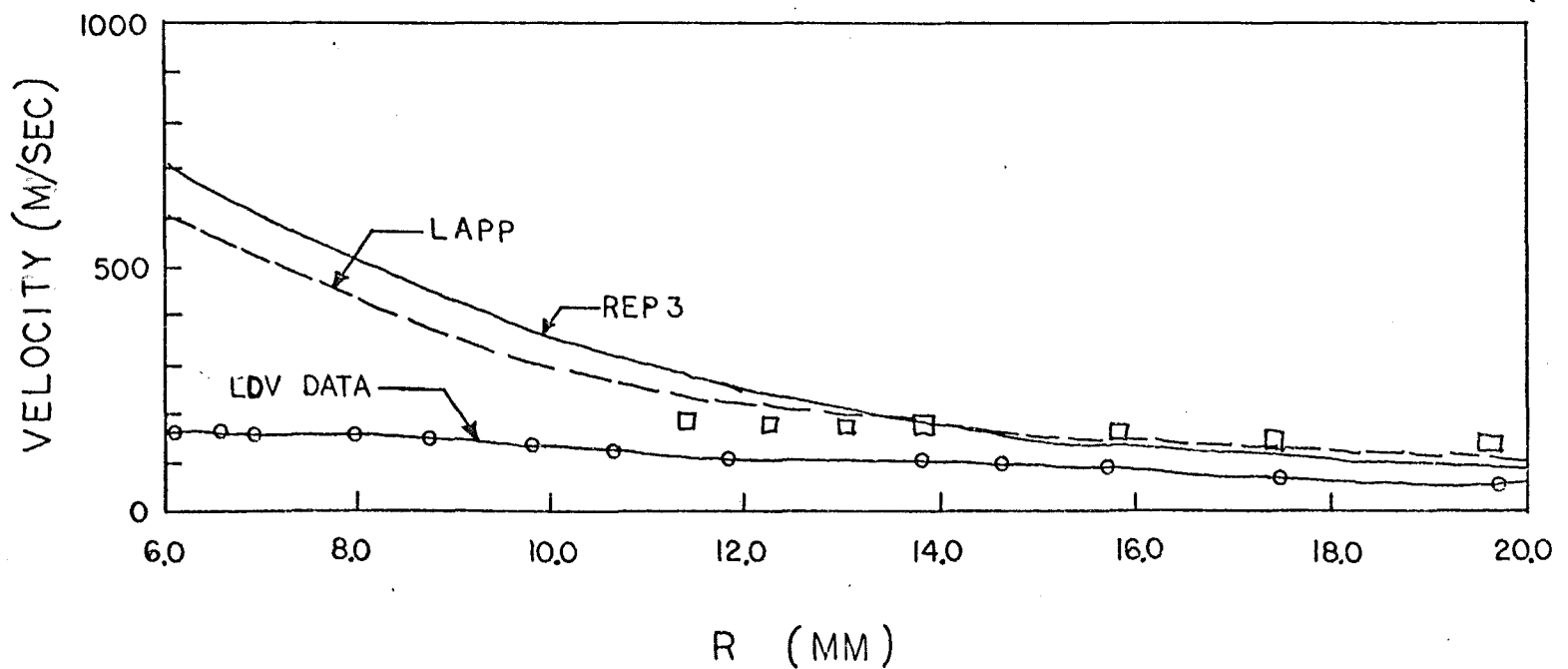
Fig. 3.28 (continued)
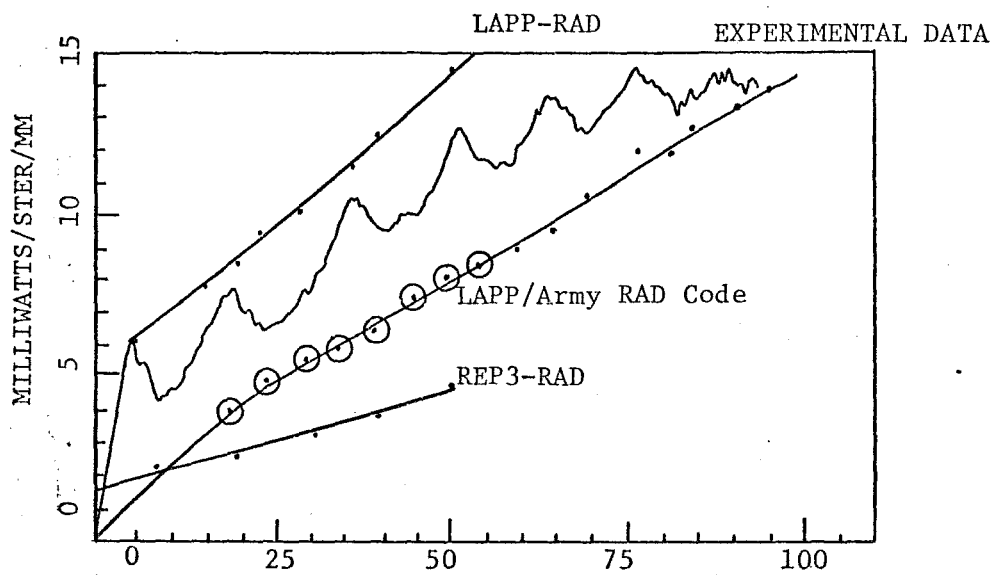
Fig. 3.29 Comparison of calculated and
measured IR radiation.

3.4 Gas Dynamics Finite Difference Computer Model

A Gas Dynamics Finite Difference Computer Model was developed as part
of the contract effort. Numerous difficulties and problems were encountered
during the development process, but the program was operational at the conclusion
of the effort. Unfortunately, the present version of the code is not entirely
satisfactory due to the fact that the computational times are large. Approxi-
mately one hour on the IMB 360 computer system was required to march the
solution 360 cycles (which corresponds to a flow time of 0.2 msec.). While
this time would be approximately 6-10 minutes on the CDC 660 computer, it is
still felt to be quite excessive since the test flow being analyzed was a relatively
simple expanding flow. In its present form, the finite difference code
successfully calculates shock waves on wedges and blunt bodies and is moderately
successful in calculating the shock-Mach disc structure in a cold gas nozzled
expansion.

Several typical nozzle expansion test cases were computed to assess
whether the numerical results were reasonable. These results are described
in the next section.

3.4.1 Overexpanded Nozzle Exhaust

In order to assess the FD model's ability to handle strong shock waves
which result in the exhaust plume from an overexpanded nozzle, the flow having
the initial characteristics given in Fig. 3.30.

The computed Mach number variation along the jet centerline is given in
Fig. 3.31. The Mach number decreased to a subsonic value in a very short
distance downstream from the exit plane and remained subsonic for 80-cm in the
flow direction.

An analytical estimate of the flow conditions was made by assuming that
an oblique shock wave would be formed at the nozzle exit and would raise the

OUTER FLOW
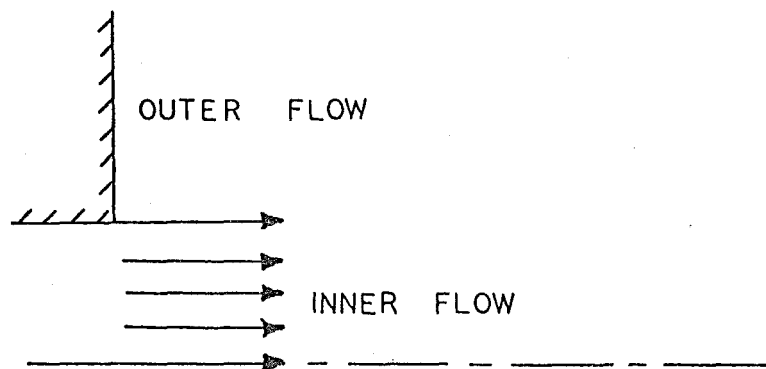
INNER FLOW

INNER FLOW	OUTER FLOW
$M_{exit} = 1.133$	$M = 0$
$T_{exit} = 300°K$	$T = 300°K$
$P_{exit} = 0.8$ atmospheres	$P = 1.0$ atmospheres

Fig. 3.3.0   INPUT FLOW PARAMETERS

CALCULATED OBLIQUE SHOCK AT EXIT (SEE ATTACHED)

Z = .05

Distance along centerline (cm)
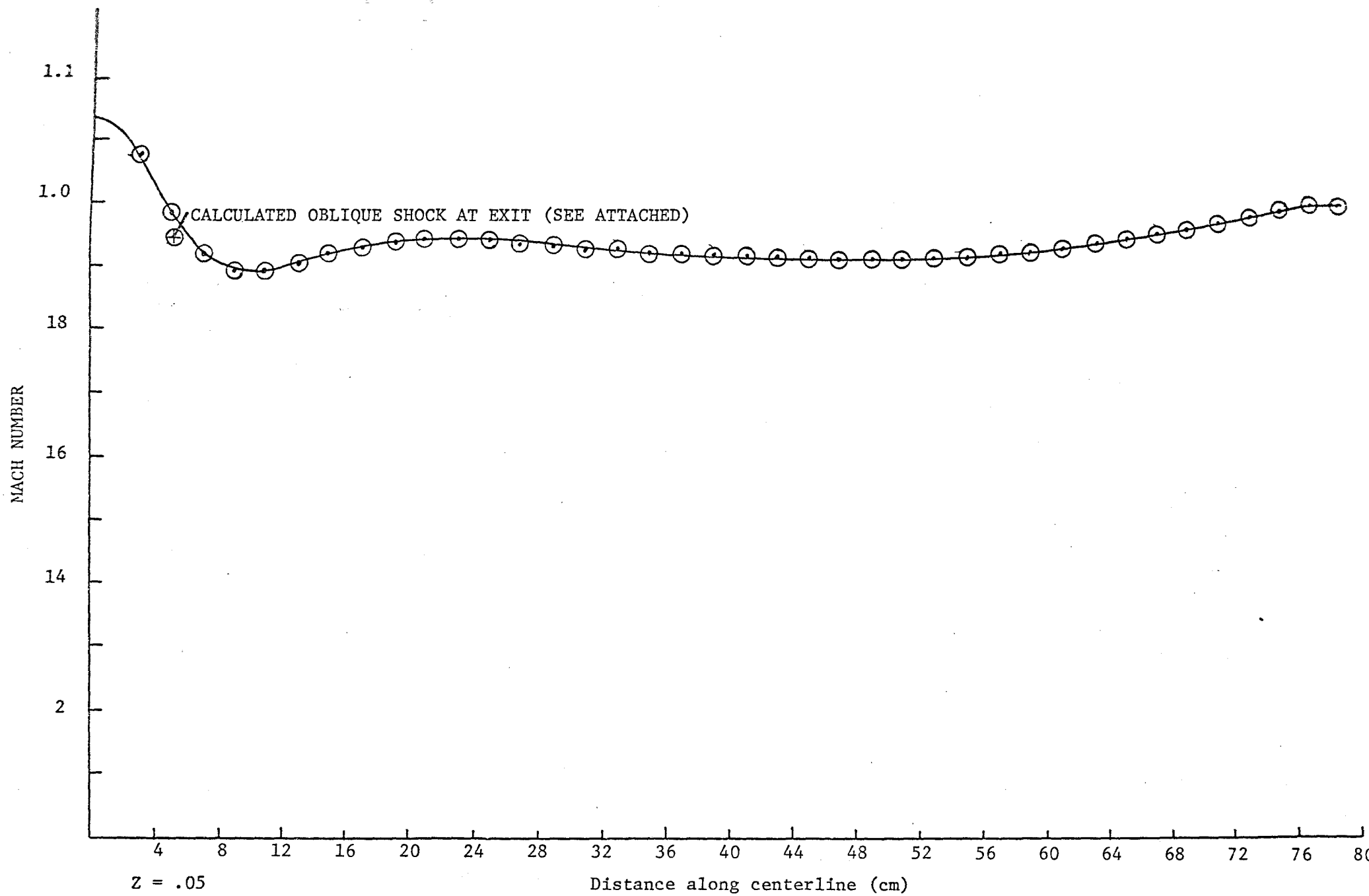
Fig. 3.31 CENTERLINE MACH NUMBER VARIATION

pressure behind the shock wave to the ambient pressure of 1.0 atm. The oblique

shock angle was then determined to be approximately 76.6° as shown in Fig. 3.32.

The shock wave would intersect the centerline axis at a distance of 0.2323-cm

downstream of the nozzle exit plane. Gas dynamics calculations yielded a

value of 0.94 for the Mach number in region (2) behind the shock wave. This

calculated value is indicated on Fig. 3.31 and is in good agreement with the

finite difference code result.

As shown in Fig. 3.32, the shock wave would reflect from the centerline

and would process the flow back parallel to the centerline axis. In doing so,

the pressure in region (3) would increase while the Mach number M_3 would be

less than M_2. This agrees qualitatively with the FD code results.

At the intersection of the reflected shock with the free boundary, an

expansion wave would be generated to reduce the pressure at the edge of the

plume back to one atm. The expansion fan would accelerate and expand the flow

in regions (4-6) until a new shock pattern would be formed between regions

(7 and 8). Then the entire pattern would repeat.

While the FD code calculations appear to be quantitatively correct, there

were no available numerical data to compare with the FD code results in the

subsonic flow region. In order to determine whether the FD code predictions

are reasonable in an expanding flow, another test case was designed in which

a supersonic flow would expand from a nozzle. The results for this flow are

described in the next section.

3.4.2 Underexpanded Nozzle Exhaust

As stated above, a test case involving the supersonic expansion of air

from a nozzle was employed so that the FD code predictions could be compared

with the results obtained using the Method of Characteristics.
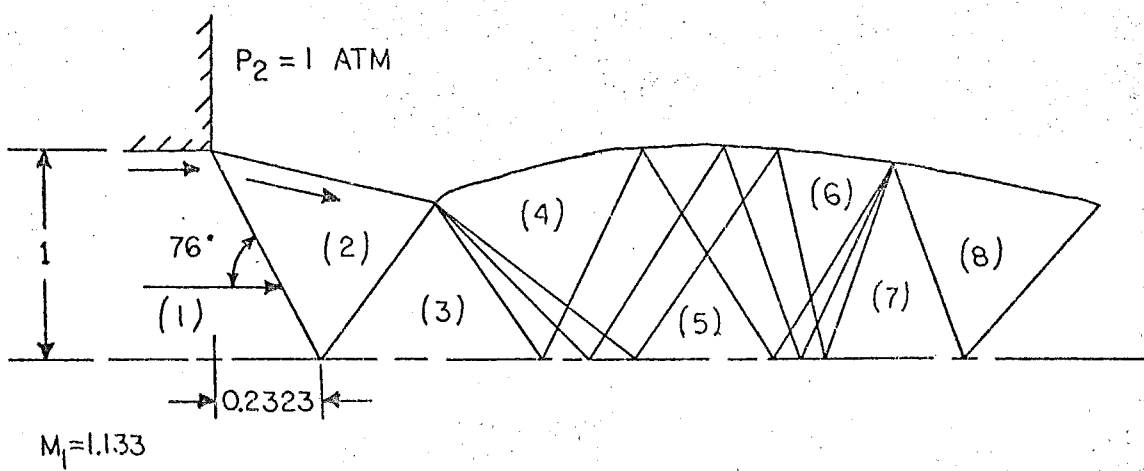
Fig. 3.32   ASSUMED SHOCK PATTERN FOR HAND CALCULATION.

FINITE DIFFERENCE
COMPUTER CODE

METHOD OF CHARACTER-
ISTICS SOLUTION

UPPER PORTION: Centerline MACH Number
Variation Along Jet
Centerline.

LOWER PORTION: X-Y Location of
Characteristics from
Hand MOC Calculation.

FLOW BOUNDARY

EXPANSION FAN

CHARACTERISTIC
LINES

M=1.133
P=2.772 ATM

M=1.436   M=1.708   M=1.990   M=2.295   M=2.635

1   2   3

X (CM)
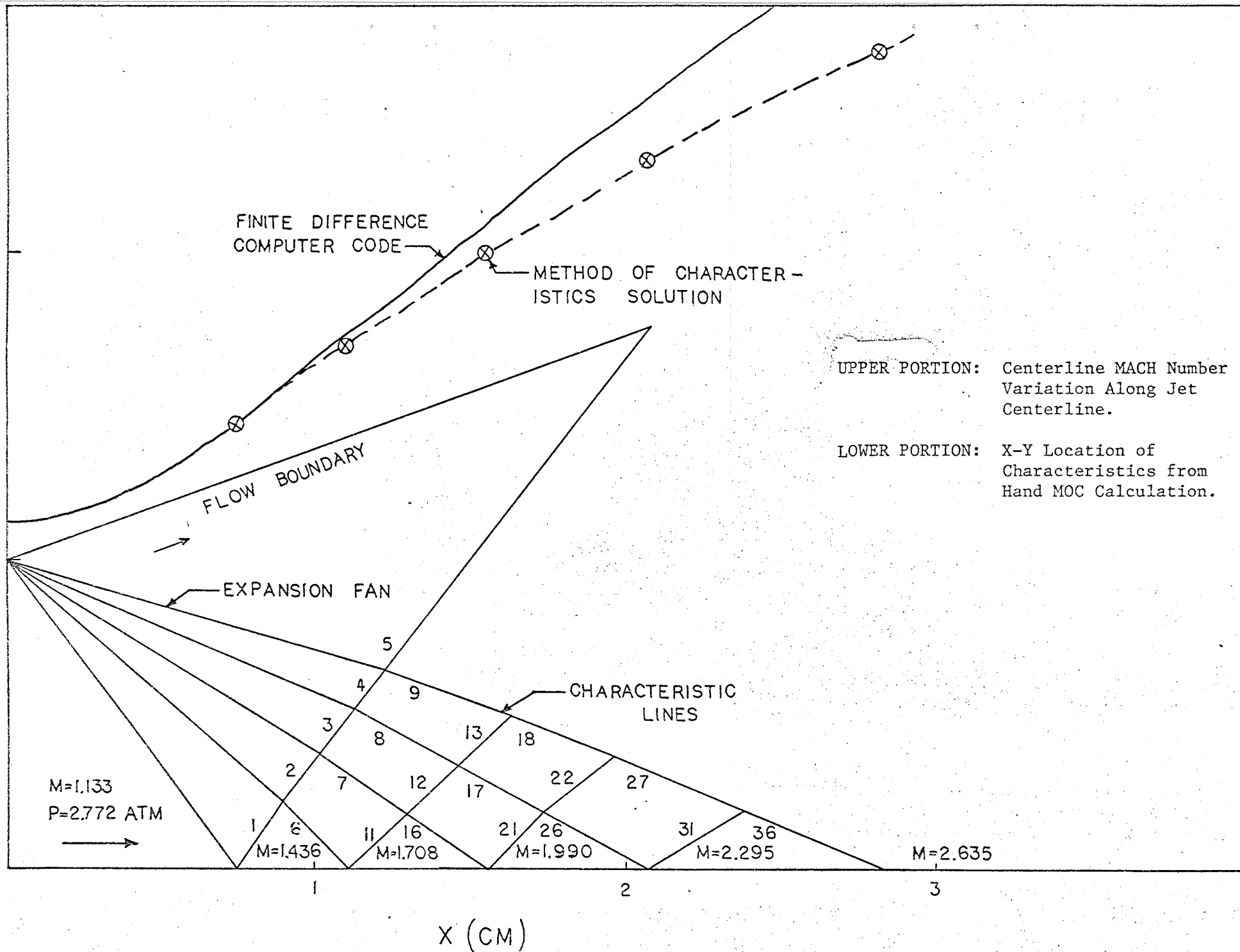
Fig. 3.33   COMPARISON OF METHOD OF CHARACTERISTICS AND FINITE DIFFERENCE MODEL RESULTS

The method of Characteristic technique used was Temple's Method as taught by the Principal Investigator in a first-year graduate course in gas dynamics. The characteristics net produced in the X-Y physical plane is shown in the lower portion of Fig. 3.33. A comparison of the MOC results (using 5 characteristics to start the calculation) and the Finite Difference Code results is presented in the upper portion of Fig. 3.33. The results are in good agreement. The lack of agreement at large distances from the nozzle exit plane is to be expected since the hand-calculated MOC solution used only five characteristics in the initial fan and is therefore expected to be more approximate than the Finite Difference Computer Code which uses a more complete set of differential equations.

Even though we were encouraged that the computer code appears to yield reasonable numerical results for an expanding plume, we are discouraged by the fact that the computer program required approximately one hour on the IBM 360 computer system to march the solution 0.3 msec. (or 360 cycles). While this time would be approximately 6-10 minutes on the CEC 6600, it still is felt to be quite excessive in view of the simple flow calculated.

3.4.3 Other Test Cases

In earlier work [21], the finite difference code was used to calculate the viscous flow between two parallel walls with one of the walls moving relative to the other. This is the so-called classical Couette Flow problem whose theoretical solution is well known [32]. The computed numerical results agreed well with the theoretical model results. In addition, the computer solution converged in 10 to 20 iteration cycles and the total computational time on the IBM 370 computer was approximately 30 seconds.

The code also successfully predicted the flow over a two-dimensional wedge in which a strong bow shock wave is formed.

In both of these cases, we have solid boundaries which restrict the flow and appear to assist in the convergence of the solution to a stable value.

3.4.4 Chemical Reactions and Turbulent Mixing Computations

Due to problems with the basic finite difference computer code, the chemical reaction and turbulent mixing portions of the code were not fully operational at the end of the program.

3.5 Results Obtained Using the REP 3 TKE Computer Model

The REP3 TKE Computer Model described earlier was revised for use on the CDC computer at MIRADCOM. The test case supplied by Dr. David Jensen of the Rocket Propulsion Establishment of Great Britain was successfully run on the MIRADCOM computer.

After the REP3 program was operational, it was utilized to calculate the flow field from a small kerosene/gaseous oxygen engine similar to the one used as the test case by Jensen. The results of these calculations are presented in Figs. 3.23-3.28. As discussed in Section 3.3, the REP 3 predictions do not agree with the experimental data. Attempts to locate any problems with the calculations or with the experimental data were unsuccessful.

One computer run was devoted to rerunning the case described in the previous paragraph. The program was rerun using a much smaller grid spacing. The results are shown in Fig. 3.34. The top curve shows the oscillations in temperature while the lower curve indicates the results for the velocity. Also shown on the graph are the locations of the radiation minima (two experimental runs are shown: Runs 65 and 85). As can be seen, the first three locations of the calculated temperature minima agree with the experimental locations. Even though the fourth through seventh minima do not agree, the results are reasonable.
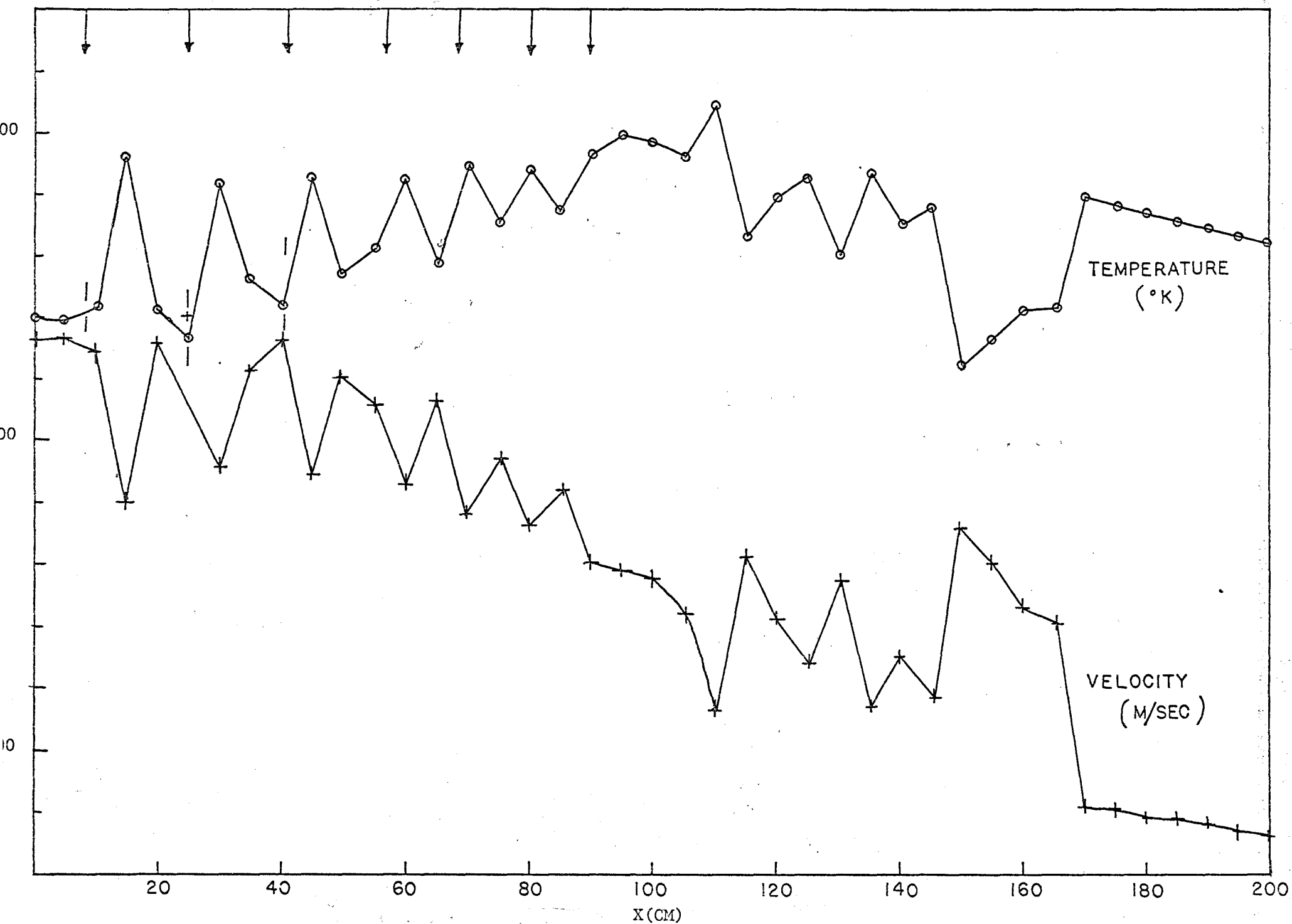
Fig. 3.34   CALCULATED RESULTS USING THE REP3 COMPUTER CODE

However, the behavior of the calculated profiles for X greater than 90-mm are disturbing in that there are a series of temperature and velocity oscillations which do not agree with any experimental or physical evidence. Furthermore, the predicted sharp drop (rise) in temperature (velocity) at 145-mm and the sharp rise (drop) in temperature (velocity) at 165-mm do not correspond to observed physical phenomena.

Clearly, further efforts are needed to ascertain whether or not the REP3 Program is correct. Unfortunately, there was no available time or funds to consider this further.

It was also discouraging that over 30 minutes of computer time on the CDC 6600 was required to obtain the small step size required to resolve the near field shock waves.

4. SUMMARY AND CONCLUSIONS

A research project was conducted which resulted in the development of an extended version of the MIRADCOM (Jackson) Infrared Radiation Computer Model.

The extended computer code was validated by comparing the predicted spectral radiance of H_2O and CO_2 in the 2.7-μm and 4.3-μm wavelength bands with experimental data and with predictions of the NASA (Reardon) Radiation Computer Code. The predicted results agree fairly well with the NASA code even though there were some slight differences. With the exception of a few results for low pressure CO_2, the predicted values were within ± 20% of the measured values.

The infrared computer code was used to predict the infrared radiation emitted in the wavelength interval 4 to 5 microns from the exhaust of a full scale turbojet aircraft. The predicted results appeared to be reasonable when compared with the available test data.

The infrared radiation band model was used to calculate the variation of infrared radiation along the exhaust plume of a small kerosene/gaseous oxygen rocket engine. The temperature and species concentration profiles were predicted using the LAPP and REP3 computer codes. The agreement between the theoretical calculations and the experimental measurements was poor. The lack of agreement was due to the fact that the calculated temperature distributions did not exhibit the spatial structure due to shock waves that are evident in the measured infrared data and are visible in photographs of the exhaust plume. There appears to be short comings in the ability of both the LAPP and REP3 codes to predict the correct spatial distributions of temperature and specie concentrations.

The Gas Dynamics Finite Difference Computer Model developed as part of this project was only partially completed and was able to produce reasonable numerical results at the expense of long computer runs and high computer memory requirements. The code successfully calculated the flow field for flow geometries having solid boundaries, but had problems with the free boundaries encountered in nozzle exhaust plumes. The results obtained for the near field of the nozzle appeared to be correct, but the downstream results were not validated.

The preliminary calculations obtained using the REP3 and TKE computer codes did not agree with the experimental data.

Due to the partial success of the finite difference and REP3 computer codes, further development and assessment are required before these codes are fully operational in a validated model.

REFERENCES

1. Edelman, R. B., and Weilerstein, G., "A Solution of the Inviscid-Viscid Equations with Applications to Bounded and Unbounded Multicomponent Reacting Flows," AIAA 7th Aerospace Science Meeting, New York, AIAA Paper 69-83, Jan. 1969.

2. Patankar, S. V., and Spalding, D. B., Heat and Mass Transfer on Boundary Layers, International Textbook Company, Ltd. London, 1970.

3. Greenwood, T., Seymore, D., Prozan, R., and Ratliff, A., "Analysis of Liquid Rocket Engine Exhaust Plumes," Journal of Spacecraft and Rockets, Vol. 8, Feb. 1971, pp. 123-128.

4. Peters, C. E., and Phares, W. J., An Integral Turbulent Kinetic Energy Analysis of Free Sheer Flows, NASA Langley Working Conference on Free Turbulent Flows, NASA Langley Research Center, Hampton, VA, July 20-21, 1972, in NASA SP-312, 1973.

5. Mikatarian, R. R., Kau, C. J., and Pergament, H. S., Air Force Rocket Propulsion Laboratory, "A Fast Computer Program for Non-equilibrium Rocket Plume Predictions," AeroChem Research Laboratories, Aug. 1972, (AFRPL-TR-72-94).

6. Wilson, A. S., "Modeling of Chemically-Reacting Turbulent Plumes," JANNAF 7th Plume Technology Meeting, June 1973.

7. Mikatarian, R. R., Prediction of Afterburning Rocket Exhaust Plume Properties Using an Eddy Breakup Model, presented at the 8th JANNAF Plume Technology Conference at the U.S. Air Force Academy, Colorado Springs, 1974.

8. Kelly, J. T. and Pergament, H. S., "A Fully Coupled Underexpanded After-burning Rocket Plume Program," AFRPL-TR-74-59, Nov. 1974 and AFRPL-TR 75-52, Dec. 1975.

9. Pergament, H. S., and Thorpe, R. D., "A Computer Code for Fully-Coupled Rocket Nozzle Flows (FULLNOZ)," Air Force Office of Scientific Research, AeroChem Research Lab, Princeton, N. J., AFOSR-TR-1563 (AeroChem TP-3221) April 1975.

10. Vaglio Laurin, R., "A Theoretical Model of Low Altitude Rocket Plume," Advanced Technology Laboratories, ATL TR 218, June 1975.

11. Jensen, D. E. and Wilson, A. S., "Prediction of Rocket Exhaust Flame Properties," Combustion and Flame, Vol. 25, pp. 43-55, 1975.

12. Spalding, D. B., Description of CHAM Computer Codes, JANNAF Exhaust Plume Working Group Low Altitude Plume Technology Workshop, Huntsville, AL, June 1977.

13. Smoot, L. D. and Purcell, W. E., "Model for Mixing of a Compressible Free Jet with a Moving Environment," AIAA Journal, Vol. 5, No. 11, pp 2049-2052, 1967, also Tufts, L. W. and Smoot, L. D., "A Turbulent Mixing Coefficient Correlation for Coaxial Jets with and without Secondary Flows," J. Spacecraft and Rockets, Vol. 8, No. 12, pp 1183-1190, 1971.

14. Stowell, D. W., and Smoot, L. D., Turbulent Mixing Correlations in Free and Confined Jets, AIAA Paper 73-1194, Nov. 1973.

15. Byrd, M., "Plume Modeling Study Results," JANNAF Exhaust Plume Working Group Low Altitude Plume Technology Workshop, Huntsville, AL, June 1977.

16. Rhodes, B., "Comparison of Experimental Results and Calculated Results using LAPP," JANNAF Exhaust Plume Working Group Low Altitude Plume Technology Workshop, Huntsville, AL, June 1977.

17. Jensen, D., "Comparison of REP3 Results with Experimental Data," JANNAF Exhaust Plume Working Group Low Altitude Plume Technology Workshop, Huntsville, AL, June 1977.

18. Harwell, K. E., Fuller, C. E. III, Jackson, H. T., Jr., and Poslajko, F., "Three Dimensional Laser Doppler Velocimeter Measurements of the Velocity Distribution in a Supersonic Jet Mixing with a Subsonic Outer Flow," AIAA Paper 76-24, Jan. 1976; also U.S. Army Missile Command TR RE-76-14, Sept. 1975.

19. Donaldson, C. DuP., and Gray, K. E., "Theoretical and Experimental Investigation of the Compressible Free-Mixing of Two Dissimilar Gases," AIAA Journal, Vol. 4, pp 2017-2025, 1966.

20. Harsha, P. T., Free Turbulent Mixing: A Critical Evaluation of Theory and Experiment, AEDC-TR-71-36, Feb. 1971.

21. Harwell, K. E. "Development of Models for the Infrared Radiation from Exhaust Plumes," Final Report, Contract DAAH01-75-C-0121, Sept. 1976.

22. Jackson, H. T., Jr., "A Model for the Spectral Emissivity of Carbon Dioxide in the 4.3 Micron Band," U.S. Army Missile Command Technical Report RE-TR-69-9, April 1970.

23. Jackson, H. T., Jr., "An Analytical Model for Prediction of the Radiation from Jet Plumes in the Mid-Infrared Spectral Region," U.S. Army Missile Command Technical Report, RE-TR-70-7, April 1970.

24. Ludwig, C. B. Malkmus, W., Reardon, J. E., Thompson, J. A. L., "Handbood of Infrared Radiation from Combustion Gases," NASA SP-3080, 1973.

25. Reardon, J. E., "A Computer Program for the Prediction of Radiation from Rocket Exhaust Plumes," Vols. I and II, Final Report, U.S. Army Contract DAAH01-73-C-0252, May 1973.

26. Sukanek, P. C. and Davis, L. P., "An Assessment of the NASA Band Model Formulation for Calculating the Radiance and Transmission of Hot and Cool Gases," AFRPL-TR-76-9, Feb. 1976.

27. Lindquist, G. H., C. B. Arnold and R. L. Spellicy, "Atmospheric Absorption Applied to Plume Emission," AFRPL-TR-75-30, Aug. 1975.

28. Simmons, F. S., H. Y. Yamada and C. B. Arnold, "Measurement of Temperature Profiles in Hot Gases by Emission-Absorption Spectroscopy," NASA-CR-72491, April 1969.

29. Simmons, F. S., "Band Models for Nonisothermal Radiating Gases," Appl. Optics 5: 11, 1801 (1966).

30. Harwell, K. E., Hyman, W. D., Jackson, H. T. Jr., and Poslajko, F., "Effects of External Flow Velocity of the Spatial Distribution of Infrared Radiation From a Rocket Exhaust Plume," AIAA Paper 76-443, July 1976, also AIAA Paper 76-143, Jan. 1976.

31. Fuller, C. E. III, "Three Dimensional Laser Doppler Velocimeter Turbulence Measurements in a Pipe Flow," Final Report, NASA Marshall Space Flight Center Contract NAS8-25896, April 1973.

32. Schlichting, H., Boundary Layer Theory, McGraw Hill, New York, 1955.

APPENDIX I

LISTING OF IR COMPUTER PROGRAM

```
IIOIXII    II  I                                                    I  II    IIXIQII
//HARWE JOB (36931,51118,REMOTE3,R-192,T-35,L-10),NGUYEN
//STEP1 EXEC FORTGCLG,FORTREG=192K,GOREG=192K
//FORT.SYSPRINT DD DUMMY
//FORT.SYSIN DD *
      COMMON/PLOT1/WAVEI,WAVEF,CENTR,TOTRAD
      COMMON /RASP/RASP
      COMMON /BANDP/ XKK(254,7),DDINV(254,7),UK(254),AKU(254)
      DIMENSION I6(3),I8(10),I7(6),I2(10),I3(6),I4(4),I5(10),I1(5)
      COMMON /RPM1/ NWAV,WAVNO(254),WAVLT(254)
      COMMON/CHECK/IREAD
      COMMON /INDATA/ X(40),R(40,30),T(40,30),PCO2(40,30),
     $   PH2O(40,30),PN2(40,30),PO2(40,30),PCO(40,30),PH2(40,30)
      COMMON /CTROL/ TITLE(12),KOUNT,NXS,NORUN
      COMMON /OTH/ PP,RJ,NRP(40)
      COMMON /SWITCH/ KSWIT   ,IXXJG
C
      DIMENSION RADSTL(254),RADXT(254),TRLAST(254)              000130
      DIMENSION CR(100),CX(100),CL(100)                        000140
      DIMENSION RADXL(254),RRN(100)
      DIMENSION STRAD(40)
      DIMENSION RAD(254),RADX(254),TRNS(254),P(254),O(254),RADSTR(254)  000230
      DIMENSION WAVL5(254)                                     000240
      DIMENSION RCALC(100)                                     000260
      DIMENSION SRAD(254),SRADSR(254)
      INTEGER IH2O(2),ICO2(2),IWRT(2)
      REAL HRADXT(40),CRADXT(40)
      REAL HCTOTX(40),HCRDXT(40)
      REAL HRADX(254),CRADX(254),SRADX(254)
      EQUIVALENCE (HRADX(1),RADX(1)),(CRADX(1),RAD(1)),
     $   (SRADX(1),TRNS(1))
      EQUIVALENCE (HCTOTX(1),CR(1)),(HCRDXT(1)  ,CX(1))
C
      DATA I6N/10/
      DATA I8N/37/
      DATA I7N/23/
      DATA I2N/33/
      DATAI3N/25/
      DATA I4N/19/
      DATA I5N/49/
      DATA I1N/20/
      DATA ASTER,RCALC/1H*,100*1H /                            000300
      DATA IDISC/8/
      DATA ISTOP/0/
      DATA IDSCT/0/
    . DATA JPASS/0/
      DATA IFLG/0/
      ISWIT = 2
      KSWIT = 2
      JSWIT=2
      LSWIT = 1
      IREAD=0
      KPZQ=0
      NZQ=1
      KNTQ=0
      IXXJG=0
C
C    SENSE SWITCH 1 SET--YES,PRINT FLOW FIELD DATA
C    SENSE SWITCH 2 SET--YES,CO2 RADIATION--NO,H2O RADIATION
C    SENSE SWITCH 3 SET--YES,AEROCHEM INPUT TAPE--NO, MOTOR DATA INPUT TAPE
C    SENSE SWITCH 4 SET--YES,H2O AND CO2 RADIATION COMBINED
 .C
```

```
      TOTRAD=0.0                                                        000590
C
C     SET PRINT LABEL
C
C
C     DETERMINE MODE OF INPUT TAPE -- MOTOR DATA OR AEROCHEM
C
  172 CONTINUE
      END FILE 9
      REWIND 9
      END FILE 8
      REWIND 8
      IF(KPZQ.EQ.1) GO TO 104
      GO TO (101,102),JSWIT
  102 CONTINUE
      CALL READER
      KPZQ=1
      GO TO 104
  101 CONTINUE
  104 CONTINUE
C
      NXS=KOUNT
      DO 111 I=1,NXS
      IF(NRP(I).GT.25) GO TO 111
      NRP1=NRP(I)+1
      ISET=NRP(I)
      DO 112 KK=NRP1,25
      R(I,KK)=R(I,ISET)
      T(I,KK)=T(I,ISET)
      PCO2(I,KK)=PCO2(I,ISET)
      PH2O(I,KK)=PH2O(I,ISET)
      PN2(I,KK)=PN2(I,ISET)
      PO2(I,KK)=PO2(I,ISET)
  112 CONTINUE
  111 CONTINUE
C
C     READ WAVELENGTHS AND CORRESPONDING BAND PARAMETERS
C     READ IN H2O BAND DATA FIRST FOLLOWED BY CO2 BAND DATA
C
   47 CONTINUE
      IF(LSWIT  .EQ.1.AND.ISTOP.EQ.3.AND.IFLG.LT.2) GO TO 21
      IF(ISTOP.EQ.3) GO TO 23
   21 CONTINUE
      WRITE (6,9911)                                                    000330
      READ (5,9912) NWAV1, NWAV2                                        000340
      WRITE (6,10035) NWAV1,NWAV2
10035 FORMAT(10H  NWAV1     ,2(1X,I5))
 9912 FORMAT(2I10)
      NWAV=1 + ((NWAV2-NWAV1)/25)                                       000360
      DO 1 I=1,NWAV                                                     000380
      IF(KNTQ.EQ.0) GO TO 9957
      GO TO 9967
 9957 READ (5,9922) WAVNO(I),(XKK(I,J),J=1,7)
 9922 FORMAT (F9.1,7E9.2)                                               000400
      GO TO 9977
 9967 READ (5,9922) WAVNO(I),(XKK(I,J),J=1,7)
 9977 CONTINUE
      WRITE (6,10037) WAVNO(I),(XKK(I,J),J=1,7)
10037 FORMAT(10H   WAV     ,F9.1,7E9.2)
      IF(KNTO.EQ.0) GO TO 9987
      GO TO 9997
 9987 READ (5,9001) WAVNO(I),(ODINV(I,J),J=1,7)
 9001 FORMAT(F6.1,F9.2,6E10.2)
      GO TO 9947
 9997 READ (5,9010) WAVNO(I),(ODINV(I,J),J=1,7)
 9010 FORMAT (F6.1,F9.2,6E10.2)
```

```
 9947 CONTINUE
      WRITE (6,10037) WAVNO(I),(DDINV(I,J),J=1,7)
      WAVLT(I)=10000./WAVNO(I)                                      000420
 9910 FORMAT (1X,8E15.7)                                            000450
    1 WAVL5(I)=WAVLT(I)**5                                          000460
      WAVEI=WAVNO(1)                                                000470
      WAVEF=WAVNO(NWAV)                                             000480
      WRITE (6,9911)                                                000490
 9911 FORMAT (1H1)                                                  000500
      DO 9913 I=1,NWAV                                              000510
      DO 9913 J=1,7                                                 000520
      IF (DDINV(I,J) .LE. 0.0) DDINV(I,J)=1.0E-20                   000530
      IF(XKK(I,J).LE.0.) XKK(I,J)=1.0E-20
 9913 CONTINUE                                                      000540
 9000 FORMAT(F9.4,7E9.3)
C
C    PRINT BAND PARAMETERS IF OPTIONED SELECTED
C
      IF(LSWIT   .EQ.1.AND.ISTOP.EQ.0.AND.IFLAG.LT.1)CALL SAVE1
      IF(ISWIT   .EQ.1) CALL BPPRT
C
   23 CONTINUE
      IF(LSWIT   .EQ.1.AND.ISTOP.EQ.3.AND.IFLG.GE.2) CALL SWAP
      IFLG=IFLG+1
C
C    DETERMINE INPUT DATA PRINT OPTIONS
C
C SUBROUTINE PRMD WRITES OUT INPUT FLOW FIELD DATA
      IF(ISWIT   .EQ.1) CALL PRMD
C                                                                  001520
C     ALPHA=ASPECT ANGLE IN DEGREES(0 DEG=NOSE-ON)                001530
C     ISTOP=1,WILL TERMINATE PROGRAM AFTER SINGLE ALPHA CALCULATION 001540
C     ISTOP=2,RETURNS TO THIS POINT FOR ANOTHER ALPHA             001550
C     ISTOP=3,RETURNS TO STMT 172 TO READ NEW SET FLOW FIELD DAT1  001560
C   SENSE SWITCH 4 WILL OVER RIDE ANY ISTOP OPTION
C                                                                  001570
  103 READ(5,1010)ALPHA,ISTOP                                      001580
 1010 FORMAT(F10.5,I5)                                             001590
      ALP=ALPHA/57.295780                                          001600
      CC=COS(ALP)                                                  001610
      SC=SIN(ALP)                                                  001620
      PI=3.1415926                                                 001630
      TRADX=0.0                                                    001640
      TOTRAD=0.0                                                   001650
      CENTER=0.0
C
      DO 185 II=1,NWAV                                             001670
  185 RADXT(II)=0.0                                                001680
C
      WRITE (6,1401)                                               001690
      DO 3000 I=1,NXS                                              001700
      NZPEX=NRP(I)
      WRITE (6,1401)                                               001710
 1401 FORMAT (1H1)                                                 001720
      WRITE (6,1404) (TITLE(JRR),JRR=1,12)                         001730
 1404 FORMAT(10X,12A4,42,/)                                        001740
      WRITE (6,1400) I,X(I),ALPHA                                  001750
 1400 FORMAT (1X,12HSTATION NO.=,I4,5X,17HAXIAL DIST. (CM)=,F10.3,5X, 001760
     #17HASPECT ANGLE (DEG)=,F5.1,/)
      TRADX=0.0                                                    001780
      IXO=I                                                        001800
      RO=R(IXO,25)                                                 001910
      IF (RO .LE. 0.0) RO=1.0E-20                                  001920
      XO=X(IXO)+.01                                                001830
      IF(ALPHA.EQ.180.0) XO=X(NXS)                                 001840
      ZPEX=NZPEX                                                   001850
```

-66-

```
C        ****CHANGE DELZ=RO/ZPEZ TO DELZ=1. FOR THE SLAP***
         DELZ=1.0
         DELZ=RO/ZPEX
C        ******* SET NZU=NZPEX FOR TOTAL PLUME *****
         ZU=RASP/DELZ
         NZU=NZPEX
C
         DO 190 II=1,NWAV                                               001870
         SRADSR(II)=0.0
  190    RADX(II)=0.0                                                   001880
         STOT=0.
C
C        THIS CARD HAS BEEN CHANGED AS
C        DO 2000 M=1,NZPEX
         DO 2000 M=1,NZU
         ZM=M                                                           001910
         ZO=DELZ*(ZM-1.)                                                001920
         IF(ALPHA.EQ.0.0) RO=2.*R(1,25)+(ZM-1.)*(R(NXS,25)-2.*R(1,25))/ZPEX001930
         IF(ALPHA.EQ.180.0) RO=(ZM-1.)*(R(NXS,25))/ ZPEX               001940
C                                                                       001950
C***********************************************************************001960
C        CALCULATE COORDINATES X,R ALONG LINE-OF-SIGHT AS FUNCTION OF ITS 001970
C        LENGTH                                                         001980
C                                                                       001990
         DELL=10.                                                       002000
         IF(ALPHA.EQ.0.0.OR.ALPHA.EQ.180.0) DELL=X(NXS)/98.            002010
  200    XL=0.                                                          002020
C
         DO 203 J=1,100                                                 002030
         N=J                                                            002040
         APR=XL*SC-SQRT(RO*RO-ZO*ZO)                                    002050
         CR(N)=SQRT(ZO*ZO+APR*APR)                                      002060
         CX(N)=XO+XL*CC                                                 002070
         CL(N)=XL                                                       002080
         IF(CX(N).LT.0.) GO TO 204                                      002090
         IF(CX(N).GT.X(NXS)) GO TO 204                                  002100
         IF(ALPHA.EQ.0.0.OR.ALPHA.EQ.180.0) GO TO 203                  002110
         DO 201 K=1,NXS                                                 002120
         KI=K                                                           002130
         IF(CX(N).LE.X(K)) GO TO 202                                    002140
  201    CONTINUE                                                       002150
  202    IF(CR(N).GT.R(KI,25) .AND. N .GT. 10) GO TO 204               002170
  203    XL=XL+DELL                                                     002180
C                                                                       002190
C     DELL TOO SMALL,INCREASE AS FOLLOWS                               002200
C                                                                       002210
         DELL=DELL*1.5
         GO TO 200
  204    CONTINUE
         IF(N.GE.50) GO TO 299
C                                                                       002260
C        DELL TOO LARGE,DECREASE AS FOLLOWS                            002270
C                                                                       002280
  205    DELL=CL(N)/50.                                                 002300
C
C        PLUME THICKNESS NEGLIGIBLE AT THIS POINT,MOVE ON TO NEXT POINT 002320
C        AFTER SETTING ALL SPECTRAL RADIATION VALUES EQUAL TO ZERO     002330
C                                                                       002340
         IF(DELL.GT..005) GO TO 200
  210    CONTINUE
C
         DO 211 II=1,NWAV
         RADSTL(II)=0.0                                                 002390
  211    RADSTR(II)=0.0                                                 002400
         GO TO 1990                                                     002450
C                                                                       002460
```

```
C*********************************************************************002470
C     CALCULATE PRESSURE AND TEMPERATURE ALONG LINE-OF-SIGHT AT EACH X,R002480
C                                                                     002490
  299 CONTINUE
      WRITE(6,307)DELZ,DELL
  307 FORMAT(2(1X,E10.4))
C
      DO 300 II=1,NWAV
      P(II)=0.0                                                        002510
      Q(II)=0.0
      TRNS(II)=1.0                                                     002530
  300 RADSTR(II)=0.0                                                   002540
C
      DO 1000 J=1,N                                                    002560
      JCHECK=J                                                         002570
C
      DO 301 L=2,NXS
      IF(JCHECK.EQ.99) LCHECK=3
      NX1=L-1
      NX2=L
      IF(CX(J).LE.X(L)) GO TO 302
  301 CONTINUE
C
  302 CONTINUE
      DO 303 L=2,25
      IF(JCHECK.EQ.99) LCHECK=3
      NR2=L
      IF(CR(J).LE.R(NX2,L)) GO TO 304
  303 CONTINUE
C
  304 CONTINUE
      DO 305 L=2,25
      NR1=L
      IF(CR(J).LE.R(NX1,L)) GO TO 306
  305 CONTINUE
C
  306 CONTINUE
      DR1=CR(J)-R(NX1,NR1-1)
      DR2=R(NX1,NR1)-R(NX1,NR1-1)
      DR3=CR(J)-R(NX2,NR2-1)
      DR4=R(NX2,NR2)-R(NX2,NR2-1)
      DX1=CX(J)-X(NX1)
      DX2=X(NX2)-X(NX1)
C
C     DR1DR2,DR3DR4,DX1DX2 WERE CREATED TO ELIMINATE INDEFINITE FORMS  002760
C
      DR1DR2=0.0                                                       002770
      DR3DR4=0.0                                                       002780
      DX1DX2=0.0                                                       002790
      IF(DR2.NE. 0.0) DR1DR2=DR1/DR2                                   002800
      IF(DR4.NE. 0.0) DR3DR4=DR3/DR4                                   002810
      IF(DX2 .NE. 0.0) DX1DX2=DX1/DX2                                  002820
      TX1=T(NX1,NR1-1)+(T(NX1,NR1)-T(NX1,NR1-1))*DR1DR2
      TX2=T(NX2,NR2-1)+(T(NX2,NR2)-T(NX2,NR2-1))*DR3DR4
      CT=TX1+(TX2-TX1)*DX1DX2                                          002850
      PH2OX1=PH2O(NX1,NR1-1)+(PH2O(NX1,NR1)-PH2O(NX1,NR1-1))*DR1DR2
      PH2OX2=PH2O(NX2,NR2-1)+(PH2O(NX2,NR2)-PH2O(NX2,NR2-1))*DR3DR4
      CPH2O=PH2OX1+(PH2OX2-PH2OX1)*DX1DX2                              00289)
C
      IF(JCHECK.EQ.99)LCHECK=11                                        002900
      PCO2X1=PCO2(NX1,NR1-1)+(PCO2(NX1,NR1)-PCO2(NX1,NR1-1))*DR1DR2
      PCO2X2=PCO2(NX2,NR2-1)+(PCO2(NX2,NR2)-PCO2(NX2,NR2-1))*DR3DR4
      CPCO2=PCO2X1+(PCO2X2-PCO2X1)*DX1DX2                              00293)
C
      PN2X1=PN2(NX1,NR1-1)+(PN2(NX1,NR1)-PN2(NX1,NR1-1))*DR1DR2
      PN2X2=PN2(NX2,NR2-1)+(PN2(NX2,NR2)-PN2(NX2,NR2-1))*DR3DR4
```

-68-

```
      CPN2=PN2X1+(PN2X2-PN2X1)*DX1DX2
      PO2X1=PO2(NX1,NR1-1)+(PO2(NX1,NR1)-PO2(NX1,NR1-1))*DR1DR2
      PO2X2=PO2(NX2,NR2-1)+(PO2(NX2,NR2)-PO2(NX2,NR2-1))*DR3DR4
      CPO2=PO2X1+(PO2X2-PO2X1)*DX1DX2
C
      PH2X1=PH2(NX1,NR1)+(PH2(NX1,NR1)-PH2(NX1,NR1-1))*DR1DR2
      PH2X2=PH2(NX2,NR2-1)+(PH2(NX2,NR2)-PH2(NX2,NR2-1))*DR3DR4
      CPH2=PH2X1+(PH2X2-PH2X1)*DX1DX2
      PCOX1=PCO(NX1,NR1)+(PCO(NX1,NR1-1)-PCO(NX1,NR1-1))*DR1DR2
      PCOX2=PCO(NX2,NR2-1)+(PCO(NX2,NR2)-PCO(NX2,NR2-1))*DR3DR4
      CPCO=PCOX1+(PCOX2-PCOX1)*DX1DX2
      IF(CT.LT.300.) CT=300.                                      002940
      IF(CPH2O.LT.0.) CPH2O=1.E-20
      IF(CPCO2.LT.0.) CPCO2=1.E-20
      IF(CPN2.LT.0.) CPN2=1.E-20
      IF(CPO2.LT.0.) CPO2=1.E-20
      IF(CPH2.LT.0.0)CPH2=1.E-20
      IF(CPCO.LT.0.0)CPH2=1.E-20
C
C     AVERAGE TEMPERATURES AND PRESSURES FOR BLOCK               002980
C
      IF(J.GT.1) GO TO 20
      CPH2OL=CPH2O
      CPCO2L=CPCO2
      CPN2L=CPN2
      CPO2L=CPO2
      CPH2L=CPH2
      CPCOL=CPCO
      CTL=CT
   20 CONTINUE
C
      PCO2AV=(CPCO2+CPCO2L)/2.                                    003000
      PH2OAV=(CPH2O+CPH2OL)/2.                                    002990
      PN2AV=(CPN2+CPN2L)*.5
      PO2AV=(CPO2+CPO2L)*.5
      PCOAV=(CPCO+CPCOL)/2.
      PH2AV=(CPH2+CPH2L)*0.5
C
      TAV=(CT+CTL)/2.                                             003020
      CPH2OL=CPH2O                                                003030
      CPCO2L=CPCO2                                                003040
      CPN2L=CPN2
      CPO2L=CPO2
      CPH2L=CPH2
      CPCOL=CPCO
      CTL=CT                                                      003070
      IF(J.EQ.1) GO TO 1000                                       003080
      CALL PARAM(TAV,DELL,PH2OAV,PN2AV,PO2AV,PCO2AV,PCOAV,PH2AV)
 1002 CONTINUE
C
      DO 2005 II=1,NWAV                                           003100
      TRLAST(II)=TRNS(II)                                         003110
      P(II)=P(II)+UK(II)
      Q(II)=Q(II)+AKU(II)                                        003130
      IF (P(II) .EQ. 0.0) P(II)=1.0E-20                          003140
      IF (Q(II) .EQ. 0.0) Q(II)=1.0E-20                          003150
      ARG=-P(II)/ SQRT(1.+.25*P(II)**2/Q(II))
      TRNS(II)=EXP(ARG)                                          003180
      RAD(II)=(TRLAST(II)-TRNS(II))*37413./WAVG5(II)/(EXP(1.439*WAVNO(II003190
     1   )/TAV)-1.)/3.1415926536                                 003200
      RADSTR(II)=RADSTR(II)+RAD(II)
      SRAD(II)=RAD(II)*10000./WAVNO(II)   **2
      SRADS2(II)=SRADS2(II)+SRAD(II)
 2005 CONTINUE
 1000 CONTINUE                                                   003230
C
```

-69-

```
      WRITE (6,2023)
 2023 FORMAT (20X,'SPECTRAL RADIATION',/,10X,'WAVNO',10X,'SRADSR')
      DO 2022 II=1,NWAV
 2001 STOT = STOT+SRADSR(II)
C     WRITE(6,2024)WAVNO(II),SRADSR(II)
C       ***TAKE OUT WRITE STATEMENT OF SRADSR(II)***
 2024 FORMAT(2(10X,E10.4))
 2022 CONTINUE
      CHECK=1.                                                     003260
C
C     RAD(II)=RADIATION FOR EACH BLOCK AT EACH WAVELENGTH (WAVLT(II))
C     RAD(II) IN(WATTS/CM2-SR-MICRON))
C     RADX(II) IN (WATTS/CM-SR-MICRON)
C     TRADX IN (WATTS/CM-SR)
C     RADXT(I) IN (WATTS/SR/MICRON)
C     RADSTR(II)=RADIATION AT EACH X AND Z SUMMED OVER EACH PATH LENGTH
C     RADX(II)=RADIATION TOTAL AT EACH X-STATION (SUMMED OVER Z)
C     TRADX=RADX(I) INTEGRATED OVER WAVELENGTH                     003290
C     RADXT(I)=RADX(I) INTEGRATED OVER ALL X-STATIONS             003300
C     TOTRAD=TRADX INTEGRATED OVER X                              003310
C
 1980 CONTINUE
 1990 IF (M.EQ.1) GO TO 1998                                       003320
      CHECK=2.                                                     003330
      IF(ALPHA.NE.0..AND.ALPHA.NE.180.) GO TO 1996
 1981 DO 1982 II=1,NWAV                                            003360
      IO=II-1
 1982 RADXT(II)=RADXT(II)+(RADSTR(II)+RADSTL(II))/2.*PI*DELZ**2*((ZM-1.)003370
     1**2-(ZM-2.)**2)                                              003380
      CHECK=3.                                                     003390
C     THIS CARD HAS BEEN CHANGED AS
C.    IF (M.EQ.NZPEX) GO TO 3001
      IF (M.EQ.NZU) GO TO 3001
      GO TO 1998                                                   003410
 1996 DO 1997 II=1,NWAV                                            003420
C     INTEGRATED RADIATION IS DOUBLED TO INCLUDE BOTH HALVES OF PLUME  003430
      RADX(II)=RADX(II)+(RADSTR(II)+RADSTL(II))
C       THIS CARD HAS BEEN CHANGED AS
C     IF (M.EQ.NZPEX) RAD(II)=RADX(II)+RADSTR(II)
      IF (M.EQ.NZU) RAD(II)=RADX(II)+RADSTR(II)
 1997 CONTINUE
 1998 DO 1999 II=1,NWAV                                            003450
      IO=II-1
 1999 RADSTL(II)=RADSTR(II)                                        003460
 2000 CONTINUE                                                     003470
      WRITE (6,2002)STOT
 2002 FORMAT (1X,'SUM UP SRADSR AT X STATION',5X,E10.4)
      WRITE(6,1402)
 1402 FORMAT(8X,'WAVE NUMBER',5X,'WAVE LENGTH',5X,'RADIATION',
     $    23X,'WAVE NUMBER',5X,'WAVE LENGTH',6X,'RADIATION'/)
      WRITE(6,14021)
14021 FORMAT(42X,'W/SR/CM/MICRON')
C
      LINCT=0
      DO 12 II=1,NWAV,2
      RADX(II)=RADX(II)*DELZ
      IF(II.GT.NWAV) RADX(II+1)=RADX(II+1)*DELZ
      IF(RADX(II).GT.0.) WRITE(6,18) RADX(II)
   18 FORMAT(' NEGATIVE RADIATION IS ILLOGICIAL ',E14.4)
      IF((II+1).GT.NWAV) GO TO 15
      WRITE(6,16) WAVNO(II),WAVLT(II),RADX(II),
     $    WAVNO(II+1),WAVLT(II+1),RADX(II+1)
   16 FORMAT(5X,F10.0,F16.4,7X,E12.5,20X,F10.0,F16.4,7X,E12.5)
      LINCT=LINCT+1
      IF(LINCT.GT.54) GO TO 12
      LINCT=0
```

-70-

```
   12 CONTINUE
      GO TO 17
   15 CONTINUE
      WRITE(6,16) WAVNO(II),WAVLT(II),RADX(II)
   17 CONTINUE
C
 1403 FORMAT (1X,F10.0,F16.4,7X,E12.5)                                003530
      DO 2997 II=2,NWAV                                               003560
      TRADX=TRADX+(WAVLT(II-1)-WAVLT(II))*
     $ (RADX(II-1)+RADX(II))*.5
 2997 CONTINUE
      IF (I.EQ.1) GO TO 2999                                          003710
      CENTER = CENTER+(X(I)-X(I-1))*0.5*(TRADX+TRADXL)*X(I)
      TOTRAD=TOTRAD+(TRADX+TRADXL)*0.5*(X(I)-X(I-1))                   003730
      STRAD(I)=(TRADX+TRADXL)*0.5*(X(I)-X(I-1))
      DO 2998 II=1,NWAV                                               003740
      RADXT(II)=RADXT(II)+((RADX(II)+RADXL(II))/2.
     $ )*(X(I)-X(I-1))*SC
 2998 CONTINUE
      WRITE(6,5000) TOTRAD
 5000 FORMAT(1H0,24HTOTAL RADIATION EMITTED=,E10.4,11H WATTS/STER)
      WRITE(6,1402)
      DO 5001 II=1,NWAV,2
      IF((II+1) .GT. NWAV) GO TO 5002
      WRITE(6,16) WAVNO(II),WAVLT(II),RADXT(II),WAVNO(II+1),WAVLT(II+1)
     +,RADXT(II+1)
 5001 CONTINUE
 5002 CONTINUE
      WRITE(6,16) WAVNO(II),WAVLT(II),RADXT(II)
 2999 TRADXL=TRADX                                                    003760
      DO 2995 II=1,NWAV                                               003770
 2995 RADXL(II)=RADX(II)                                              003780
      RRN(I)=TRADX                                                    003790
      WRITE (6,1492) I,TRADX                                          003800
 1492 FORMAT(/5X,'TOTAL RADIATION FOR STATION',I3,1X,1H=,1X,E12.5,
     1        'WATTS/SR/CM')
C
C    CHECK FOR COMBINE RUN.  IF SO OUTPUT DATA TO DISC
C
      IF(LSWIT  .EQ.2) GO TO 22
      WRITE(IDISC) NWAV,I,TRADX
      WRITE(IDISC) (WAVNO(JJ),WAVLT(JJ),RADX(JJ),JJ=1,NWAV)
      IDSCT=IDSCT+1
   22 CONTINUE
 3000 CONTINUE                                                        003820
      WRITE (6,1401)                                                  003830
      CENTR=0.0                                                       003880
 3001 CONTINUE
 3003 CENTR=CENTER *SC/TOTRAD
      TOTRAD=TOTRAD*SC                                                003920
      IF (TOTRAD .EQ.0.) TOTRAD=1.*10.**(-30)
      IF(LSWIT  .EQ.1) WRITE(IDISC) TOTRAD,(RADXT(J),J=1,NWAV)
 3004 WRITE (6,1404) (TITLE(J),J=1,8 )                                003910
      WRITE (6,1405)
 1405 FORMAT (70X,'STATION RADIATION (W/SR)')
      WRITE (6,1407)(X(II),RRN(II),STRAD(II),RCALC(II),II=1,NXS)
 1407 FORMAT (F15.2,28X,E13.7,20X,E13.7,1X,A1)
C
      WRITE (6,8421)                                                  004030
C    CALL FINAL PLOT ROUTINE
C
C
 8421 FORMAT(/10X,83H* RADIATION VALUE WAS CALCULATED BASED ON THE SLOPE004040
     *  BETWEEN THE PREVIOUS TWO POINTS)                              004050
      WRITE(6,1211) TOTRAD
 1211 FORMAT(1H0,24HTOTAL RADIATION EMITTED=,E10.4,11H WATTS/STER)     004080
```

```
      IF(LSWIT  .EQ.1) WRITE(IDISC) TOTRAD
      WRITE(6,1254) CENTR                                           004090
 1254 FORMAT(1H0,9HCENTROID=,E11.4,'CM')
C
C    CHECK FOR COMBINED RUN. SENSE SWITCH 4 WILL OVER RIDE THE ISTOP OPTION
C
      IF(LSWIT  .EQ.1) GO TO 24
      GO TO (107,103,172),ISTOP                                     004280
C
C    DETERMINE IF ANOTHER PASS IS TO BE PREFORMED
C
   24 CONTINUE
      JPASS=JPASS+1
      IDISC=IDISC+1
      KSWIT=1
      IF(JPASS.LT.2) GO TO 47
      KSWIT=2
      JPASS=0
      IDISC=8
C
C    READ H2O AND CO2 RADIATION BACK FROM DISC.
C    SUM AND OUTPUT
C
      END FILE 9
      REWIND 9
      END FILE 8
      REWIND 8
      WRITE(6,27)
   27 FORMAT(1H1,30X,' C O M B I N E D   H 2 0   C O 2   R A D I A T I O N
     S  S U M S')
      WRITE(6,28) NWAV1,NWAV2
   28 FORMAT(1H ,/,43X,'SUMMED OVER WAVE NUMBERS ',2I6)
C
      DO 25 JK=1,NXS
      READ(8) NWAV,I,CTRADX
      READ(9) NWAV,I,HTRADX
      CALL ERRCHK(2)
      READ(8) (WAVNO(JJ),WAVLT(JJ),CRADX(JJ),JJ=1,NWAV)
      READ(9) (WAVNO(JJ),WAVLT(JJ),HRADX(JJ),JJ=1,NWAV)
      CALL ERRCHK(3)
      DO 26 JJ=1,NWAV
      SRADX(JJ)=HRADX(JJ)+CRADX(JJ)
   26 CONTINUE
      HCTOTX(JK)=HTRADX+CTRADX
C
      WRITE(6,9911)
      WRITE(6,1402)
      DO 29 JJ=1,NWAV,2
      IF((JJ+1).GT.NWAV) GO TO 30
      WRITE(6,16) WAVNO(JJ),WAVLT(JJ),SRADX(JJ),
     S   WAVNO(JJ+1),WAVLT(JJ+1),SRADX(JJ+1)
   29 CONTINUE
      GO TO 31
   30 CONTINUE
      WRITE(6,16) WAVNO(JJ),WAVLT(JJ),SRADX(JJ)
   31 CONTINUE
C
      WRITE(6,32) I,HCTOTX(JK)
   32 FORMAT(//10X,' TOTAL COMBINED RADIATION FOR STATION ',I3,
     S   ' IS ',E12.4)
      IF(HCTOTX(IS).EQ.0.0.) GO TO 25
   25 CONTINUE
C
      READ(8) CTORAD ,(CRADXT(J),J=1,NWAV)
      READ(9) HTORAD ,(HRADXT(J),J=1,NWAV)
      CALL ERRCHK(4)
```

-72-

```
      WRITE(6,9911)
      WRITE(6,34)
   34 FORMAT(20X,'WAVNO',10X,'WAVELENGTH',10X,'HCRADXT'//)
C     PUNCH CARDS FOR ATMOSPHERIC TRANSMISSION PROGRAM
      NN=NWAV
      DO 33 JJ=1,NWAV
      HCRDXT(JJ)=HRADXT(JJ)+CRADXT(JJ)
      WRITE(6,35) WAVNO(JJ),WAVLT(JJ),HCRDXT(JJ)
   35 FORMAT(17X,E12.4,6X,E12.4,6X,E12.4)
   33 CONTINUE
      STORAD=HTORAD+CTORAD
      WRITE(6,43) (TITLE(J),J=1,8)
   43 FORMAT(1H ///,' SUMMARIES FOR ',7A10,A2/)
      WRITE(6,36) HTORAD
      WRITE(6,37) CTORAD
   36 FORMAT(10X,'TOTAL H2O RADIATION',E14.4)
   37 FORMAT(10X,'TOTAL CO2 RADIATION',E14.4)
      WRITE(6,41)
   41 FORMAT(29X,'---------------')
      WRITE(6,42) STORAD
   42 FORMAT(' TOTAL COMBINED RADIATION',4X,E14.4)
C
      GO TO (107,107,172),ISTOP
  107 CONTINUE
      STOP
      END                                                    004420
      SUBROUTINE READER
C
C     THIS ROUTINE WILL READ ONE COMPLETE BLOCK OF
C     MOTOR DATA PER CALL
C
      COMMON /INDATA/ X(40),R(40,30),T(40,30),PCO2(40,30),
     S   PH2O(40,30),PN2(40,30),PO2(40,30),PCO(40,30),PH2(40,30)
      COMMON /CTROL/ TITLE(12),KOUNT,NXS,NORUN
      COMMON /OTH/ PP,RJ,NRP(40)
      COMMON /RASP/RASP
      DATA JJ/1/
C
      READ(5,100) (TITLE(J),J=1,12)
      WRITE(6,100) (TITLE(J),J=1,12)
  100 FORMAT(12A4)
      READ(5,101)RASP          ──→ This is the radius of the detector. This value does not effect †
      READ(5,300) PP,RJ,NRP(1)
      RJ=RJ*100.
      WRITE(6,300) PP,RJ,NRP(1)
  300 FORMAT(2E10.4,I4)
      KOUNT=0
C
C     NOW READ IN THE ENTIRE BLOCK OF MOTOR DATA
C
   30 CONTINUE
      READ(5,400) X(JJ),ILAST
      X(JJ)=X(JJ)*RJ
      WRITE (6,700)X(JJ)
  400 FORMAT (E10.3,69X,I1)
  700 FORMAT (1X,E10.3)
      IF(ILAST.EQ.1) GO TO 14
  103 FORMAT(I5)
      READ(5,103)NRP(JJ)
      IX=NRP(JJ)
      DO 12 KK=1,IX
C     THE PUNCH DATA INPUT FOR RADIATION PROGRAM IN
C     CHANGE READ (5,500) R(JJ,KK), T(JJ,KK), CARD TO
C     THE FOLLOWING ORDER   PPCO2, PPH2O,PPN2,PPO2
C     +PH2(JJ,KK),PO2(JJ,KK)
C     READ(5,500) R(JJ,KK),T(JJ,KK),PCO2(JJ,KK),PH2O(JJ,KK),
```

-73-

```
      READ(5,500)R(JJ,KK),T(JJ,KK),PCO2(JJ,KK),PH2O(JJ,KK)
  500 FORMAT(E10.3,20X,3E10.3)
      R(JJ,KK)=R(JJ,KK)*RJ
      PCO(JJ,KK)=1.0E-20
      PH2(JJ,KK)=1.0E-20
      PO2(JJ,KK)=1.0E-20
      PN2(JJ,KK)=1.0E-20
      WRITE(6,600) R(JJ,KK),T(JJ,KK),PN2(JJ,KK),PCO(JJ,KK),PCO2(JJ,KK),
     +PH2O(JJ,KK),PO2(JJ,KK)
  600 FORMAT (1X,8E10.4)
   12 CONTINUE
      JJ=JJ+1
  101 FORMAT(E10.4)
      KOUNT=KOUNT+1
      GO TO 30
   14 CONTINUE
      CALL LIMIT(KOUNT,40,1)
      CALL LIMIT(NRP(1),30,2)
C
      RETURN
      END
      SUBROUTINE LIMIT(IARG,LIM,NPS)
C
      IF(IARG.GE.0.AND.IARG.LE.LIM) RETURN
C
      WRITE(6,10) IARG,LIM,NPS
   10 FORMAT(' ILLEGAL INPUT PARAMETER ',
     $    2I10/' CALLED FROM LOCATION ',I8)
C
      STOP
      END
      SUBROUTINE SWAP
C
      COMMON /BANDP/ XKK(254,7),DDINV(254,7),UK(254),AKU(254)
      COMMON /RPN1/ NWAV,WAVVD(254),WAVLT(254)
C
      DIMENSION XSAVE(254,7),DSAVE(254,7)
C
      DO 10 JJ=1,NWAV
      DO 10 KK=1,7
      XHOLD=XKK(JJ,KK)
      DHOLD=DDINV(JJ,KK)
      XKK(JJ,KK)=XSAVE(JJ,KK)
      DDINV(JJ,KK)=DSAVE(JJ,KK)
      XSAVE(JJ,KK)=XHOLD
      DSAVE(JJ,KK)=DHOLD
   10 CONTINUE
C
      NWVOLD=NWAV
      NWAV=NWLST
      NWLST=NWVOLD
C
      RETURN
C
      ENTRY SAVE1
C
      DO 11 JJ=1,NWAV
      DO 11 KK=1,7
      XSAVE(JJ,KK)=XKK(JJ,KK)
      DSAVE(JJ,KK)=DDINV(JJ,KK)
   11 CONTINUE
C
      NWLST=NWAV
C
      RETURN
      END
```

```
      SUBROUTINE PRMD
C
      COMMON /INDATA/ X(40),R(40,30),T(40,30),PCO2(40,30),
     $   PH2O(40,30),PH2(40,30),PO2(40,30),PCO(40,30),PH2(40,30)
      COMMON /CTROL/ TITLE(12),KOUNT,NXS,NORUN
      COMMON /OTH/ PP,RJ,NRP(40)
C
      WRITE(6,10)
   10 FORMAT(1H1)
      WRITE(6,11) NORUN
   11 FORMAT(1H ,25X,' M O T O R ',I3//)
      WRITE(6,12) KOUNT
   12 FORMAT(1H ,9X,'NUMBER OF X STATIONS IS',I4)
C
      DO 14 JJ=1,KOUNT
      NRP1=NRP(JJ)
      WRITE(6,15) JJ,X(JJ),NRP1
   15 FORMAT(//' X(',I2,') = ',E12.4,
     $   8X,' NUMBER OF POINTS AT THIS X STATION IS',I4)
      WRITE(6,16)
   16 FORMAT(1H ,4X,'R',13X,'T',11X,'CO2',10X,
     $   'H2O',11X,'N2',11X,'O2'/)
      DO 14 KK=1,NRP1
      WRITE(6,18) R(JJ,KK),T(JJ,KK),PCO2(JJ,KK),
     $   PH2O(JJ,KK),PN2(JJ,KK),PO2(JJ,KK)
   18 FORMAT(1H ,6(E12.4,1X))
   14 CONTINUE
C
      RETURN
      END
      SUBROUTINE BPPRT
C
C   THIS ROUTINE PRINTS THE BAND PARAMETERS TOGETHER
C   WITH THE ASSOCIATED WAVENUMBERS AND WAVELENGTHS
C
      COMMON /BANDP/ XKK(254,7),DDINV(254,7),UK(254),AKU(254)
      COMMON /RPN1/ NWAV,WAVNO(254),WAVLT(254)
C
      WRITE(6,11)
   11 FORMAT(1H1,51X,'B A N D   P A R A M E T E R S'//)
      LINCT=0
      WRITE(6,12)
   12 FORMAT(10X,'WAVENUMBER',1X,'WAVELENGTH',20X,
     $   'XKK AND DDINV PARAMETERS'/)
C
      DO 10 JJ=1,NWAV
      WRITE(6,14) WAVNO(JJ),WAVLT(JJ),(XKK(JJ,K),K=1,7)
      WRITE(6,14) WAVNO(JJ),WAVLT(JJ),(DDINV(JJ,K),K=1,7)
   14 FORMAT(14X,F5.0,4X,F8.1, 7X,7E12.4)
      WRITE(6,15)
   15 FORMAT(1H )
      LINCT=LINCT+3
      IF(LINCT.LT.56) GO TO 10
      LINCT=0
      WRITE(6,16)
   16 FORMAT(1H1)
      WRITE(6,12)
   10 CONTINUE
C
      RETURN
      END
      SUBROUTINE LIMITS(ARRAY,N7,KLOW,KUPPER)
C
      REAL ARRAY(254)
C
      RHLOW= 1.E-40
```

```
      DO 10 JJ=1,NO
      IF(ARRAY(JJ).GT.RHIGH) RHIGH=ARRAY(JJ)
  10  CONTINUE
C
      IUP=ALOG10(RHIGH)+1
      ILP=IUP-3
      RUPPER=10.**IUP
      RLOW=10.**ILP
C
      RETURN
      END
      SUBROUTINE ERRCHK(ILOC)
      RETURN
      END
      SUBROUTINE PARAM(TAV,XL,PH2O,PN2,PO2,PCO2,PCO,PH2)
      COMMON/CHECK/IREAD
      COMMON /BANDP/ XKK(254,7),DDINV(254,7),UK(254),AKU(254)
      COMMON /RPN1/ NWAV,WAVNO(254),WAVLT(254)
      COMMON /SWITCH/ KSWIT  ,IXXJG
      REAL TT(7)
      REAL LOG1,LOG2
C
      DATA TT(1),TT(2),TT(3),TT(4),TT(5),TT(6),TT(7)/300.,600.,1000.,
     $1500.,2000.,2500.,3000./
      DATA IDBG/-1/                                               004470
      T=TAV
      IXXJG=IXXJG+ 1
      IF (KSWIT.NE.2) GO TO 23
      TT(3)=1200.
      TT(4)=1500.
      TT(5)=1800.
      TT(6)=2400.
  23  CONTINUE
      IDBG=IDBG+1                                                 004480
C     CALCULATE OPTICAL DEPTH, U, AND WIDTH, GAMMA                004490
C
      T273=273./T
      SQT273=SQRT(T273)
      IF(KSWIT  .EQ.2) GO TO 18
      U=T273*PH2O*XL
      GAMMA=120.1*PH2O/T+SQT273*(.09*(PH2O+PN2)+.04*PO2+.12*PCO2
     $     +.05*PH2+0.1*PCO)
      GO TO 19
  18  CONTINUE
      U=T273*PCO2*XL
      GAMMA=0.01*PCO2*T273+(.07*PN2+0.055*PO2+0.09*PCO2+PH2*.08
     $     +PCO*0.06)*SQT273
  19  CONTINUE
C
C     SELECTION OF TEMPERATURES TO BE USED IN INTERPOLATIONS      004530
      I=1
      DO 30 KK=1,7
      K=KK
      TT1=ABS(T-TT(K))
      IF (TT1.GE.E-20) GO TO 31
  30  CONTINUE
      GO TO 32
  31  XK=XKK(I,K)
      DDINV=DDINV(I,K)
      GO TO 16
  32  CONTINUE
      DO 8 J=3,7
      K=1
      IF(TT(J)-T) 8,8,9
  8   CONTINUE
  9   CONTINUE
```

-76-

```fortran
      IF(T.GE.TT(K-1)) K=K+1
      TTK=TT(K)-TT(K-2)
      TTK1=TT(K)-TT(K-1)
      TTK2=TT(K-1)-TT(K-2)
      DIV=TTK*TTK1*TTK2
C
 1000 CONTINUE
      LOG1=ALOG(XKK(I,K-1)/XKK(I,K-2))
      LOG2=ALOG(XKK(I,K)/XKK(I,K-2))
      B=((TTK**2)*LOG1-(TTK2**2)*LOG2)/DIV
      C=(TTK2*LOG2-TTK*LOG1)/DIV
      XK=EXP(ALOG(XKK(I,K-2))+B*(T-TT(K-2))+C*(T-TT(K-2))**2)
C
      IF(T.LT.TT(2)) GO TO 14
      DLOG=ALOG(DDINV(I,K-2))
      DINV=EXP((ALOG(DDINV(I,K-1))-DLOG)*(T-TT(K-2))/(TT(K-1)-TT(K-2))
     C     +DLOG)
      GO TO 16
C
   14 CONTINUE
      DLOG=ALOG(DDINV(I,1))
      DINV=EXP((ALOG(DDINV(I,2))-DLOG)*(T-TT(1))/(TT(2)-TT(1))+DLOG)
C
   16 CONTINUE
C
C     CALCULATE PARAMETERS
C
      UK(I)=XK*U
      AKU(I)=GAMMA*DINV*UK(I)
      IF (TT1.LE.E-20) GO TO 17
C
      KDEX=K-2
      IDEX=K-1
      FLOW=.9*AMIN1(XKK(I,KDEX),XKK(I,IDEX))
      FHIGH=1.1*AMAX1(XKK(I,KDEX),XKK(I,IDEX))
      IF(XK.GE.FLOW.AND.XK.LE.FHIGH) GO TO 17
      B=ALOG(XKK(I,K-1)/XKK(I,K-2))/TTK2
      XK=EXP(ALOG(XKK(I,K-2))+B*(T-TT(K-2)))
      IF(XK.LT.FLOW.OR.XK.GT.FHIGH) WRITE(6,20)
     $    WAVNO(I),I,XK,T,U,GAMMA,TTK,B,C,DINV,UK(I),AKU(I)
   20 FORMAT(1X,/,' XK STILL OUT OF RANGE AT WAVNO = ',F10.0,' AND I = '
     $    ,I5,/,1X,5E14.4/,1X,5E14.4)
   17 CONTINUE
      I=I+1
      IF (I-NWAV)29,29,15
   29 IF (TT1.GE.E-20)GO TO 31
      IF(I-NWAV) 1000,1000,15
C
   15 CONTINUE
      IREAD=IREAD+1
      RETURN
      END
//GO.FT08F001 DD DSN=HARWE.PLOT8,UNIT=SYSDA,DISP=(NEW,DELETE),
//    DCB=(RECFM=VSB,LRECL=100,BLKSIZE=1000,BUFNO=1),
//    SPACE=(CYL,(5,5),RLSE)
//GO.FT09F001 DD DSN=HARWE.PLOT9,UNIT=SYSDA,DISP=(NEW,DELETE),
//    DCB=(RECFM=VSB,LRECL=100,BLKSIZE=1000,BUFNO=1),
//    SPACE=(CYL,(5,5),RLSE)
//GO.SYSIN DD *
```

APPENDIX II

INPUT INSTRUCTIONS AND SAMPLE INPUT DATA

APPENDIX II

The computer program input is composed of two parts: the flow field section and the band parameter section. The flow field of a plume can be generated by several computer codes like the NASA MOC code or the AeroChem code [3 and 5]. The flow field program provides the temperature and partial pressure at different locations along the plume. This information is necessary to calculate the optical depth and the radiance of the plume. The band parameter input is composed of the coefficient of absorption part and the line density part. It is tabulated according to the wave number and temperature. Subroutine READER reads in the flow field data and subroutine PARAM calculates the transmissivity τ.

Table A.1 lists all input parameters, format of the read statements, and their meaning, in the same order as encountered in the program for the flow field. Table A.2 lists the input parameters required for the radiation calculations. Tables A.1 and A.2 indicate all input data needed for operation of the code. A listing of a sample input data case is included as Table A.3.

Card #	Parameter	Format	Meaning
1	Title	12A4	Title of the Flowfield
2	PP	E10.4	Total Pressure
	RJ	E10.4	Radius of the Nozzle
	NRP(1)	I4	# of Radial Points at the Beginning of the Plume
3	X(JJ)	E10.3	Axial Location
	ILAST	69X,I1	Control value. ILAST = 1 for the end of the flow field
4	NRP(JJ)	I5	# of Radial Points at Axial Location X(JJ)
5	R(JJ,KK)	E10.3	Radial Location at Point (JJ,KK)
	T(JJ,KK)	E10.3	Temperature at Point (JJ,KK)
	PCO_2(JJ,KK)	E10.3	Partial Pressure of CO_2 at Point (JJ,KK)
	PH_2O(JJ,KK)	E10.3	Partial Pressure of H_2O at Point (JJ,KK)

Repeat card 5 for NRP(JJ) times.

Go back to card 3 for another axial point.

At the end of the flow field, set ILAST = 1. Such value of ILAST will terminate the reader subroutine and return to the MAIN ROUTINE.

TABLE A.2

Card #	Parameter	Format	Meaning
1	NWAV 1	I10	Wave number, lower limit
	NWAV 2	I10	Wave number, upper limit
2	WAV NO(I)	F9.1	Wave number
	XKK(I,J)	7E9.2	Coefficient of absorption K @ 300,600,1200,1500, 1800,2400,3000 °K of wave number WAVNO(I).
3	WAVNO(I)	F9.1	Wave number (must be the same as WAVNO(I) in card 2).
	DDINV(I,J)	7E9.2	Line density at temperature of 300,600,1200,1500,1800, 2400,3000 °K of wave number WAVNO(I).

Repeat card 2 and 3 for N = (NWAV 2 - NWAV 1)/25 +1

4	ALPHA	F10.5	Aspect angle of the line of sight
	ISTOP	I5	ISTOP = 1, will terminate the program after single alpha calculation. ISTOP = 2 will return to this point for another ALPHA calculation. ISTOP = 3, will read in a new set of flow field.

TABLE A.3

PR1.0X

```
.1000E 010.3930E 00   12
  0.0
0.0          0.2400E 040.1000E-190.1000E-190.7546E-010.2563E 000.1000E-19
0.3930E-010.2400E 040.1000E-190.1000E-190.7546E-010.2563E 000.1000E-19
0.7860E-010.2400E 040.1000E-190.1000E-190.7546E-010.2563E 000.1000E-19
0.1179E 000.2400E 040.1000E-190.1000E-190.7546E-010.2563E 000.1000E-19
0.1572E 000.2400E 040.1000E-190.1000E-190.7546E-010.2563E 000.1000E-19
0.1965E 000.2400E 040.1000E-190.1000E-190.7546E-010.2563E 000.1000E-19
0.2358E 000.2400E 040.1000E-190.1000E-190.7546E-010.2563E 000.1000E-19
0.2751E 000.2400E 040.1000E-190.1000E-190.7546E-010.2563E 000.1000E-19
0.3144E 000.2400E 040.1000E-190.1000E-190.7546E-010.2563E 000.1000E-19
0.3537E 000.2400E 040.1000E-190.1000E-190.7546E-010.2563E 000.1000E-19
0.3930E 000.2400E 040.1000E-190.1000E-190.7546E-010.2563E 000.1000E-19
0.4606E 000.2880E 030.1000E-190.1000E-190.2885E-060.2885E-060.1000E-19
  0.410E 00
0.0          0.2477E 040.1000E-190.1000E-190.7954E-010.2625E 000.1000E-19
0.3993E-010.2477E 040.1000E-190.1000E-190.7954E-010.2625E 000.1000E-19
0.7982E-010.2477E 040.1000E-190.1000E-190.7954E-010.2625E 000.1000E-19
0.1197E 000.2477E 040.1000E-190.1000E-190.7954E-010.2625E 000.1000E-19
0.1596E 000.2477E 040.1000E-190.1000E-190.7954E-010.2625E 000.1000E-19
0.1996E 000.2477E 040.1000E-190.1000E-190.7954E-010.2625E 000.1000E-19
0.2395E 000.2477E 040.1000E-190.1000E-190.7954E-010.2625E 000.1000E-19
0.2794E 000.2477E 040.1000E-190.1000E-190.7953E-010.2625E 000.1000E-19
0.3193E 000.2475E 040.1000E-190.1000E-190.7947E-010.2623E 000.1000E-19
0.3591E 000.2448E 040.1000E-190.1000E-190.7834E-010.2592E 000.1000E-19
0.3997E 000.2228E 040.1000E-190.1000E-190.6844E-010.2279E 000.1000E-19
0.4531E 000.1212E 040.1000E-190.1000E-190.2709E-010.8465E-010.1000E-19
0.5439E 000.5520E 030.1000E-190.1000E-190.6866E-020.2061E-010.1000E-19
0.6449E 000.3539E 030.1000E-190.1000E-190.1660E-020.4986E-020.1000E-19
0.7459E 000.3020E 030.1000E-190.1000E-190.3467E-030.1067E-020.1000E-19
0.8363E 000.2880E 030.1000E-190.1000E-190.2885E-060.2885E-060.1000E-19
  0.814E 00
0.0          0.2487E 040.1000E-190.1000E-190.8209E-010.2609E 000.1000E-19
0.3997E-010.2487E 040.1000E-190.1000E-190.8209E-010.2609E 000.1000E-19
0.7994E-010.2487E 040.1000E-190.1000E-190.8209E-010.2609E 000.1000E-19
0.1199E 000.2487E 040.1000E-190.1000E-190.8209E-010.2609E 000.1000E-19
0.1599E 000.2487E 040.1000E-190.1000E-190.8209E-010.2609E 000.1000E-19
0.1999E 000.2487E 040.1000E-190.1000E-190.8209E-010.2609E 000.1000E-19
0.2398E 000.2487E 040.1000E-190.1000E-190.8209E-010.2609E 000.1000E-19
0.2798E 000.2486E 040.1000E-190.1000E-190.8207E-010.2607E 000.1000E-19
0.3197E 000.2473E 040.1000E-190.1000E-190.8185E-010.2594E 000.1000E-19
0.3598E 000.2412E 040.1000E-190.1000E-190.8035E-010.2512E 000.1000E-19
0.4016E 000.2173E 040.1000E-190.1000E-190.7212E-010.2137E 000.1000E-19
0.4559E 000.1479E 040.1000E-190.1000E-190.4261E-010.1220E 000.1000E-19
0.5357E 000.8166E 030.1000E-190.1000E-190.1581E-010.4558E-010.1000E-19
0.6308E 000.5012E 030.1000E-190.1000E-190.5747E-020.1687E-010.1000E-19
0.7318E 000.3739E 030.1000E-190.1000E-190.2240E-020.6671E-020.1000E-19
0.8269E 000.3231E 030.1000E-190.1000E-190.9029E-030.2708E-020.1000E-19
0.9188E 000.3017E 030.1000E-190.1000E-190.3501E-030.1053E-020.1000E-19
0.1005E 010.2925E 030.1000E-190.1000E-190.1148E-030.3454E-030.1000E-19
  0.122E 01
0.0          0.2497E 040.1000E-190.1000E-190.8402E-010.2598E 000.1000E-19
0.4005E-010.2497E 040.1000E-190.1000E-190.8402E-010.2598E 000.1000E-19
0.8009E-010.2497E 040.1000E-190.1000E-190.8402E-010.2598E 000.1000E-19
0.1201E 000.2497E 040.1000E-190.1000E-190.8402E-010.2598E 000.1000E-19
0.1601E 000.2497E 040.1000E-190.1000E-190.8402E-010.2598E 000.1000E-19
0.2002E 000.2497E 040.1000E-190.1000E-190.8402E-010.2598E 000.1000E-19
0.2402E 000.2495E 040.1000E-190.1000E-190.8404E-010.2596E 000.1000E-19
```

```
0.2802E 000.2489E 040.1000E-190.1000E-190.8411E-010.2588E 000.1000E-19
0.3202E 000.2463E 040.1000E-190.1000E-190.8420E-010.2550E 000.1000E-19
0.3608E 000.2386E 040.1000E-190.1000E-190.8346E-010.2413E 000.1000E-19
0.4052E 000.2161E 040.1000E-190.1000E-190.7718E-010.2032E 000.1000E-19
0.4602E 000.1643E 040.1000E-190.1000E-190.5494E-010.1359E 000.1000E-19
0.5349E 000.1050E 040.1000E-190.1000E-190.2660E-010.6755E-010.1000E-19
0.6253E 000.6700E 030.1000E-190.1000E-190.1164E-010.3069E-010.1000E-19
0.7239E 000.4783E 030.1000E-190.1000E-190.5360E-020.1466E-010.1000E-19
0.8210E 000.3843E 030.1000E-190.1000E-190.2630E-020.7400E-020.1000E-19
0.9145E 000.3379E 030.1000E-190.1000E-190.1339E-020.3842E-020.1000E-19
0.1004E 010.3136E 030.1000E-190.1000E-190.6796E-030.1974E-020.1000E-19
0.1089E 010.3004E 030.1000E-190.1000E-190.3265E-030.9567E-030.1000E-19
0.1172E 010.2929E 030.1000E-190.1000E-190.1286E-030.3786E-030.1000E-19
 0.161E 01
0.0        0.2506E 040.1000E-190.1000E-190.8543E-010.2591E 000.1000E-19
0.4009E-010.2506E 040.1000E-190.1000E-190.8543E-010.2591E 000.1000E-19
0.8017E-010.2506E 040.1000E-190.1000E-190.8543E-010.2591E 000.1000E-19
0.1203E 000.2506E 040.1000E-190.1000E-190.8543E-010.2591E 000.1000E-19
0.1604E 000.2505E 040.1000E-190.1000E-190.8544E-010.2591E 000.1000E-19
0.2004E 000.2504E 040.1000E-190.1000E-190.8549E-010.2589E 000.1000E-19
0.2405E 000.2500E 040.1000E-190.1000E-190.8565E-010.2583E 000.1000E-19
0.2805E 000.2488E 040.1000E-190.1000E-190.8609E-010.2562E 000.1000E-19
0.3208E 000.2456E 040.1000E-190.1000E-190.8687E-010.2496E 000.1000E-19
0.3625E 000.2375E 040.1000E-190.1000E-190.8701E-010.2325E 000.1000E-19
0.4087E 000.2168E 040.1000E-190.1000E-190.8206E-010.1964E 000.1000E-19
0.4649E 000.1746E 040.1000E-190.1000E-190.6401E-010.1416E 000.1000E-19
0.5368E 000.1228E 040.1000E-190.1000E-190.3708E-010.8346E-010.1000E-19
0.6237E 000.8267E 030.1000E-190.1000E-190.1848E-010.4325E-010.1000E-19
0.7196E 000.5889E 030.1000E-190.1000E-190.9346E-020.2284E-010.1000E-19
0.8170E 000.4590E 030.1000E-190.1000E-190.5004E-020.1271E-010.1000E-19
0.9122E 000.3867E 030.1000E-190.1000E-190.2813E-020.7375E-020.1000E-19
0.1003E 010.3461E 030.1000E-190.1000E-190.1627E-020.4369E-020.1000E-19
0.1091E 010.3220E 030.1000E-190.1000E-190.9414E-030.2572E-020.1000E-19
0.1175E 010.3072E 030.1000E-190.1000E-190.5280E-030.1462E-020.1000E-19
0.1257E 010.2980E 030.1000E-190.1000E-190.2741E-030.7655E-030.1000E-19
0.1337E 010.2922E 030.1000E-190.1000E-190.1138E-030.3194E-030.1000E-19
 0.197E 01
0.0        0.2513E 040.1000E-190.1000E-190.8639E-010.2588E 000.1000E-19
0.3029E-010.2513E 040.1000E-190.1000E-190.8640E-010.2588E 000.1000E-19
0.1605E 000.2512E 040.1000E-190.1000E-190.8647E-010.2586E 000.1000E-19
0.2407E 000.2503E 040.1000E-190.1000E-190.8708E-010.2568E 000.1000E-19
0.3218E 000.2454E 040.1000E-190.1000E-190.8937E-010.2444E 000.1000E-19
0.4126E 000.2170E 040.1000E-190.1000E-190.8555E-010.1916E 000.1000E-19
0.5388E 000.1356E 040.1000E-190.1000E-190.4562E-010.9387E-010.1000E-19
0.7168E 000.6935E 030.1000E-190.1000E-190.1377E-010.3044E-010.1000E-19
0.9102E 000.4412E 030.1000E-190.1000E-190.4631E-020.1104E-010.1000E-19
0.1091E 010.3494E 030.1000E-190.1000E-190.1787E-020.4492E-020.1000E-19
0.1260E 010.3120E 030.1000E-190.1000E-190.6857E-030.1781E-020.1000E-19
0.1420E 010.2941E 030.1000E-190.1000E-190.1732E-030.4571E-030.1000E-19
 0.237E 01
0.0        0.2520E 040.1000E-190.1000E-190.8721E-010.2585E 000.1000E-19
0.8037E-010.2520E 040.1000E-190.1000E-190.8725E-010.2585E 000.1000E-19
0.1607E 000.2513E 040.1000E-190.1000E-190.8753E-010.2578E 000.1000E-19
0.2411E 000.2505E 040.1000E-190.1000E-190.8875E-010.2543E 000.1000E-19
0.3232E 000.2410E 040.1000E-190.1000E-190.9155E-010.2383E 000.1000E-19
0.4152E 000.2174E 040.1000E-190.1000E-190.8831E-010.1864E 000.1000E-19
0.5419E 000.1452E 040.1000E-190.1000E-190.5263E-010.1015E 000.1000E-19
0.7125E 000.8104E 030.1000E-190.1000E-190.1972E-010.3975E-010.1000E-19
0.9015E 000.5167E 030.1000E-190.1000E-190.7556E-020.1639E-010.1000E-19
0.1068E 010.3720E 030.1000E-190.1000E-190.3294E-020.7446E-020.1000E-19
0.1259E 010.3373E 030.1000E-190.1000E-190.1503E-020.3539E-020.1000E-19
```

```
0.1423E 010.3106E 030.1000E-190.1000E-190.6750E-030.1638E-020.1000E-19
0.1579E 010.2967E 030.1000E-190.1000E-190.2550E-030.6309E-030.1000E-19
0.1732E 010.2904E 030.1000E-190.1000E-190.6951E-040.1739E-030.1000E-19
 0.278E 01
0.0        0.2527E 040.1000E-190.1000E-190.8788E-010.2584E 000.1000E-19
0.8041E-010.2526E 040.1000E-190.1000E-190.8800E-010.2582E 000.1000E-19
0.1608E 000.2522E 040.1000E-190.1000E-190.8859E-010.2569E 000.1000E-19
0.2415E 000.2507E 040.1000E-190.1000E-190.9047E-010.2516E 000.1000E-19
0.3250E 000.2443E 040.1000E-190.1000E-190.9379E-010.2329E 000.1000E-19
0.4201E 000.2176E 040.1000E-190.1000E-190.9074E-010.1824E 000.1000E-19
0.5459E 000.1531E 040.1000E-190.1000E-190.5911E-010.1070E 000.1000E-19
0.7109E 000.9199E 030.1000E-190.1000E-190.2524E-010.4748E-010.1000E-19
0.8964E 000.5924E 030.1000E-190.1000E-190.1075E-010.2131E-010.1000E-19
0.1082E 010.4403E 030.1000E-190.1000E-190.5030E-020.1047E-010.1000E-19
0.1258E 010.3664E 030.1000E-190.1000E-190.2517E-020.5458E-020.1000E-19
0.1425E 010.3290E 030.1000E-190.1000E-190.1291E-020.2840E-020.1000E-19
0.1584E 010.3086E 030.1000E-190.1000E-190.6375E-030.1462E-020.1000E-19
0.1738E 010.2972E 030.1000E-190.1000E-190.2812E-030.6559E-030.1000E-19
0.1888E 010.2912E 030.1000E-190.1000E-190.9628E-040.2268E-030.1000E-19
 0.318E 01
0.0        0.2533E 040.1000E-190.1000E-190.8851E-010.2582E 000.1000E-19
0.8049E-010.2532E 040.1000E-190.1000E-190.8875E-010.2578E 000.1000E-19
0.1610E 000.2527E 040.1000E-190.1000E-190.8974E-010.2557E 000.1000E-19
0.2422E 000.2509E 040.1000E-190.1000E-190.9225E-010.2487E 000.1000E-19
0.3271E 000.2440E 040.1000E-190.1000E-190.9586E-010.2276E 000.1000E-19
0.4244E 000.2178E 040.1000E-190.1000E-190.9266E-010.1790E 000.1000E-19
0.5498E 000.1597E 040.1000E-190.1000E-190.6451E-010.1110E 000.1000E-19
0.7109E 000.1013E 040.1000E-190.1000E-190.3073E-010.5451E-010.1000E-19
0.8933E 000.6643E 030.1000E-190.1000E-190.1408E-010.2612E-010.1000E-19
0.1078E 910.4885E 030.1000E-190.1000E-190.6973E-020.1354E-010.1000E-19
0.1256E 010.3982E 030.1000E-190.1000E-190.3705E-020.7492E-020.1000E-19
0.1425E 010.3504E 030.1000E-190.1000E-190.2050E-020.4280E-020.1000E-19
0.1587E 010.3232E 030.1000E-190.1000E-190.1136E-020.2433E-020.1000E-19
0.1743E 010.3067E 030.1000E-190.1000E-190.5969E-030.1302E-020.1000E-19
0.1895E 010.2967E 030.1000E-190.1000E-190.2762E-030.6103E-030.1000E-19
0.2043E 010.2911E 030.1000E-190.1000E-190.9776E-040.2177E-030.1000E-19
 0.358E 01
0.0        0.2539E 040.1000E-190.1000E-190.8918E-010.2578E 000.1000E-19
0.8056E-010.2537E 040.1000E-190.1000E-190.8957E-010.2571E 000.1000E-19
0.1612E 000.2532E 040.1000E-190.1000E-190.9098E-010.2542E 000.1000E-19
0.2431E 000.2512E 040.1000E-190.1000E-190.9399E-010.2454E 000.1000E-19
0.3295E 000.2437E 040.1000E-190.1000E-190.9756E-010.2226E 000.1000E-19
0.4288E 000.2178E 040.1000E-190.1000E-190.9396E-010.1760E 000.1000E-19
0.5537E 000.1649E 040.1000E-190.1000E-190.6862E-010.1140E 000.1000E-19
0.7113E 000.1096E 040.1000E-190.1000E-190.3588E-010.6073E-010.1000E-19
0.8905E 000.7337E 030.1000E-190.1000E-190.1752E-010.3077E-010.1000E-19
0.1075E 010.5361E 030.1000E-190.1000E-190.9100E-020.1666E-010.1000E-19
0.1254E 010.4334E 030.1000E-190.1000E-190.5055E-020.9604E-020.1000E-19
0.1426E 010.3743E 030.1000E-190.1000E-190.2935E-020.5756E-020.1000E-19
0.1590E 010.3399E 030.1000E-190.1000E-190.1736E-020.3494E-020.1000E-19
0.1748E 010.3186E 030.1000E-190.1000E-190.1014E-020.2082E-020.1000E-19
0.1901E 010.3049E 030.1000E-190.1000E-190.5542E-030.1156E-020.1000E-19
0.2051E 010.2961E 030.1000E-190.1000E-190.2642E-030.5565E-030.1000E-19
0.2198E 010.2909E 030.1000E-190.1000E-190.9535E-040.2020E-030.1000E-19
 0.398E 01
0.0        0.2544E 040.1000E-190.1000E-190.9001E-010.2571E 000.1000E-19
0.8064E-010.2543E 040.1000E-190.1000E-190.9054E-010.2561E 000.1000E-19
0.1616E 000.2537E 040.1000E-190.1000E-190.9235E-010.2523E 000.1000E-19
0.2442E 000.2515E 040.1000E-190.1000E-190.9570E-010.2420E 000.1000E-19
0.3322E 000.2433E 040.1000E-190.1000E-190.9909E-010.2176E 000.1000E-19
0.4331E 000.2173E 040.1000E-190.1000E-190.9517E-010.1731E 000.1000E-19
```

```
0.5581E 000.1693E 040.1000E-190.1000E-190.7210E-010.1162E 000.1000E-19
0.7125E 000.1170E 040.1000E-190.1000E-190.4070E-010.6621E-010.1000E-19
0.8886E 000.8011E 030.1000E-190.1000E-190.2103E-010.3526E-010.1000E-19
0.1072E 010.5881E 030.1000E-190.1000E-190.1136E-010.1976E-010.1000E-19
0.1252E 010.4690E 030.1000E-190.1000E-190.6533E-020.1176E-010.1000E-19
0.1425E 010.3997E 030.1000E-190.1000E-190.3933E-020.7303E-020.1000E-19
0.1592E 010.3583E 030.1000E-190.1000E-190.2431E-020.4631E-020.1000E-19
0.1752E 010.3322E 030.1000E-190.1000E-190.1509E-020.2934E-020.1000E-19
0.1906E 010.3151E 030.1000E-190.1000E-190.9148E-030.1808E-020.1000E-19
0.2057E 010.3033E 030.1000E-190.1000E-190.5147E-030.1030E-020.1000E-19
0.2206E 010.2948E 030.1000E-190.1000E-190.2278E-030.4590E-030.1000E-19
0.2351E 010.2901E 030.1000E-190.1000E-190.6977E-040.1411E-030.1000E-19
 0.439E 01
0.0        0.2550E 040.1000E-190.1000E-190.9103E-010.2561E 000.1000E-19
0.8084E-010.2548E 040.1000E-190.1000E-190.9171E-010.2548E 000.1000E-19
0.1621E 000.2543E 040.1000E-190.1000E-190.9383E-010.2501E 000.1000E-19
0.2457E 000.2519E 040.1000E-190.1000E-190.9739E-010.2383E 000.1000E-19
0.3352E 000.2430E 040.1000E-190.1000E-190.1005E 000.2133E 000.1000E-19
0.4378E 000.2180E 040.1000E-190.1000E-190.9637E-010.1705E 000.1000E-19
0.5624E 000.1731E 040.1000E-190.1000E-190.7518E-010.1179E 000.1000E-19
0.7145E 000.1237E 040.1000E-190.1000E-190.4521E-010.7091E-010.1000E-19
0.8882E 000.8657E 030.1000E-190.1000E-190.2457E-010.3953E-010.1000E-19
0.1070E 010.6382E 030.1000E-190.1000E-190.1374E-010.2284E-010.1000E-19
0.1250E 010.5062E 030.1000E-190.1000E-190.8129E-020.1396E-010.1000E-19
0.1425E 010.4276E 030.1000E-190.1000E-190.5036E-020.8901E-020.1000E-19
0.1593E 010.3785E 030.1000E-190.1000E-190.3212E-020.5821E-020.1000E-19
0.1755E 010.3471E 030.1000E-190.1000E-190.2074E-020.3839E-020.1000E-19
0.1912E 010.3263E 030.1000E-190.1000E-190.1332E-020.2507E-020.1000E-19
0.2064E 010.3120E 030.1000E-190.1000E-190.8290E-030.1582E-020.1000E-19
0.2213E 010.3019E 030.1000E-190.1000E-190.4757E-030.9164E-030.1000E-19
0.2360E 010.2942E 030.1000E-190.1000E-190.2133E-030.4132E-030.1000E-19
 0.482E 01
0.0        0.2556E 040.1000E-190.1000E-190.9228E-010.2547E 000.1000E-19
0.8108E-010.2555E 040.1000E-190.1000E-190.9306E-010.2531E 000.1000E-19
0.1628E 000.2549E 040.1000E-190.1000E-190.9541E-010.2475E 000.1000E-19
0.2474E 000.2522E 040.1000E-190.1000E-190.9904E-010.2345E 000.1000E-19
0.3385E 000.2426E 040.1000E-190.1000E-190.1018E 000.2089E 000.1000E-19
0.4425E 000.2181E 040.1000E-190.1000E-190.9742E-010.1679E 000.1000E-19
0.5671E 000.1763E 040.1000E-190.1000E-190.7776E-010.1190E 000.1000E-19
0.7172E 000.1296E 040.1000E-190.1000E-190.4930E-010.7481E-010.1000E-19
0.8878E 000.9266E 030.1000E-190.1000E-190.2807E-010.4354E-010.1000E-19
0.1068E 010.6878E 030.1000E-190.1000E-190.1620E-010.2587E-010.1000E-19
0.1249E 010.5436E 030.1000E-190.1000E-190.9816E-020.1616E-010.1000E-19
0.1424E 010.4556E 030.1000E-190.1000E-190.6221E-020.1053E-010.1000E-19
0.1594E 010.3996E 030.1000E-190.1000E-190.4066E-020.7050E-020.1000E-19
0.1757E 010.3632E 030.1000E-190.1000E-190.2705E-020.4786E-020.1000E-19
0.1915E 010.3386E 030.1000E-190.1000E-190.1803E-020.3245E-020.1000E-19
0.2070E 010.3216E 030.1000E-190.1000E-190.1184E-020.2162E-020.1000E-19
0.2220E 010.3094E 030.1000E-190.1000E-190.7499E-030.1384E-020.1000E-19
0.2367E 010.3005E 030.1000E-190.1000E-190.4354E-030.8097E-030.1000E-19
0.2513E 010.2936E 030.1000E-190.1000E-190.1967E-030.3675E-030.1000E-19
 0.522E 01
0.0        0.2563E 040.1000E-190.1000E-190.9362E-010.2530E 000.1000E-19
0.8143E-010.2562E 040.1000E-190.1000E-190.9446E-010.2512E 000.1000E-19
0.1637E 000.2555E 040.1000E-190.1000E-190.9693E-010.2448E 000.1000E-19
0.2493E 000.2524E 040.1000E-190.1000E-190.1005E 000.2309E 000.1000E-19
0.3417E 000.2422E 040.1000E-190.1000E-190.1029E 000.2049E 000.1000E-19
0.4468E 000.2181E 040.1000E-190.1000E-190.9824E-010.1655E 000.1000E-19
0.5714E 000.1767E 040.1000E-190.1000E-190.7974E-010.1195E 000.1000E-19
0.7196E 000.1344E 040.1000E-190.1000E-190.5271E-010.7754E-010.1000E-19
0.8882E 000.9794E 030.1000E-190.1000E-190.3122E-010.4699E-010.1000E-19
```

```
0.1067E 010.7326E 030.1000E-190.1000E-190.1851E-010.2859E-010.1000E-19
0.1247E 010.5786E 030.1000E-190.1000E-190.1145E-010.1819E-010.1000E-19
0.1423E 010.4826E 030.1000E-190.1000E-190.7391E-020.1205E-010.1000E-19
0.1594E 010.4207E 030.1000E-190.1000E-190.4924E-020.8219E-020.1000E-19
0.1759E 010.3793E 030.1000E-190.1000E-190.3344E-020.5697E-020.1000E-19
0.1919E 010.3511E 030.1000E-190.1000E-190.2288E-020.3965E-020.1000E-19
0.2074E 010.3312E 030.1000E-190.1000E-190.1555E-020.2734E-020.1000E-19
0.2226E 010.3169E 030.1000E-190.1000E-190.1035E-020.1840E-020.1000E-19
0.2375E 010.3065E 030.1000E-190.1000E-190.6592E-030.1182E-020.1000E-19
0.2521E 010.2988E 030.1000E-190.1000E-190.3833E-030.6920E-030.1000E-19
0.2665E 010.2929E 030.1000E-190.1000E-190.1732E-030.3139E-030.1000E-19
   0.563E 01
0.0       0.2570E 040.1000E-190.1000E-190.9535E-010.2504E 000.1000E-19
0.8194E-010.2568E 040.1000E-190.1000E-190.9621E-010.2483E 000.1000E-19
0.1649E 000.2559E 040.1000E-190.1000E-190.9864E-010.2411E 000.1000E-19
0.2516E 000.2521E 040.1000E-190.1000E-190.1019E 000.2261E 000.1000E-19
0.3454E 000.2411E 040.1000E-190.1000E-190.1034E 000.2000E 000.1000E-19
0.4516E 000.2172E 040.1000E-190.1000E-190.9795E-010.1625E 000.1000E-19
0.5761E 000.1802E 040.1000E-190.1000E-190.8038E-010.1197E 000.1000E-19
0.7219E 000.1385E 040.1000E-190.1000E-190.5537E-010.8035E-010.1000E-19
0.8870E 000.1031E 040.1000E-190.1000E-190.3439E-010.5043E-010.1000E-19
0.1063E 010.7806E 030.1000E-190.1000E-190.2112E-010.3160E-010.1000E-19
0.1243E 010.6178E 030.1000E-190.1000E-190.1338E-010.2051E-010.1000E-19
0.1420E 010.5134E 030.1000E-190.1000E-190.8807E-020.1383E-010.1000E-19
0.1592E 010.4450E 030.1000E-190.1000E-190.5979E-020.9596E-020.1000E-19
0.1758E 010.3985E 030.1000E-190.1000E-190.4146E-020.6785E-020.1000E-19
0.1920E 010.3664E 030.1000E-190.1000E-190.2907E-020.4837E-020.1000E-19
0.2077E 010.3434E 030.1000E-190.1000E-190.2037E-020.3438E-020.1000E-19
0.2230E 010.3266E 030.1000E-190.1000E-190.1409E-020.2406E-020.1000E-19
0.2380E 010.3141E 030.1000E-190.1000E-190.9464E-030.1632E-020.1000E-19
0.2527E 010.3047E 030.1000E-190.1000E-190.6039E-030.1049E-020.1000E-19
0.2672E 010.2977E 030.1000E-190.1000E-190.3497E-030.6104E-030.1000E-19
0.2816E 010.2924E 030.1000E-190.1000E-190.1572E-030.2752E-030.1000E-19
   0.603E 01
0.0       0.2576E 040.1000E-190.1000E-190.9741E-010.2466E 000.1000E-19
0.8261E-010.2573E 040.1000E-190.1000E-190.9823E-010.2442E 000.1000E-19
0.1664E 000.2559E 040.1000E-190.1000E-190.1004E 000.2363E 000.1000E-19
0.2545E 000.2512E 040.1000E-190.1000E-190.1031E 000.2205E 000.1000E-19
0.3497E 000.2392E 040.1000E-190.1000E-190.1035E 000.1946E 000.1000E-19
0.4571E 000.2156E 040.1000E-190.1000E-190.9720E-010.1591E 000.1000E-19
0.5809E 000.1808E 040.1000E-190.1000E-190.8048E-010.1194E 000.1000E-19
0.7243E 000.1420E 040.1000E-190.1000E-190.5747E-010.8274E-010.1000E-19
0.8858E 000.1081E 040.1000E-190.1000E-190.3732E-010.5386E-010.1000E-19
0.1060E 010.8300E 030.1000E-190.1000E-190.2376E-010.3472E-010.1000E-19
0.1237E 010.6601E 030.1000E-190.1000E-190.1547E-010.2302E-010.1000E-19
0.1414E 010.5478E 030.1000E-190.1000E-190.1041E-010.1579E-010.1000E-19
0.1587E 010.4727E 030.1000E-190.1000E-190.7203E-020.1114E-010.1000E-19
0.1756E 010.4209E 030.1000E-190.1000E-190.5093E-020.8017E-020.1000E-19
0.1919E 010.3842E 030.1000E-190.1000E-190.3647E-020.5833E-020.1000E-19
0.2078E 010.3578E 030.1000E-190.1000E-190.2624E-020.4255E-020.1000E-19
0.2233E 010.3383E 030.1000E-190.1000E-190.1877E-020.3060E-020.1000E-19
0.2384E 010.3235E 030.1000E-190.1000E-190.1319E-020.2184E-020.1000E-19
0.2532E 010.3122E 030.1000E-190.1000E-190.8950E-030.1494E-020.1000E-19
0.2679E 010.3035E 030.1000E-190.1000E-190.5731E-030.9622E-030.1000E-19
0.2823E 010.2970E 030.1000E-190.1000E-190.3312E-030.5583E-030.1000E-19
0.2966E 010.2920E 030.1000E-190.1000E-190.1483E-030.2505E-030.1000E-19
   0.644E 01
0.0       0.2581E 040.1000E-190.1000E-190.9948E-010.2424E 000.1000E-19
0.8339E-010.2577E 040.1000E-190.1000E-190.1002E 000.2398E 000.1000E-19
0.1641E 000.2558E 040.1000E-190.1000E-190.1022E 000.2313E 000.1000E-19
0.2574E 000.2503E 040.1000E-190.1000E-190.1043E 000.2150E 000.1000E-19
```

```
0.3539E 000.2375E 040.1000E-190.1000E-190.1039E 000.1894E 000.1000E-19
0.4622E 000.2144E 040.1000E-190.1000E-190.9715E-010.1557E 000.1000E-19
0.5856E 000.1816E 040.1000E-190.1000E-190.8119E-010.1189E 000.1000E-19
0.7274E 000.1452E 040.1000E-190.1000E-190.5955E-010.8455E-010.1000E-19
0.8866E 000.1125E 040.1000E-190.1000E-190.3996E-010.5680E-010.1000E-19
0.1058E 010.8747E 030.1000E-190.1000E-190.2616E-010.3752E-010.1000E-19
0.1234E 010.6993E 030.1000E-190.1000E-190.1740E-010.2531E-010.1000E-19
0.1410E 010.5801E 030.1000E-190.1000E-190.1190E-010.1761E-010.1000E-19
0.1584E 010.4988E 030.1000E-190.1000E-190.8367E-020.1258E-010.1000E-19
0.1753E 010.4421E 030.1000E-190.1000E-190.6006E-020.9176E-020.1000E-19
0.1918E 010.4015E 030.1000E-190.1000E-190.4374E-020.6778E-020.1000E-19
0.2078E 010.3718E 030.1000E-190.1000E-190.3208E-020.5036E-020.1000E-19
0.2235E 010.3499E 030.1000E-190.1000E-190.2352E-020.3733E-020.1000E-19
0.2387E 010.3332E 030.1000E-190.1000E-190.1708E-020.2737E-020.1000E-19
0.2537E 010.3202E 030.1000E-190.1000E-190.1212E-020.1957E-020.1000E-19
0.2685E 010.3099E 030.1000E-190.1000E-190.8209E-030.1334E-020.1000E-19
0.2830E 010.3017E 030.1000E-190.1000E-190.5117E-030.8352E-030.1000E-19
0.2973E 010.2955E 030.1000E-190.1000E-190.2782E-030.4554E-030.1000E-19
0.3116E 010.2911E 030.1000E-190.1000E-190.1157E-030.1897E-030.1000E-19
 0.685E 01
0.0         0.2584E 040.1000E-190.1000E-190.1015E 000.2378E 000.1000E-19
0.8430E-010.2579E 040.1000E-190.1000E-190.1022E 000.2350E 000.1000E-19
0.1700E 000.2555E 040.1000E-190.1000E-190.1039E 000.2260E 000.1000E-19
0.2604E 000.2493E 040.1000E-190.1000E-190.1054E 000.2095E 000.1000E-19
0.3581E 000.2360E 040.1000E-190.1000E-190.1045E 000.1845E 000.1000E-19
0.4669E 000.2134E 040.1000E-190.1000E-190.9739E-010.1525E 000.1000E-19
0.5907E 000.1823E 040.1000E-190.1000E-190.8207E-010.1180E 000.1000E-19
0.7314E 000.1479E 040.1000E-190.1000E-190.6151E-010.8585E-010.1000E-19
0.8882E 000.1164E 040.1000E-190.1000E-190.4239E-010.5924E-010.1000E-19
0.1057E 010.9151E 030.1000E-190.1000E-190.2838E-010.4001E-010.1000E-19
0.1232E 010.7354E 030.1000E-190.1000E-190.1920E-010.2741E-010.1000E-19
0.1408E 010.6104E 030.1000E-190.1000E-190.1332E-010.1930E-010.1000E-19
0.1581E 010.5238E 030.1000E-190.1000E-190.9485E-020.1394E-010.1000E-19
0.1752E 010.4627E 030.1000E-190.1000E-190.6893E-020.1028E-010.1000E-19
0.1917E 010.4185E 030.1000E-190.1000E-190.5085E-020.7681E-020.1000E-19
0.2079E 010.3858E 030.1000E-190.1000E-190.3783E-020.5784E-020.1000E-19
0.2236E 010.3614E 030.1000E-190.1000E-190.2822E-020.4360E-020.1000E-19
0.2390E 010.3428E 030.1000E-190.1000E-190.2096E-020.3268E-020.1000E-19
0.2542E 010.3283E 030.1000E-190.1000E-190.1537E-020.2415E-020.1000E-19
0.2690E 010.3169E 030.1000E-190.1000E-190.1099E-020.1737E-020.1000E-19
0.2836E 010.3077E 030.1000E-190.1000E-190.7482E-030.1189E-020.1000E-19
0.2981E 010.3002E 030.1000E-190.1000E-190.4606E-030.7345E-030.1000E-19
0.3124E 010.2937E 030.1000E-190.1000E-190.2166E-030.3460E-030.1000E-19
 0.694E 01
0.0         0.2585E 040.1000E-190.1000E-190.1020E 000.2367E 000.1000E-19
0.8646E-010.2559E 040.1000E-190.1000E-190.1031E 000.2300E 000.1000E-19
0.1731E 000.2554E 040.1000E-190.1000E-190.1042E 000.2249E 000.1000E-19
0.2648E 000.2380E 040.1000E-190.1000E-190.1044E 000.2000E 000.1000E-19
0.3594E 000.2357E 040.1000E-190.1000E-190.1046E 000.1834E 000.1000E-19
0.5926E 000.1824E 040.1000E-190.1000E-190.8226E-010.1178E 000.1000E-19
0.8873E 000.1172E 040.1000E-190.1000E-190.4290E-010.5972E-010.1000E-19
0.1232E 010.7430E 030.1000E-190.1000E-190.1959E-010.2786E-010.1000E-19
0.1581E 010.5292E 030.1000E-190.1000E-190.9723E-020.1423E-010.1000E-19
0.1917E 010.4222E 030.1000E-190.1000E-190.5240E-020.7877E-020.1000E-19
0.2237E 010.3639E 030.1000E-190.1000E-190.2927E-020.4498E-020.1000E-19
0.2543E 010.3301E 030.1000E-190.1000E-190.1607E-020.2512E-020.1000E-19
0.2837E 010.3086E 030.1000E-190.1000E-190.7893E-030.1247E-020.1000E-19
0.3125E 010.2941E 030.1000E-190.1000E-190.2297E-030.3648E-030.1000E-19
 0.741E 01
0.0         0.2581E 040.1000E-190.1000E-190.1040E 000.2304E 000.1000E-19
0.8646E-010.2560E 040.1000E-190.1000E-190.1048E 000.2230E 000.1000E-19
```

```
0.1754E 000.2543E 040.1000E-190.1000E-190.1057E 000.2186E 000.1000E-19
0.2596E 000.2440E 040.1000E-190.1000E-190.1050E 000.1980E 000.1000E-19
0.3639E 000.2339E 040.1000E-190.1000E-190.1049E 000.1780E 000.1000E-19
0.5981E 000.1827E 040.1000E-190.1000E-190.8317E-010.1161E 000.1000E-19
0.8909E 000.1205E 040.1000E-190.1000E-190.4494E-010.6173E-010.1000E-19
0.1229E 010.7812E 030.1000E-190.1000E-190.2161E-010.3016E-010.1000E-19
0.1576E 010.5580E 030.1000E-190.1000E-190.1108E-010.1586E-010.1000E-19
0.1914E 010.4420E 030.1000E-190.1000E-190.6102E-020.8951E-020.1000E-19
0.2236E 010.3775E 030.1000E-190.1000E-190.3492E-020.5231E-020.1000E-19
0.2545E 010.3398E 030.1000E-190.1000E-190.2002E-020.3048E-020.1000E-19
0.2843E 010.3168E 030.1000E-190.1000E-190.1107E-020.1705E-020.1000E-19
0.3133E 010.3027E 030.1000E-190.1000E-190.5517E-030.8733E-030.1000E-19
0.3419E 010.2940E 030.1000E-190.1000E-190.2273E-030.3553E-030.1000E-19
  0.785E 01
0.0       0.2576E 040.1000E-190.1000E-190.1059E 000.2251E 000.1000E-19
0.8882E-010.2554E 040.1000E-190.1000E-190.1065E 000.2180E 000.1000E-19
0.1776E 000.2532E 040.1000E-190.1000E-190.1071E 000.2126E 000.1000E-19
0.2672E 000.2430E 040.1000E-190.1000E-190.1060E 000.1920E 000.1000E-19
0.3682E 000.2324E 040.1000E-190.1000E-190.1053E 000.1730E 000.1000E-19
0.6036E 000.1828E 040.1000E-190.1000E-190.8376E-010.1145E 000.1000E-19
0.8941E 000.1232E 040.1000E-190.1000E-190.4684E-010.6325E-010.1000E-19
0.1229E 010.8136E 030.1000E-190.1000E-190.2334E-010.3207E-010.1000E-19
0.1574E 010.5833E 030.1000E-190.1000E-190.1228E-010.1726E-010.1000E-19
0.1912E 010.4602E 030.1000E-190.1000E-190.6905E-020.9932E-020.1000E-19
0.2236E 010.3906E 030.1000E-190.1000E-190.4052E-020.5947E-020.1000E-19
0.2547E 010.3497E 030.1000E-190.1000E-190.2413E-020.3599E-020.1000E-19
0.2847E 010.3244E 030.1000E-190.1000E-190.1412E-020.2132E-020.1000E-19
0.3140E 010.3082E 030.1000E-190.1000E-190.7800E-030.1189E-020.1000E-19
0.3427E 010.2980E 030.1000E-190.1000E-190.3857E-030.5921E-030.1000E-19
0.3710E 010.2919E 030.1000E-190.1000E-190.1499E-030.2310E-030.1000E-19
  0.830E 01
0.0       0.2568E 040.1000E-190.1000E-190.1077E 000.2190E 000.1000E-19
0.8980E-010.2544E 040.1000E-190.1000E-190.1080E 000.2120E 000.1000E-19
0.1798E 000.2520E 040.1000E-190.1000E-190.1085E 000.2066E 000.1000E-19
0.2700E 000.2414E 040.1000E-190.1000E-190.1070E 000.1870E 000.1000E-19
0.3726E 000.2308E 040.1000E-190.1000E-190.1056E 000.1681E 000.1000E-19
0.6091E 000.1828E 040.1000E-190.1000E-190.8418E-010.1129E 000.1000E-19
0.8976E 000.1257E 040.1000E-190.1000E-190.4858E-010.6440E-010.1000E-19
0.1229E 010.8429E 030.1000E-190.1000E-190.2496E-010.3374E-010.1000E-19
0.1572E 010.6070E 030.1000E-190.1000E-190.1342E-010.1856E-010.1000E-19
0.1910E 010.4777E 030.1000E-190.1000E-190.7691E-020.1087E-010.1000E-19
0.2236E 010.4039E 030.1000E-190.1000E-190.4610E-020.6646E-020.1000E-19
0.2549E 010.3594E 030.1000E-190.1000E-190.2820E-020.4132E-020.1000E-19
0.2851E 010.3319E 030.1000E-190.1000E-190.1720E-020.2552E-020.1000E-19
0.3146E 010.3141E 030.1000E-190.1000E-190.1017E-020.1525E-020.1000E-19
0.3435E 010.3024E 030.1000E-190.1000E-190.5569E-030.8411E-030.1000E-19
0.3719E 010.2942E 030.1000E-190.1000E-190.2409E-030.3654E-030.1000E-19
  0.876E 01
0.0       0.2559E 040.1000E-190.1000E-190.1093E 000.2128E 000.1000E-19
0.9118E-010.2530E 040.1000E-190.1000E-190.1095E 000.2070E 000.1000E-19
0.1821E 000.2508E 040.1000E-190.1000E-190.1097E 000.2005E 000.1000E-19
0.2777E 000.2400E 040.1000E-190.1000E-190.1070E 000.1820E 000.1000E-19
0.3770E 000.2291E 040.1000E-190.1000E-190.1056E 000.1635E 000.1000E-19
0.6143E 000.1827E 040.1000E-190.1000E-190.8446E-010.1113E 000.1000E-19
0.9011E 000.1277E 040.1000E-190.1000E-190.5011E-010.6525E-010.1000E-19
0.1229E 010.8692E 030.1000E-190.1000E-190.2647E-010.3519E-010.1000E-19
0.1570E 010.6292E 030.1000E-190.1000E-190.1451E-010.1975E-010.1000E-19
0.1909E 010.4948E 030.1000E-190.1000E-190.8457E-020.1177E-010.1000E-19
0.2236E 010.4169E 030.1000E-190.1000E-190.5158E-020.7316E-020.1000E-19
0.2551E 010.3692E 030.1000E-130.1000E-190.3222E-020.4545E-020.1000E-19
0.2850E 010.3392E 030.1000E-190.1000E-190.2016E-020.2948E-020.1000E-19
```

```
0.3152E 010.3194E 030.1000E-190.1000E-190.1232E-020.1819E-020.1000E-19
0.3441E 010.3061E 030.1000E-190.1000E-190.7069E-030.1051E-020.1000E-19
0.3727E 010.2972E 030.1000E-190.1000E-190.3605E-030.5390E-030.1000E-19
0.4009E 010.2917E 030.1000E-190.1000E-190.1433E-030.2150E-030.1000E-19
  0.921E 01
0.0       0.2548E 040.1000E-190.1000E-190.1108E 000.2066E 000.1000E-19
0.9188E-010.2520E 040.1000E-190.1000E-190.1107E 000.2005E 000.1000E-19
0.1844E 000.2493E 040.1000E-190.1000E-190.1107E 000.1945E 000.1000E-19
0.2824E 000.2380E 040.1000E-190.1000E-190.1083E 000.1767E 000.1000E-19
0.3814E 000.2275E 040.1000E-190.1000E-190.1059E 000.1589E 000.1000E-19
0.6194E 000.1825E 040.1000E-190.1000E-190.8460E-010.1096E 000.1000E-19
0.9051E 000.1295E 040.1000E-190.1000E-190.5143E-010.6584E-010.1000E-19
0.1230E 010.8932E 030.1000E-190.1000E-190.2787E-010.3648E-010.1000E-19
0.1570E 010.6500E 030.1000E-190.1000E-190.1556E-010.2085E-010.1000E-19
0.1908E 010.5110E 030.1000E-190.1000E-190.9201E-020.1261E-010.1000E-19
0.2236E 010.4292E 030.1000E-190.1000E-190.5694E-020.7955E-020.1000E-19
0.2553E 010.3786E 030.1000E-190.1000E-190.3615E-020.5135E-020.1000E-19
0.2859E 010.3463E 030.1000E-190.1000E-190.2312E-020.3328E-020.1000E-19
0.3157E 010.3250E 030.1000E-190.1000E-190.1461E-020.2125E-020.1000E-19
0.3448E 010.3106E 030.1000E-190.1000E-190.8896E-030.1305E-020.1000E-19
0.3735E 010.3007E 030.1000E-190.1000E-190.4981E-030.7352E-030.1000E-19
0.4016E 010.2936E 030.1000E-190.1000E-190.2189E-030.3242E-030.1000E-19
  0.966E 01
0.0       0.2535E 040.1000E-190.1000E-190.1120E 000.2003E 000.1000E-19
0.9294E-010.2500E 040.1000E-190.1000E-190.1118E 000.1945E 000.1000E-19
0.1868E 000.2477E 040.1000E-190.1000E-190.1116E 000.1686E 000.1000E-19
0.2861E 000.2360E 040.1000E-190.1000E-190.1087E 000.1710E 000.1000E-19
0.3858E 000.2257E 040.1000E-190.1000E-190.1059E 000.1545E 000.1000E-19
0.6249E 000.1821E 040.1000E-190.1000E-190.8462E-010.1079E 000.1000E-19
0.9090E 000.1310E 040.1000E-190.1000E-190.5257E-010.6623E-010.1000E-19
0.1232E 010.9150E 030.1000E-190.1000E-190.2917E-010.3760E-010.1000E-19
0.1569E 010.6696E 030.1000E-190.1000E-190.1656E-010.2186E-010.1000E-19
0.1907E 010.5264E 030.1000E-190.1000E-190.9924E-020.1340E-010.1000E-19
0.2235E 010.4410E 030.1000E-190.1000E-190.6220E-020.8566E-020.1000E-19
0.2554E 010.3877E 030.1000E-190.1000E-190.4006E-020.5611E-020.1000E-19
0.2861E 010.3534E 030.1000E-190.1000E-190.2609E-020.3704E-020.1000E-19
0.3161E 010.3305E 030.1000E-190.1000E-190.1687E-020.2422E-020.1000E-19
0.3453E 010.3147E 030.1000E-190.1000E-190.1056E-020.1529E-020.1000E-19
0.3741E 010.3034F 030.1000E-190.1000E-190.6082E-030.8861E-030.1000E-19
0.4024E 010.2949E 030.1000E-190.1000E-190.2730E-030.3991E-030.1000E-19
0.4303E 010.2901E 030.1000E-190.1000E-190.8437E-040.1236E-030.1000E-19
  0.101E 02
0.0       0.2521E 040.1000E-190.1000E-190.1131E 000.1942F 000.1000E-19
0.9511E-010.2490F 040.1000E-190.1000E-190.1127E 000.1890E 000.1000E-19
0.1891E 000.2460E 040.1000E-190.1000E-190.1122E 000.1828E 000.1000E-19
0.2861E 000.2350F 040.1000E-190.1000E-190.1090E 000.1660E 000.1000E-19
0.3901E 000.2239F 040.1000E-190.1000E-190.1057E 000.1502E 000.1000E-19
0.6300E 000.1810E 040.1000E-190.1000E-190.8450E-010.1061E 000.1000E-19
0.9129E 000.1323E 040.1000E-190.1000E-190.5351E-010.6543E-010.1000E-19
0.1233E 010.9345E 030.1000E-190.1000E-190.3035E-010.3857E-010.1000E-19
0.1569E 010.6876E 030.1000E-190.1000E-190.1750E-010.2278E-010.1000E-19
0.1906E 010.5409E 030.1000E-190.1000E-190.1062E-010.1414E-010.1000E-19
0.2235E 010.4523E 030.1000E-190.1000E-190.6730E-020.9144E-020.1000E-19
0.2554E 010.3956E 030.1000E-190.1000E-190.4387E-020.6063E-020.1000E-19
0.2803E 010.3602E 030.1000E-190.1000E-190.2897E-020.4060E-020.1000E-19
0.3104E 010.3357E 030.1000E-190.1000E-190.1904E-020.2699E-020.1000E-19
0.3458E 010.3188E 030.1000E-190.1000E-190.1223E-020.1749E-020.1000E-19
0.3747E 010.3069E 030.1000E-190.1000E-190.7486E-030.1078E-020.1000E-19
0.4032E 010.2986F 030.1000E-190.1000E-190.4176E-030.6042E-030.1000E-19
0.4311E 010.2926E 030.1000E-190.1000E-190.1823E-030.2645E-030.1000E-19
  0.105E 02
```

```
0.0         0.2504E 040.1000E-190.1000E-190.1139E 000.1880E 000.1000E-19
0.9432E-010.2470E 040.1000E-190.1000E-190.1132E 000.1825E 000.1000E-19
0.1914E 000.2441E 040.1000E-190.1000E-190.1126E 000.1770E 000.1000E-19
0.2928E 000.2330E 040.1000E-190.1000E-190.1090E 000.1615E 000.1000E-19
0.3946E 000.2220E 040.1000E-190.1000E-190.1053E 000.1460E 000.1000E-19
0.6398E 000.1801E 040.1000E-190.1000E-190.8391E-010.1025E 000.1000E-19
0.9208E 000.1341E 040.1000E-190.1000E-190.5492E-010.6639E-010.1000E-19
0.1237E 010.9680E 030.1000E-190.1000E-190.3242E-010.4012E-010.1000E-19
0.1570E 010.7205E 030.1000E-190.1000E-190.1925E-010.2440E-010.1000E-19
0.1905E 010.5682E 030.1000E-190.1000E-190.1195E-010.1550E-010.1000E-19
0.2235E 010.4741E 030.1000E-190.1000E-190.7724E-020.1023E-010.1000E-19
0.2556E 010.4139E 030.1000E-190.1000E-190.5140E-020.6924E-020.1000E-19
0.2867E 010.3737E 030.1000E-190.1000E-190.3473E-020.4749E-020.1000E-19
0.3170E 010.3464E 030.1000E-190.1000E-190.2354E-020.3257E-020.1000E-19
0.3467E 010.3272E 030.1000E-190.1000E-190.1574E-020.2200E-020.1000E-19
0.3757E 010.3134E 030.1000E-190.1000E-190.1015E-020.1428E-020.1000E-19
0.4044E 010.3030E 030.1000E-190.1000E-190.5980E-030.8466E-030.1000E-19
0.4327E 010.2948E 030.1000E-190.1000E-190.2727E-030.3872E-030.1000E-19
0.4606E 010.2901E 030.1000E-190.1000E-190.8526E-040.1212E-030.1000E-19
 0.110E 02
0..0         0.2485E 040.1000E-190.1000E-190.1145E 000.1820E 000.1000E-19
0.9628E-010.2453E 040.1000E-190.1000E-190.1136E 000.1767E 000.1000E-19
0.1938E 000.2421E 040.1000E-190.1000E-190.1128E 000.1714E 000.1000E-19
0.2959E 000.2310E 040.1000E-190.1000E-190.1090E 000.1570E 000.1000E-19
0.3989E 000.2200E 040.1000E-190.1000E-190.1049E 000.1419E 000.1000E-19
0.6351E 000.1809E 040.1000E-190.1000E-190.8426E-010.1043E 000.1000E-19
0.9169E 000.1333E 040.1000E-190.1000E-190.5430E-010.6648E-010.1000E-19
0.1235E 010.9522E 030.1000E-190.1000E-190.3143E-010.3941E-010.1000E-19
0.1569E 010.7046E 030.1000E-190.1000E-190.1840E-010.2363E-010.1000E-19
0.1906E 010.5549E 030.1000E-190.1000E-190.1129E-010.1484E-010.1000E-19
0.2235E 010.4634E 030.1000E-190.1000E-190.7232E-020.9697E-020.1000E-19
0.2555E 010.4053E 030.1000E-190.1000E-190.4766E-020.6502E-020.1000E-19
0.2865E 010.3669E 030.1000E-190.1000E-190.3186E-020.4409E-020.1000E-19
0.3168E 010.3411E 030.1000E-190.1000E-190.2130E-020.2983E-020.1000E-19
0.3462E 010.3231E 030.1000E-190.1000E-190.1402E-020.1982E-020.1000E-19
0.3752E 010.3103E 030.1000E-190.1000E-190.8881E-030.1264E-020.1000E-19
0.4036E 010.3010E 030.1000E-190.1000E-190.5152E-030.7373E-030.1000E-19
0.4319E 010.2939E 030.1000E-190.1000E-190.2323E-030.3335E-030.1000E-19
 0.0
```

```
NWAV1      2000  2500
WAV    2000.0 0.0           0.0         0.0         0.13E-03 0.0          0.13E 00 0.66E 00
WAV    2000.0 0.25E 01 0.15E 02 0.18E 03 0.40E 03 0.87E 03 0.28E 04 0.70E 04
WAV    2025.0 0.0           0.0         0.0         0.78E-03 0.0          0.26E 00 0.11E 01
WAV    2025.0 0.25E 01 0.15E 02 0.18E 03 0.40E 03 0.87E 03 0.28E 04 0.63E 04
WAV    2050.0 0.0           0.0         0.0         0.37E-02 0.0          0.50E 00 0.17E 01
WAV    2050.0 0.25E 01 0.15E 02 0.18E 03 0.40E 03 0.87E 03 0.27E 04 0.51E 04
WAV    2075.0 0.0           0.0         0.0         0.15E-01 0.0          0.95E 00 0.26E 01
WAV    2075.0 0.25E 01 0.15E 02 0.18E 03 0.40E 03 0.87E 03 0.27E 04 0.44E 04
WAV    2100.0 0.0           0.0         0.0         0.52E-01 0.29E 00 0.17E 01 0.37E 01
WAV    2100.0 0.25E 01 0.15E 02 0.18E 03 0.40E 03 0.86E 03 0.25E 04 0.36E 04
WAV    2125.0 0.0           0.0         0.0         0.18E 00 0.69E 00 0.28E 01 0.50E 01
WAV    2125.0 0.25E 01 0.15E 02 0.18E 03 0.40E 03 0.82E 03 0.21E 04 0.29E 04
WAV    2150.0 0.0           0.0         0.0         0.52E 00 0.15E 01 0.45E 01 0.73E 01
WAV    2150.0 0.25E 01 0.15E 02 0.18E 03 0.40E 03 0.75E 03 0.17E 04 0.23E 04
WAV    2175.0 0.0           0.0         0.31E 00 0.14E 01 0.31E 01 0.67E 01 0.87E 01
WAV    2175.0 0.25E 01 0.15E 02 0.18E 03 0.39E 03 0.65E 03 0.13E 04 0.17E 04
WAV    2200.0 0.0           0.75E-03 0.11E 01 0.32E 01 0.56E 01 0.93E 01 0.11E 02
WAV    2200.0 0.25E 01 0.15E 02 0.16E 03 0.35E 03 0.55E 03 0.96E 03 0.13E 04
WAV    2225.0 0.0           0.18E-01 0.32E 01 0.66E 01 0.93E 01 0.12E 02 0.12E 02
WAV    2225.0 0.25E 01 0.14E 02 0.14E 03 0.26E 03 0.40E 03 0.73E 03 0.90E 03
WAV    2250.0 0.78E-04 0.28E 00 0.78E 01 0.12E 02 0.14E 02 0.14E 02 0.12E 02
WAV    2250.0 0.25E 01 0.14E 02 0.11E 03 0.17E 03 0.28E 03 0.46E 03 0.63E 03
WAV    2275.0 0.21E-01 0.26E 01 0.15E 02 0.17E 02 0.17E 02 0.15E 02 0.12E 02
WAV    2275.0 0.25E 01 0.12E 02 0.75E 02 0.14E 03 0.20E 03 0.37E 03 0.41E 03
WAV    2300.0 0.19E 01 0.16E 02 0.22E 02 0.20E 02 0.19E 02 0.16E 02 0.13E 02
WAV    2300.0 0.23E 01 0.78E 01 0.85E 02 0.11E 03 0.22E 03 0.34E 03 0.41E 03
WAV    2325.0 0.37E 02 0.36E 02 0.23E 02 0.20E 02 0.18E 02 0.13E 02 0.93E 01
WAV    2325.0 0.14E 01 0.57E 01 0.42E 02 0.73E 02 0.79E 02 0.11E 03 0.13E 03
WAV    2350.0 0.11E 02 0.21E 02 0.23E 02 0.20E 02 0.17E 02 0.11E 02 0.72E 01
WAV    2350.0 0.28E 01 0.80E 01 0.24E 02 0.34E 02 0.37E 02 0.49E 02 0.56E 02
WAV    2375.0 0.24E 02 0.34E 02 0.20E 02 0.14E 02 0.11E 02 0.60E 01 0.27E 01
WAV    2375.0 0.11E 01 0.21E 01 0.55E 01 0.75E 01 0.70E 01 0.68E 01 0.63E 01
WAV    2400.0 0.0           0.0         0.0         0.0         0.0         0.0         0.0
WAV    2400.0 0.0           0.0         0.0         0.0         0.0         0.0         0.0
WAV    2425.0 0.0           0.0         0.0         0.0         0.0         0.0         0.0
WAV    2425.0 0.0           0.0         0.0         0.0         0.0         0.0         0.0
WAV    2450.0 0.0           0.0         0.0         0.0         0.0         0.0         0.0
WAV    2450.0 0.0           0.0         0.0         0.0         0.0         0.0         0.0
WAV    2475.0 0.0           0.0         0.0         0.0         0.0         0.0         0.0
WAV    2475.0 0.0           0.0         0.0         0.0         0.0         0.0         0.0
WAV    2500.0 0.0           0.0         0.0         0.0         0.0         0.0         0.0
WAV    2500.0 0.0           0.0         0.0         0.0         0.0         0.0         0.0
```

APPENDIX III

SAMPLE CASE OUTPUT

WAVE NUMBER	WAVE LENGTH	RADIATION		WAVE NUMBER	WAVE LENGTH	RADIATION
		W/SR/CM/MICRON				
2000.	5.0000	0.98137E-03		2025.	4.9383	0.20115E-02
2050.	4.8780	0.39446E-02		2075.	4.8193	0.76348E-02
2100.	4.7619	0.17107E-01		2125.	4.7059	0.29450E-01
2150.	4.6512	0.49696E-01		2175.	4.5977	0.77929E-01
2200.	4.5455	0.11446E 00		2225.	4.4944	0.15660E 00
2250.	4.4444	0.19604E 00		2275.	4.3956	0.22414E 00
2300.	4.3478	0.25091E 00		2325.	4.3011	0.22054E 00
2350.	4.2553	0.17916E 00		2375.	4.2105	0.78166E-01
2400.	4.1667	0.0		2425.	4.1237	0.0
2450.	4.0816	0.0		2475.	4.0404	0.0
2500.	4.0000	0.0				

TOTAL RADIATION EMITTED=0.8259E-01 WATTS/STER

WAVE NUMBER	WAVE LENGTH	RADIATION		WAVE NUMBER	WAVE LENGTH	RADIATION
2000.	5.0000	0.11605E-02		2025.	4.9383	0.23865E-02
2050.	4.8780	0.45994E-02		2075.	4.8193	0.91333E-02
2100.	4.7619	0.19295E-01		2125.	4.7059	0.33014E-01
2150.	4.6512	0.55326E-01		2175.	4.5977	0.85780E-01
2200.	4.5455	0.12457E 00		2225.	4.4944	0.16815E 00
2250.	4.4444	0.20694E 00		2275.	4.3956	0.23378E 00
2300.	4.3478	0.26036E 00		2325.	4.3011	0.22397E 00
2350.	4.2553	0.18512E 00		2375.	4.2105	0.82563E-01
2400.	4.1667	0.0		2425.	4.1237	0.0
2450.	4.0816	0.0		2475.	4.0404	0.0
2500.	4.0000	0.0				

TOTAL RADIATION FOR STATION 4 = 0.78207E-01WATTS/SR/CM

PR1.OX
STATION NO.= 28   AXIAL DIST. (CM)=   11.035   ASPECT ANGLE (DEG)= 90.0

SUM UP SRADSR AT X STATION   0.0

WAVE NUMBER	WAVE LENGTH	RADIATION	WAVE NUMBER	WAVE LENGTH	RADIATION
		W/SR/CM/MICRON			
2000.	5.0000	0.0	2025.	4.9383	0.0
2050.	4.8780	0.0	2075.	4.8193	0.0
2100.	4.7619	0.0	2125.	4.7059	0.0
2150.	4.6512	0.0	2175.	4.5977	0.0
2200.	4.5455	0.0	2225.	4.4944	0.0
2250.	4.4444	0.0	2275.	4.3956	0.0
2300.	4.3478	0.0	2325.	4.3011	0.0
2350.	4.2553	0.0	2375.	4.2105	0.0
2400.	4.1667	0.0	2425.	4.1237	0.0
2450.	4.0816	0.0	2475.	4.0404	0.0
2500.	4.0000	0.0			

TOTAL RADIATION EMITTED=0.1663E 01 WATTS/STER

WAVE NUMBER	WAVE LENGTH	RADIATION	WAVE NUMBER	WAVE LENGTH	RADIATION
2000.	5.0000	0.10455E-01	2025.	4.9383	0.21407E-01
2050.	4.8780	0.41942E-01	2075.	4.8193	0.81130E-01
2100.	4.7619	0.26070E 00	2125.	4.7059	0.47098E 00
2150.	4.6512	0.82891E 00	2175.	4.5977	0.13972E 01
2200.	4.5455	0.21785E 01	2225.	4.4944	0.31900E 01
2250.	4.4444	0.42830E 01	2275.	4.3956	0.50712E 01
2300.	4.3478	0.56955E 01	2325.	4.3011	0.51826E 01
2350.	4.2553	0.39996E 01	2375.	4.2105	0.16854E 01
2400.	4.1667	0.0	2425.	4.1237	0.0
2450.	4.0816	0.0	2475.	4.0404	0.0
2500.	4.0000	0.0			

TOTAL RADIATION FOR STATION 28 =   0.0   WATTS/SR/CM

LAPP GAS DYNAMICS — ARMY RADIATION CODE

PRJ.UX	W/SR/cm	STATION RADIATION (W/SR)
0.0	0.5837254E-01	~~0.4032077E-50~~
0.41	0.6468284E-01	0.2522010E-01
0.81	0.7061887E-01	0.2730462E-01
1.22	0.7820714E-01	0.3006312E-01
1.61	0.8649528E-01	0.3262293E-01
1.97	0.9388489E-01	0.3232552E-01
2.37	0.1016850E 00	0.3915963E-01
2.78	0.1099497E 00	0.4252582E-01
3.18	0.1185645E 00	0.4656448E-01
3.58	0.1266638E 00	0.4842820E-01
3.98	0.1350878E 00	0.5225714E-01
4.39	0.1435786E 00	0.5804345E-01
4.82	0.1524286E 00	0.6281853E-01
5.22	0.1602380E 00	0.6266773E-01
5.63	0.1665467E 00	0.6678170E-01
6.03	0.1720112E 00	0.6852239E-01
6.44	0.1782773E 00	0.7089573E-01
6.85	0.1849118E 00	0.7493514E-01
6.94	0.1851284E 00	0.1672365E-01
7.41	0.1922510E 00	0.8823474E-01
7.85	0.1983629E 00	0.8673418E-01
8.30	0.2038116E 00	0.9088081E-01
8.76	0.2088537E 00	0.9325266E-01
9.21	0.2134077E 00	0.9542012E-01
9.66	0.2167625E 00	0.9805322E-01
10.12	0.2199754E 00	0.9955025E-01
10.58	0.2249740E 00	0.1014207E 00
11.04	0.0	0.5172247E-01

* RADIATION VALUE WAS CALCULATED BASED ON THE SLOPE BETWEEN THE PREVIOUS TWO POINTS

TOTAL RADIATION EMITTED=0.1563E 01 WATTS/STER

CENTROID= 0.6655E 01CM

```
NWAV1      2000   2500
  WAV       2000.0 0.78E-02 0.40E-01 0.77E-01 0.11E 00 0.13E 00 0.14E 00 0.15E 00
  WAV       2000.0 0.95E-01 0.17E 00 0.45E 00 0.14E 01 0.39E 01 0.98E 01 0.24E 02
  WAV       2025.0 0.54E-02 0.35E-01 0.65E-01 0.87E-01 0.11E 00 0.12E 00 0.13E 00
  WAV       2025.0 0.12E 00 0.21E 00 0.50E 00 0.15E 01 0.36E 01 0.91E 01 0.23E 02
  WAV       2050.0 0.38E-02 0.25E-01 0.51E-01 0.71E-01 0.89E-01 0.10E 00 0.11E 00
  WAV       2050.0 0.11E 00 0.19E 00 0.48E 00 0.15E 01 0.40E 01 0.10E 02 0.26E 02
  WAV       2075.0 0.26E-02 0.18E-01 0.51E-01 0.55E-01 0.72E-01 0.83E-01 0.96E-01
  WAV       2075.0 0.12E 00 0.22E 00 0.55E 00 0.18E 01 0.45E 01 0.12E 02 0.28E 02
  WAV       2100.0 0.18E-02 0.12E-01 0.29E-01 0.44E-01 0.61E-01 0.69E-01 0.84E-01
  WAV       2100.0 0.14E 00 0.26E 00 0.57E 00 0.17E 00 0.41E 01 0.12E 02 0.35E 02
  WAV       2125.0 0.13E-02 0.85E-02 0.21E-01 0.38E-01 0.58E-01 0.64E-01 0.73E-01
  WAV       2125.0 0.20E 00 0.39E 00 0.68E 00 0.17E 01 0.36E 01 0.11E 02 0.36E 02
  WAV       2150.0 0.88E-03 0.68E-02 0.15E-01 0.28E-01 0.45E-01 0.52E-01 0.63E-01
  WAV       2150.0 0.22E 00 0.42E 00 0.13E 01 0.27E 01 0.50E 01 0.17E 02 0.65E 02
  WAV       2175.0 0.62E-02 0.40E-02 0.11E-01 0.21E-01 0.37E-01 0.45E-01 0.53E-01
  WAV       2175.0 0.23E 00 0.43E 00 0.10E 01 0.21E 01 0.40E 01 0.14E 02 0.89E 02
  WAV       2200.0 0.48E-03 0.30E-02 0.93E-02 0.19E-01 0.33E-01 0.40E-01 0.46E-01
  WAV       2200.0 0.23E 00 0.45E 00 0.11E 01 0.25E 01 0.49E 01 0.19E 02 0.12E 03
  WAV       2225.0 0.41E-03 0.18E-02 0.70E-02 0.15E-01 0.30E-01 0.37E-01 0.40E-01
  WAV       2225.0 0.24E 00 0.45E 00 0.11E 01 0.27E 01 0.53E 01 0.21E 02 0.13E 03
  WAV       2250.0 0.32E-03 0.12E-02 0.45E-02 0.10E-01 0.25E-01 0.33E-01 0.35E-01
  WAV       2250.0 0.25E 00 0.48E 00 0.12E 01 0.29E 01 0.58E 01 0.23E 02 0.13E 03
  WAV       2275.0 0.23E-03 0.72E-03 0.36E-02 0.93E-02 0.23E-01 0.31E-01 0.31E-01
  WAV       2275.0 0.25E 00 0.50E 00 0.12E 01 0.31E 01 0.63E 01 0.25E 02 0.14E 03
  WAV       2300.0 0.20E-03 0.54E-03 0.32E-02 0.75E-02 0.20E-01 0.28E-01 0.29E-01
  WAV       2300.0 0.27E 00 0.52E 00 0.12E 01 0.34E 01 0.69E 01 0.28E 02 0.15E 03
  WAV       2325.0 0.15E-03 0.38E-03 0.19E-02 0.60E-02 0.18E-01 0.27E-01 0.28E-01
  WAV       2325.0 0.27E 00 0.53E 00 0.13E 01 0.37E 01 0.75E 01 0.31E 02 0.16E 03
  WAV       2350.0 0.10E-03 0.26E-03 0.12E-02 0.48E-02 0.16E-01 0.25E-01 0.28E-01
  WAV       2350.0 0.28E 00 0.55E 00 0.13E 01 0.40E 01 0.82E 01 0.34E 02 0.17E 03
  WAV       2375.0 0.85E-04 0.19E-03 0.91E-03 0.36E-02 0.13E-01 0.24E-01 0.26E-01
  WAV       2375.0 0.29E 00 0.55E 00 0.14E 01 0.43E 01 0.90E 01 0.37E 02 0.18E 03
  WAV       2400.0 0.76E-04 0.14E-03 0.71E-03 0.32E-02 0.12E-01 0.24E-01 0.25E-01
  WAV       2400.0 0.30E 00 0.53E 00 0.14E 01 0.46E 01 0.98E 01 0.41E 02 0.19E 03
  WAV       2425.0 0.62E-04 0.13E-03 0.61E-03 0.23E-02 0.10E-01 0.22E-01 0.25E-01
  WAV       2425.0 0.31E 00 0.60E 00 0.15E 01 0.50E 01 0.11E 02 0.45E 02 0.21E 03
  WAV       2450.0 0.48E-04 0.11E-03 0.52E-03 0.20E-02 0.92E-02 0.20E-01 0.25E-01
  WAV       2450.0 0.32E 00 0.63E 00 0.15E 01 0.54E 01 0.12E 02 0.50E 02 0.22E 03
  WAV       2475.0 0.37E-04 0.11E-03 0.44E-03 0.17E-02 0.79E-02 0.18E-01 0.25E-01
  WAV       2475.0 0.33E 00 0.65E 00 0.16E 01 0.58E 01 0.13E 02 0.55E 02 0.24E 03
  WAV       2500.0 0.36E-04 0.10E-03 0.38E-03 0.17E-02 0.67E-02 0.17E-01 0.25E-01
  WAV       2500.0 0.34E 00 0.67E 00 0.16E 01 0.64E 01 0.14E 02 0.61E 02 0.25E 03
```